kOMUNIKÁCIE
COMMUNICATIONS

Dear reader,

this volume of the Communications is mainly devoted to fatigue of structural materials. Fatigue properties of structural materials have been studied for more than 150 years:

- *1829 – Wilhelm Albert first discusses the phenomenon on observing the failure of iron mine-hoist chains in Clausthal mines;*
- *1839 – the term fatigue becomes current when Jean-Victor Poncelet in his lectures at the military school at Metz describes metals as being tired;*
- *1843 – William John Macquorn Rankine in his investigation of railroad axle failures following the Versailles accident recognises the importance of stress concentration;*
- *1849 – Eaton Hodgkinson is granted a small sum of money to report to the UK Parliament on his work in ascertaining by direct experiment, the effects of continued changes of load upon iron structures and to what extent they could be loaded without danger to their ultimate security*
- *1860 – the first systematic investigations of fatigue life by Sir William Fairbairn and August Wőhler. Wőhler's study of railroad axles lead him to the idea of a fatigue limit and to propose the use of S-N curves in mechanical design; and so on ...*

Although fatigue has been studied extensively over many years, further study is warranted because the knowledge base, although large, is partly obsolete and new materials and treatments are continuously being developed. With regard to the above facts the editorial board addressed the institutions whose activities on the fatigue field are significant. The reaction of authors was spontaneous. Let me thank to all of them (Institute of Physics of Materials, Academy of Sciences of the Czech Republic, Brno; Czech Technical University of Prague, Prague; Charles University, Prague; Brno University of Technology, Brno; University of Defence, Brno; SVÚM, a.s., Prague; Technical University of Košice, Košice; University of Žilina, Žilina) who contributed to the Communications – Scientific Letters of the University of Žilina, No. 4, 2006.

Otakar Bokůvka

https://doi.org/10.26552/com.C.2006.4.5-9

Jaroslav Polák – Jiří Man – Martin Petrenec *

MECHANISMS OF THE EARLY FATIGUE DAMAGE IN METALLIC MATERIALS

The early stages of the fatigue damage in f.c.c. and b.c.c. metals are studied using high resolution techniques. The localization of the cyclic plastic strain results in formation persistent slip bands (PSBs) with specific dislocation structure. Characteristic surface relief is formed at locations where PSBs emerge on the surface. It consists of extrusions and intrusions separated by the original flat surface. Atomic force microscopy is used to study the details of the surface relief. The experimental findings are discussed in terms of the point defect model of fatigue crack initiation.

1. Introduction

The basic facts concerning the surface relief formation in fatigued metals were documented already at the beginning of the 20th century by Ewing and Humfrey [1] by observing the surface of fatigued Swedish iron. The optical microscope used in these and later studies could not reveal details of the emerging extrusions and intrusions and eventually the early initiation of fatigue cracks. Later studies using replicas in transmission electron microscope or classical scanning electron microscope (see. e.g. [2]) yield higher resolution but it is not possible to obtain quantitative information in three dimensions.

Transmission electron microscopy allowed studying dislocation structure of fatigued metals [2]. Early studies in single crystals revealed specific structure of the bands, responsible for the localization of the cyclic strain – persistent slip bands (PSBs). Oriented foil technique [3] allows studying dislocation structure in individual grains of polycrystalline materials. PSBs accommodate high cyclic plastic strain. Due to high cyclic plastic strain amplitude localized in PSBs pronounced surface relief in the form persistent slip markings (PSMs) is formed in areas where PSBs emerge on the surface.

In this contribution the characteristic dislocation structures corresponding to cyclic slip localization in polycrystalline f.c.c. and b.c.c. stainless steels observed using transmission electron microscope are shown. The characteristic surface relief produced during cyclic straining of these materials – PSMs – using AFM (Topometrics) is documented. The experimental data are used to discuss the models of fatigue crack initiation.

2. Experimental

Polycrystalline specimens made of 316L austenitic stainless steel and X10CrAl24 ferritic stainless steel were used in the present study. Smooth cylindrical specimens having 8 mm in diameter and 12 mm in gage length were slightly notched to produce surface suitable for surface observations. The dimensions of the specimen are shown in Fig. 1. The area of the notch was mechanically and electrolytically polished to facilitate the observations of the surface relief. The specimens were cycled in computer controlled MTS 880 electrohydraulic machine. Symmetrical strain cycle with the strain rate $\dot{\epsilon} = 2.5 \times 10^{-3}\ s^{-1}$ was applied at room temperature. The plastic strain amplitude derived from the half-width of the hysteresis loop was kept constant using the computer "outer loop". Further experimental details concerning the materials and testing procedure can be found elsewhere [3, 4].

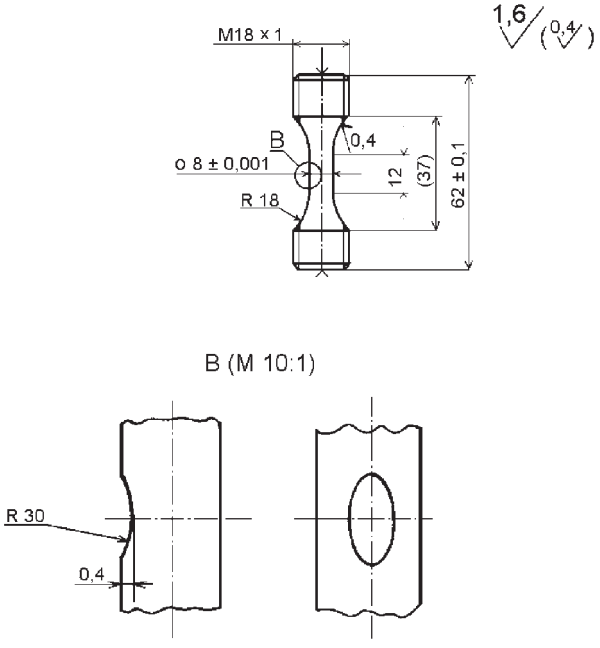

Fig. 1 Dimensions of the specimen with a shallow notch.

* **Jaroslav Polák, Jiří Man, Martin Petrenec**
Institute of Physics of Materials, Academy of Sciences of the Czech Republic, Žižkova 22, Brno, Czech Republic, polak@ipm.cz

The cycling was interrupted at a selected number of cycles; the specimen was taken from the testing machine and inspected in AFM. Replica technique was applied to reveal the depth and the shape of extrusions and intrusions [5].

Some fatigued specimens were cut and thin foils with the foil plane parallel to the specimen axis were produced. They were observed in transmission electron microscope Philips CM12. Orientation of the foil relative to the loading axis was determined with the help of electron diffraction and Kikuchi lines.

3. Results

3.1. Dislocation structures

Dislocation structures corresponding to cyclic slip localization were studied mostly in polycrystalline specimens cycled with medium and low plastic strain amplitudes. Previous studies in austenitic steel and in austenitic grains of duplex steel [6–8] revealed the presence of specific bands (PSBs) with irregular ladder structure embedded in the matrix. The density of individual PSBs is highest for medium plastic strain amplitudes ($\sim 2 \times 10^{-3}$).

Figure 2 shows characteristic dislocation structures in austenitic and in ferritic stainless steels in specimens cycled with medium plastic strain amplitudes up to the end of the fatigue life. Orientation of individual grains is shown by the position of the stress axis in a stereographic triangle. The trace of the primary slip plane and Schmid factors of mostly stressed systems are also shown. Individual ladder-like bands, parallel to the primary slip plane in Fig. 2a consist of alternating dislocation-rich walls and dislocation-poor channels, both approximately perpendicular to the foil plane. This structure corresponds to the dislocation arrangement in fatigued single crystals [2].

Ladder-like dislocation structures were also found in fatigued ferritic stainless steel cycled with constant low plastic strain amplitude. Figure 2b shows a micrograph of a grain oriented for single slip in a section close to $(1\bar{2}1)$ plane with three bands of ladder-like structure parallel to the traces of $(\bar{1}01)$ or $(\bar{1}\bar{1}2)$ planes. The matrix is formed by random arrangement of dislocations [9]. Dislocation walls consisting of dipole and multipole configurations are more regular than in case of austenitic steel (Fig. 2a). Screw dislocation segments in the channels are hanging between neighbor dislocation walls.

3.2. Surface relief evolution

Typical shapes of PSMs in 316L steel fatigued to fracture as recorded by AFM are shown in Fig. 3. Since the real shape of PSMs is distorted in the AFM [5] it was necessary to record not only the AFM image of the metallic surface (Fig. 3a) but also the inverted AFM image of the plastic replica taken at the identical location (Fig. 3b). Comparing these two images enough information on the real shape of typical PSMs in fatigued 316L steel can be obtained. The band-like extrusions emanate from the material in a direction of the active Burgers vector and their height fluctuates only moderately. One or two thin parallel intrusions, observed on the image of plastic replica (Fig. 3b), penetrate into the material at the boundary between PSB and the matrix, preferably on the side of the extrusion where the angle between the surface and the slip plane emerging from the crystal is acute.

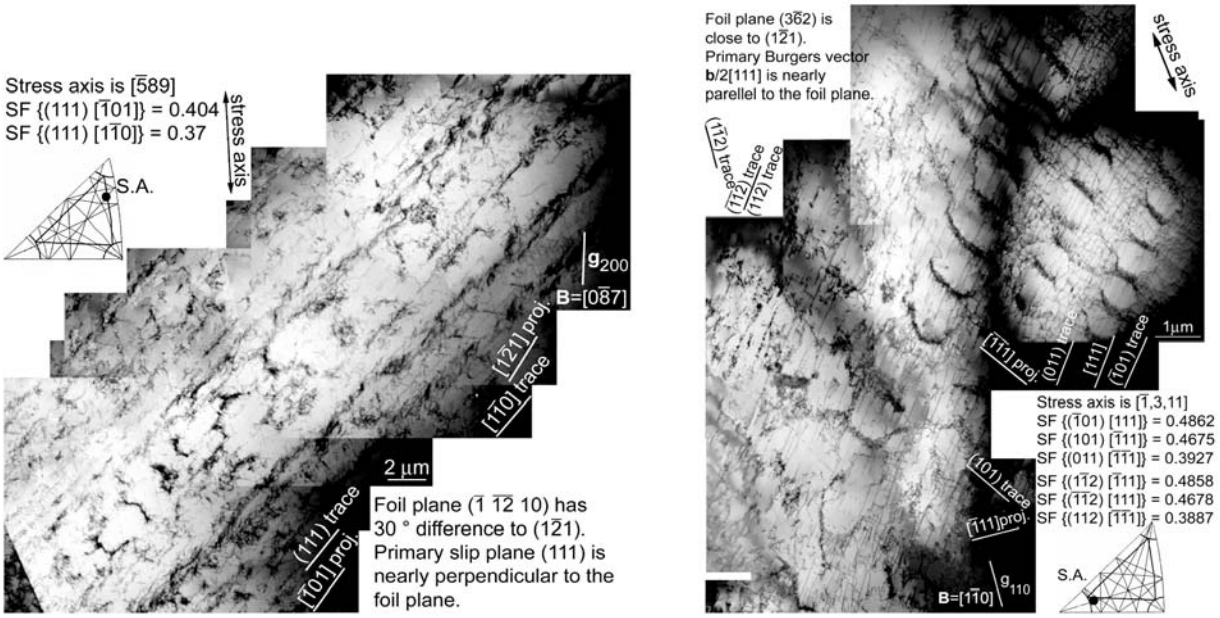

Fig. 2 Ladder-like structures of PSBs and matrix in specimens cycled to fracture (a) austenitic steel, $\epsilon_{ap} = 1 \times 10^{-3}$ (b) ferritic steel, $\epsilon_{ap} = 2 \times 10^{-3}$. (Direction of the stress axis (S.A.) is shown in a basic triangle).

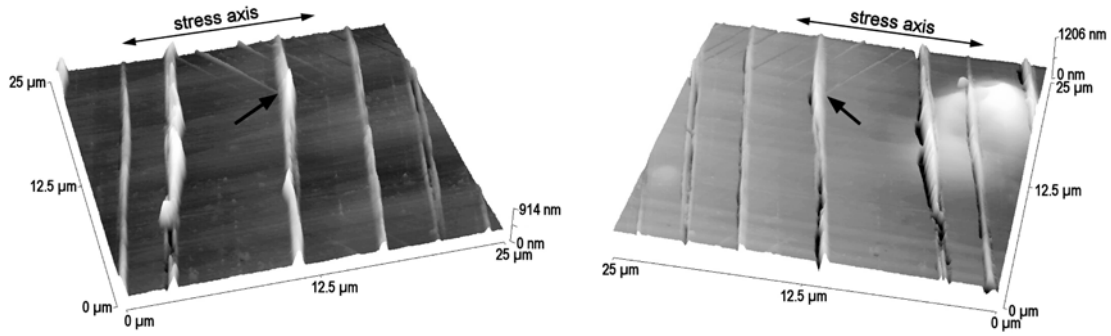

Fig. 3 AFM images of the surface relief of individual PSMs in 316L steel on the metallic specimen (a) and on the plastic replica (b); $\epsilon_{ap} = 2 \times 10^{-3}$, N = 20 000 cycles.

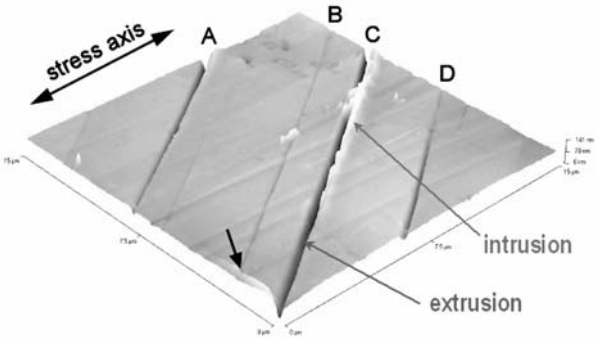

Fig. 4 AFM image of the plastic replica of the austenitic grain after 500 loading cycles with $\epsilon_{ap} = 1 \times 10^{-3}$.

The growth of extrusions and intrusions in constant plastic strain amplitude cycling has been followed quantitatively using AFM. The extrusions start to grow very early in life (0.1% Nf). The initial rate of extrusion growth is high, decreases later and for most of the fatigue life the stabilized value 2.5×10^{-11} m/cycle in cycling with constant plastic strain amplitude 2×10^{-3} is reached [10]. The growth of intrusions can be measured using plastic replica technique. Only early stages of intrusion formation could be documented since intrusions are very thin and deep and plastic replica reproduces their shape only when their depth is less than 0.5 μm, exceptionally up to 1 μm. Figure 4 shows the AFM image of the plastic replica of a grain of 316L steel cycled with plastic strain amplitude $\epsilon_{ap} = 1 \times 10^{-3}$ for 500 cycles (1.1 % N_f). Four PSMs denoted A, B, C, D are present. An intrusion starts growing at one side of an extrusion C while extrusions in all PSMs are already well developed. The first signs of this intrusion were detected at 350 cycles (0.8 % N_f). Figure 5 shows the height of an extrusion and the depth of parallel intrusions accompanying the extrusion early in fatigue life. The plot and also more detailed observations [10] reveal that while the extrusions start very early in fatigue life the intrusions appear and start to grow after some lag (~ 350 cycles in this grain). In most cases the rate of intrusion growth is much higher than that of the extrusion. This could be connected with the fact that intrusions are much thinner than extrusions.

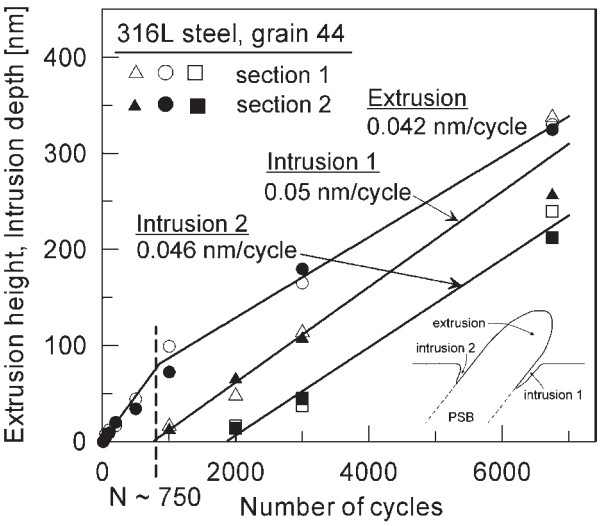

Fig. 5 Simultaneous growth of extrusions and intrusions in the grain 0of austenitic steel at the beginning of cycling with $\epsilon_{ap} = 1 \times 10^{-3}$.

Similar observations on the shape and the growth of extrusions and intrusions were made on ferritic stainless steel. Figure 6 shows the AFM image of one grain of ferritic stainless steel cycled with $\epsilon_{ap} = 2 \times 10^{-3}$ for 9 000 cycles (close to N_f). Figure 6a shows the image of the metallic surface and Fig. 6b the image of the plastic replica. While only extrusions seem to be detected in Fig. 6a, Fig. 6b shows both extrusions and parallel intrusions. The variation of the extrusion height and intrusion depth along PSMs is higher than in austenitic steel. Therefore for the quantitative measurement of extrusion growth in ferritic stainless steel the mean integral height of extrusions was evaluated [11]. Also in ferritic steel the initial growth rate of extrusions is higher and stabilizes later for most of the fatigue life.

4. Discussion

Experimental data on the dislocation structure of PSBs and on the details of the surface relief simultaneously with the knowledge of the dislocation motion and interactions in metallic materials allow us to specify the mechanisms leading to the early formation of

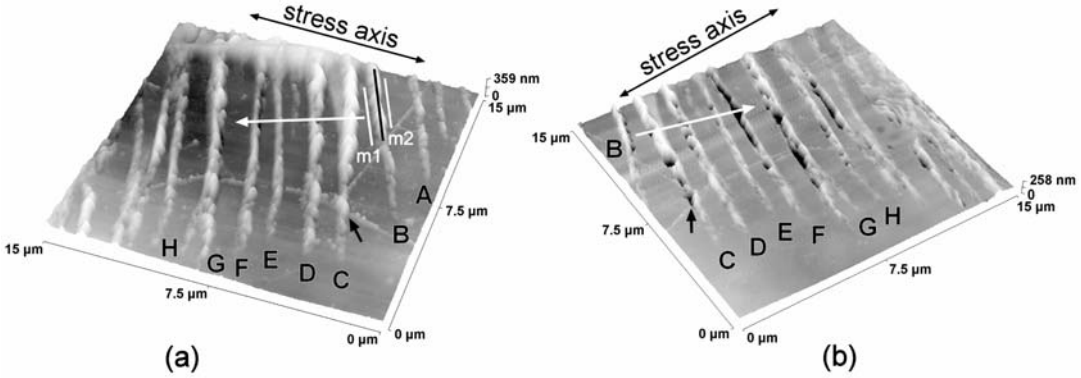

Fig. 6 AFM images showing the surface relief of individual PSMs in a grain of ferritic steel taken on the metallic specimen (a) and on the plastic replica (b); $\epsilon_{ap} = 2 \times 10^{-3}$, $N = 9\,000$.

the surface damage in the form of PSMs. Fig. 7 shows schematically the dislocation arrangement of a PSB. It consists of alternat-

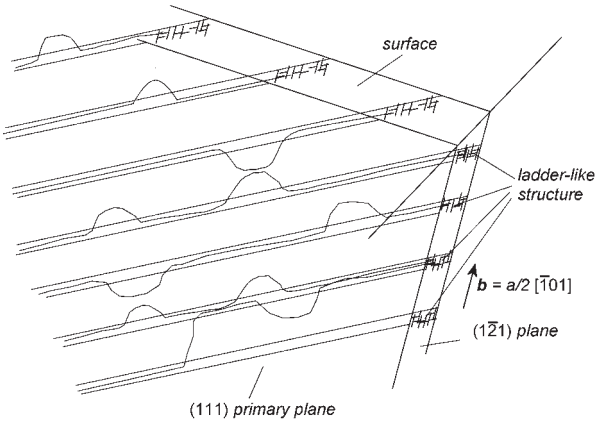

Fig. 7 Schematic picture showing dislocation structure of a PSB.

ing dislocation walls composed from edge dipoles and multipoles alternating with dislocation free channels. Dislocation loops are emitted from the walls and expand in the primary slip plane without obstruction into the neighbor channel. When reaching the opposite wall the edge segment is built in the neighbor wall in the multipole configuration. The screw parts move apart carrying the majority of the local plastic strain until they annihilate by cross slip with a screw dislocation segment on a parallel plane moving in the opposite direction. This deformation mechanism can result only in random relief formation. To account for the extrusion and intrusion formation some redistribution of matter must be considered.

Point defect models of fatigue crack initiation predict the formation of extrusions and/or intrusions. Formation of point defects in cyclic straining has been proved experimentally [12]. Essmann et al. [13] (EGM model) consider the formation of unit dipoles, i.e. rows of vacancies or interstitials by encountering two opposite edge dislocations on a neighbor planes or by the motion of a non-conservative jog on a screw dislocation. Due to lower formation energy vacancy production prevails. Only a static extrusion whose height is proportional to the saturated vacancy concentration was considered in EGM model [13]. Polák's model [14] extends the EGM model by considering the migration of vacancies from the PSB to the matrix. The reversed migration of the atoms from the matrix to the PSB leads to an accumulation of matter in a PSB. The compression stresses are relaxed by plastic straining and result in a steady growth of an extrusion in agreement with experiment. In the areas, where vacancies are annihilated in the matrix, i.e. mostly at the boundary between the matrix and PSB, the matter is missing and intrusions arise and steadily deepen.

The vacancy production rate $p(\epsilon_{ap})$ depends on the local plastic strain amplitude ϵ_{ap}. The net vacancy production rate is reduced by two processes: (i) the sweeping and annihilation of vacancies by moving dislocation loops (ii) the migration of vacancies from the PSB to the matrix i.e.

$$\frac{dc}{dN} = p(\epsilon_{ap}) - (A + M(T))c \qquad (1)$$

where A is the relative annihilation rate of vacancies (fraction of vacancy concentration annihilated in one cycle) mostly due to encounter with moving edge dislocations and $M(T)$ is the vacancy migration rate characterizing the flow of vacancies out of the PSB to the matrix (fraction of vacancy concentration leaving the PSB/matrix boundary). The relative annihilation rate A is independent of temperature but the vacancy migration rate $M(T)$ is strongly temperature dependent and is determined by the vacancy diffusion coefficient and geometrical parameters, e.g. thickness of the PSB.

Vacancy concentration will be obtained by integrating eq. (1)

$$c = \frac{P}{A + M(T)} [1 - \exp(-(A + M(T))N] \qquad (2)$$

Saturated vacancy concentration $c_S = p/(A+M(T))$ in PSB will be achieved for each temperature. The flow of atoms from the matrix to the PSB is equal to the net flow of vacancies from PSB to the matrix in saturation. The steady growth rate of the extrusion height dh/dN is thus

$$\frac{dh}{dN} = l\left(\frac{dc}{dN}\right)_{PSB-matrix} = l\frac{pM(T)}{A + M(T))} \quad (3)$$

where l is the depth of the PSB bellow the surface. The growth rate of the extrusion is proportional to the vacancy production rate and depends on the fraction of vacancies annihilated athermally and by migration to the matrix. Migration rate is proportional to the jump frequency and is given by the term $\exp(-E_M/kT)$ where k is Boltzmann constant and E_M vacancy migration energy. The shape and the depth of intrusions depend on the arrangement of edge dislocations in the matrix.

The production of vacancies in PSB and their migration to the matrix has been modeled in two dimensions using the Monte Carlo method [15]. The growth of extra-vacancy concentration has been obtained. The width of a growing extrusion is the same as the width of a PSB while two thin and deep intrusions are produced at the boundary between the PSB and the matrix. After the initial delay, corresponding to the formation of saturated vacancy concentration, a linear growth of extrusion and two parallel intrusions is observed. Intrusion represents a very sharp notch and irreversible cyclic straining leads to the formation of new surfaces and thus to crack initiation.

6. Conclusions

The analysis of experimental results on the early fatigue damage in polycrystalline f.cc. and b.c.c. steels and the comparison with physically based models lead to the following conclusions:

(i) Localization of the cyclic plastic strain results in the early formation of PSBs.

(ii) PSBs have specific dislocation structure consisting of alternating thin dislocation rich walls and wide dislocation free channels.

(iii) Intensive cyclic plastic straining within the PSB leads to the dislocation interaction and vacancy formation and finally PSMs consisting of an extrusion and parallel intrusions arise on the surface.

(iv) Surface intrusions represent high stress and strain raisers and cyclic plastic strain within PSB is concentrated to the tip of the intrusions and usually one intrusion changes into a crack capable of further growth.

Acknowledgements

The authors acknowledge the support by the grant No. 1QS200410502 of the Academy of Sciences of the Czech Republic.

References

[1] EWING, J. A., W. HUMFREY, J. C.: *Phil. Trans. Roy*. Soc. A200 (1903) 241–250.
[2] POLÁK, J.: *Comprehensive Structural Integrity,* I. Milne, R. O. Ritchie, B. Karihaloo, (Eds.) Vol. 4, Elsevier, 2003, Amsterdam, pp. 1–39.
[3] POLÁK, J., PETRENEC, M., MAN, J.: *Mater. Sci.* Eng. A400-401 (2005) 405–408.
[4] POLÁK, J., OBRTLÍK, K., HÁJEK, M.: *Fatigue Fract.* Eng. Mater. Struct. 17 (1994) 773–782.
[5] POLÁK, J., MAN, J., OBRTLÍK, K., KRUML, T.: *Metallkd.* 94 (2003) 1327–1330.
[6] GERLAND, M., MENDEZ, J., VIOLAN, P., AIT SAADI, B.: *Mater. Sci.* Eng. A118 (1989) 83–95.
[7] OBRTLÍK, K., KRUML, T., POLÁK, J.: *Mater. Sci*. Eng. A187 (1994) 1-9.
[8] KRUML, T., POLÁK, J., OBRTLÍK, K., DEGALLAIX, S. : *Acta Mater. 45* (1997) 5145–5151.
[9] PETRENEC, M., POLÁK, J., OBRTLÍK, K., MAN, J.: *Acta Mater.54* (2006) 3429--3443.
[10] MAN, J., OBRTLÍK, K., POLÁK, J.: *Mater. Sci.* Eng. A351 (2003) 123–132.
[11] MAN, J., PETRENEC, M., OBRTLÍK, K., POLÁK, J.: *Acta Mater. 52* (2004) 5551–5561.
[12] POLÁK, J.: *Mater. Sci.* Eng. 89.(1987) 35–43.
[13] ESSMANN, U., GÖSELE, U., MUGHRABI, H.: *Phil. Mag.* A 44 (1981) 405–426.
[14] POLÁK, J.: *Mater. Sci.* Eng. 92 (1987) 71–80.
[15] POLÁK, J., ZOUHAR, L. to be published.

https://doi.org/10.26552/com.C.2006.4.10-14

kamUNikácie
COMMUNICATIONS

Jiří Kunz – Jan Siegl – Ivan Nedbal *

QUANTITATIVE FRACTOGRAPHY – WELL SPRING OF INTIMATE KNOWLEDGE IN FATIGUE CRACK GROWTH HISTORY

Quantitative fractography of fatigued structure parts can offer very useful and valuable information on the fatigue process. One of main contribution of this experimental method is a detailed description of fatigue crack growth in time and in space. The fractographic reconstitution of fatigue process history is conditioned by the existence and detectability of a fractographic feature characteristics of which is correlated with the fatigue crack growth rate. In the paper presented, three various fractographic features are used for the fractographic reconstitution – striations (in the case of constant amplitude loading), beach marks (for simple program loading) and special inserted fracture marks (for complex program loading). All three methods described are illustrated on case studies, all from the area of testing and development of aircraft structure parts.

1. Introduce

Since long ago, the application of engineering materials has been accompanied by failures of structural parts, tools and other things which are made of them. Prevention of the failures the many of which have been catastrophic is conditioned by the development of effective failure analysis methods. The cost of failure analysis may exceed the value of the fractured part, but the cost of service failures usually far exceeds the cost of failure analysis [1]. For these purposes, fractography is undoubtedly the most effectual experimental method; it provides insights into the fracture process that are not accessible by any other means. Topography of fracture surface created by a growing crack is a result of interaction between material microstructure and service conditions, especially character of loading, temperature, environment etc. [2]. Information on a failure process is encoded in the fracture morphology. Main tasks of fractography is to decode this information, i.e., to find a correlation between identified fracture morphological features and corresponding physical processes which originated these features. Each fractographic features can be characterized by a set of qualitative and/or quantitative parameters. Qualitative parameters give fundamental information dealing with the fracture character (static or fatigue, brittle or ductile, transgranular or intergranular etc.). Quantitative parameters are measurable characteristics of fracture surface, e.g., the area percentage of the particular fractographic feature, its size (e.g., ductile dimple diameter, striation spacing, and cleavage facet size), local crack growth direction etc. A typical feature of current fractography is an effort to increase the mass of quantitative data supplying better and deeper understanding of the fracture processes and an integration of the experimental results with the theoretical knowledge of fracture mechanics.

Primary cause of a major part of all fractures in practice is material fatigue. One of the main contributions of quantitative fractography is the reconstitution of fatigue process history, i.e., setting of dependence of crack length (or other variable expressing the failure extent) on the number of cycles (or on the other time related variable, e.g., service time, number of flights, etc.). The reconstitution is conditioned by the existence and detectability of a fractographic feature, some quantitative characteristic of which is corre- lated with the fatigue crack growth rate.

2. Reconstitution of fatigue crack growth based on striation spacing measurements

The most suitable fractographic features for a detailed description of fatigue crack growth are striations. If it is possible to distinguish individual striations and to measure their spacing, then the reconstitution of the fatigue process can be done very thoroughly, even cycle by cycle. The methods of this fractographic reconstitution developed at our department are described in detail in [3–5]. Results of the microfractographic measuring by means of a scanning electron microscope are usually presented in the form of dependence of the striation spacing (denoted s) on the crack length (denoted a), i.e., $s = s(a)$. Next processing of the experimental data set (s_i, a_i), $i = 1, 2, ..., k$, consists of two steps:

a) Transformation from a micro volume into a macro volume, i.e., conversion of the striation spacing (giving the information about the fatigue crack growth rate in the micro volume) into the macroscopic crack growth rate which is crucial quantity for the evaluation of fatigue life and loading capacity of the fatigued body.
b) Transformation of the dependence on the space coordinate (i.e., on the crack length a) into the functionality on a time-dependent variables expressing the service time (e.g., number of loading cycles N).

The decisive problem of the first step is the relation between striation spacing s and the macroscopic crack growth rate $v = da/dN$ [5]. These two variables are not generally identical; the equality

* **Jiří Kunz, Jan Siegl, Ivan Nedbal**
Department of Materials, Faculty of Nuclear Sciences and Physical Engineering, Czech Technical University in Prague, Trojanova 13, 120 00 Prague 2, Czech Republic, E-mail: jiri.kunz@fjfi.cvut.cz

$v = s$ is valid only under special conditions depending namely on the stress and strain field around the crack tip, temperature etc. The ratio $D = v/s$ is a function of the stress intensity factor range ΔK and it can vary within several orders (approximately, $10^{-3} < < D < 10^{1}$); it is influenced by the following phenomena:

1) discontinuous propagation of a fatigue crack front both in time and space, or in other words, existence of the so called "idle cycles",
2) deviation of local directions of a fatigue crack growth from a macroscopic one,
3) synergy of striation formation micromechanism with other ones, e.g., ductile dimple fracture, inter crystalline decohesion, quasi cleavage, etc.

The relation between striation spacing and the macroscopic crack growth rate D must be a priori known or experimentally determined. For practical application of the suggested reconstitution technique, preferably the form $D = D(s)$ (i.e., D-factor as a function of striation spacing s) making possible to use a simple fundamental equation

$$N_x = \int_{a_i}^{a_x} \frac{da}{D(s) \cdot s(a)} + N_i \,, \qquad (1)$$

where the number of cycles N_x corresponds to the given crack length a_x, and (N_i, a_i) is a priori known or determined couple of corresponding data, e.g., the total elapsed number of cycles, and crack length corresponding to the boundary between fatigue and final fracture.

An application of the method mentioned will be illustrated on the following case study: During the full-scale fatigue test, a model specimen of a wing spar of a small transport airplane was loaded by cyclic four-point bending with a constant amplitude [7]. The thin web plate was riveted to the L-profile flange plates. All the main structural components were made of AlCu4Mg1 alloy type 2124. The fatigue test was finished after $N = 117\,500$ applied loading cycles.

The fatigue cracks under study initiated in the hole of rivets connecting the spar web and the lower flange plate. The critical area is presented in Fig.1. During the full-scale test, the crack propagating upwards in the spar web was optically monitored. In the first period of the test, when the flange plate covered the crack (see Fig.1), direct observation was impossible. This reason results in the fact that optical information on the crack growth in the web was available only in the last 42% of the test duration.

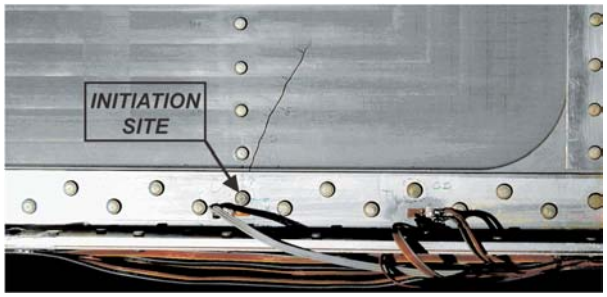

Fig. 1. Detail of critical area of wing spar – the studied fatigue crack in the spar web initiated on the rivet hole. The first period is covered by the lower flange plate.

After the residual strength test and dismantling the tested wing spar, fracture surfaces were observed by means of a binocular light and scanning electron microscope. The limited set of macroscopic data on the fatigue crack propagation was completed by fractographic results [8]. Initiation of the fatigue crack in the rivet hole was of a multiple character. Regardless of the crack length, striations were a typical microfractographic feature. Striation spacing s was measured and presented as a function of the crack length a, where a is the distance of micro-area under study and rivet hole axis.

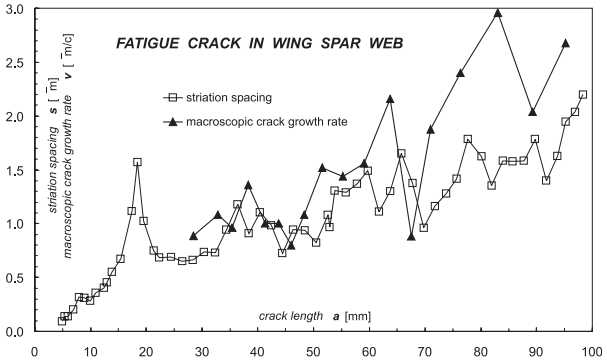

Fig. 2. Striation spacing and macroscopic crack growth rate vs. crack length.

In Fig. 2, the microfractographic data $s = s(a)$ are compared with macroscopic crack growth rates $v = v(a)$ corresponding to the results of the direct optical monitoring. This comparison is in accordance with general experience [5] – in the range of the middle crack length, equation $v = s$ may be approximately acceptable, while for longer cracks, inequality $v > s$ is obvious.

Microfractographic data set (s_i, a_i), $i = 1, 2, ..., k$, was used for the reconstitution of the fatigue crack growth process history. Precision and exactness of the reconstitution results strongly depend on the volume and quality of input information. The fractographic reconstitution of the fatigue crack growth in the spar web was based on the knowledge of the empirical relation $D = D(s)$

$$D(s) = 1.797 \cdot 10^{45} \frac{s^{0.1108}}{(79.55 - s)^{23.84}}$$

$$\text{for } (0.09 \le s \le 4.74)\ \mu\text{m}, \qquad (2)$$

determined by our previous laboratory experiments of similar Al-alloy [5]. The results obtained are in a very good agreement with the macroscopic data – see Fig. 3.

For comparison, the results of the fractographic reconstitution based on a widely used but usually not verified assumption $v = s$, i.e. $D = 1$, are presented in the same graph; in this case, the agree-

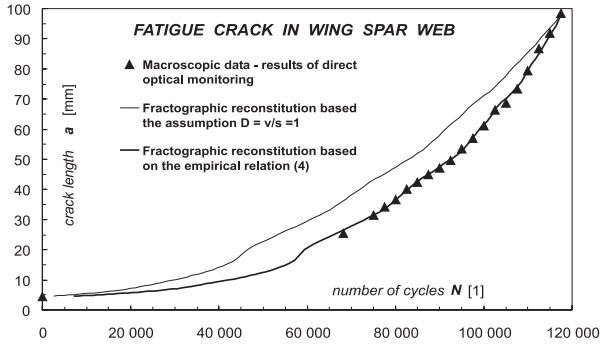

Fig. 3. Comparison of fractographic reconstitution of fatigue crack growth curve with macroscopic data.

ment of the reconstitution results with the macroscopic data is very poor (Fig. 3). In the both cases of fractographic reconstitution, the couple of data $N_f = 117\,500$ and $a_f = 98.5$ mm corresponding to the fatigue test termination, was used as the "initial condition" in the relation (1). Growth of the fatigue crack under study in the area inaccessible to a routine visual monitoring was also obtained by means of this fractographic reconstitution.

3. Fractographic Reconstitution of Fatigue Crack Growth under Simple Program Spectrum Loading

In the case of program loading spectrum, e.g., flight simulation loading, the reconstitution of a fatigue crack growth is based on a fractographic identification of morphological features created by specific inherent part of the spectrum (e.g., gust cycle, the most severe flight etc.). Spacing between two neighboring beach marks is equal to a crack length increment during the corresponding loading block. If the beach marks are readable and their spacing is measurable, neither marking nor special modification of original loading spectrum is needful. In this case, there is no trouble with the relation between a microscopic and macroscopic crack growth rate. The application of this method for fractographic reconstitution of a fatigue crack growth in aircraft structure parts is presented, e.g., in [9, 10].

In addition to the crack growth rate, observation of beach marks has been giving information on the crack front shape and its changes in time and space. On this base, two dimensional description of fatigue degradation of a body cross section is possible.

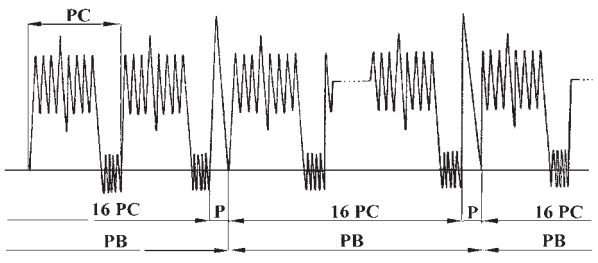

Fig. 4. Loading program used in full-scale test of L 410 UVP aircraft wing.

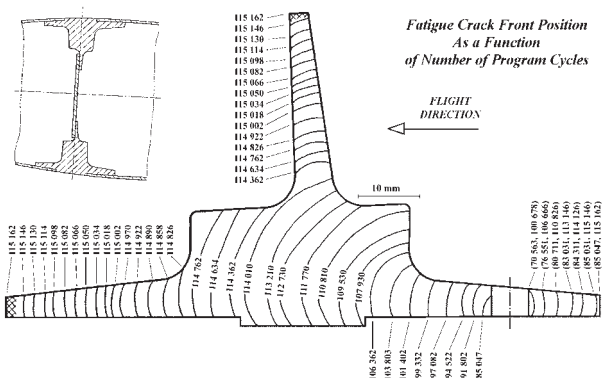

Fig. 5. Fractographic reconstitution of fatigue process in wing beam (loading program PB = 16 PC + P - see Fig. 4).

As an example, in the full-scale test of transport aircraft wing, the loading program block (PB) consists of 16 program cycles (PC) simulating 16 flights and one severe cycle (P) simulating the gust 6.8 m/s, was applied – see Fig.4 [11],[12]. The program block consists of 193 various cycles. Periodically repeated gust cycles resulted in microscopically detectable beach marks on fracture surfaces of the fatigued wing parts. The distance between two neighboring beach marks represents the fatigue crack increment during the one PB. The beach mark spacing s_p as a function of fatigue crack length a was obtained by means of the quantitative fractographic analysis. On the base of the $s_p = s_p(a)$ relation, position and shape of the fatigue crack front in time (i.e., as a function of the overall applied number of program cycles) was determined – e.g., see Fig. 5.

4. Fractographic Reconstitution of Fatigue Crack Growth Based on Fracture Marking by Special Cycles Inserted into the Complex Program Loading Spectrum

In the case of real structures tested under the complex loading spectrum (i.e., flight by flight, random etc.), a sophisticated method of fatigue fracture marking has to be applied. As an example, a full-scale fatigue test of the main beam of fighter body will be given [13]. Service conditions were simulated by means of a flight-by-flight loading spectrum. The applied complex loading spectrum consists of many cycles with a very different amplitude. This fact disables fractographic reconstitution of the fatigue crack process based on the striation spacing measurements. Therefore, special coded marking loading blocks were applied in the test. One marking set consists of 12 different marks symbols of which are given in the table in Fig. 6.

The symbols used are similar to Morse code: the "dot" consists of 100 constant amplitude cycles, the "dash" consists of the same 800 cycles. Individual "dots" and "dashes" were separated by

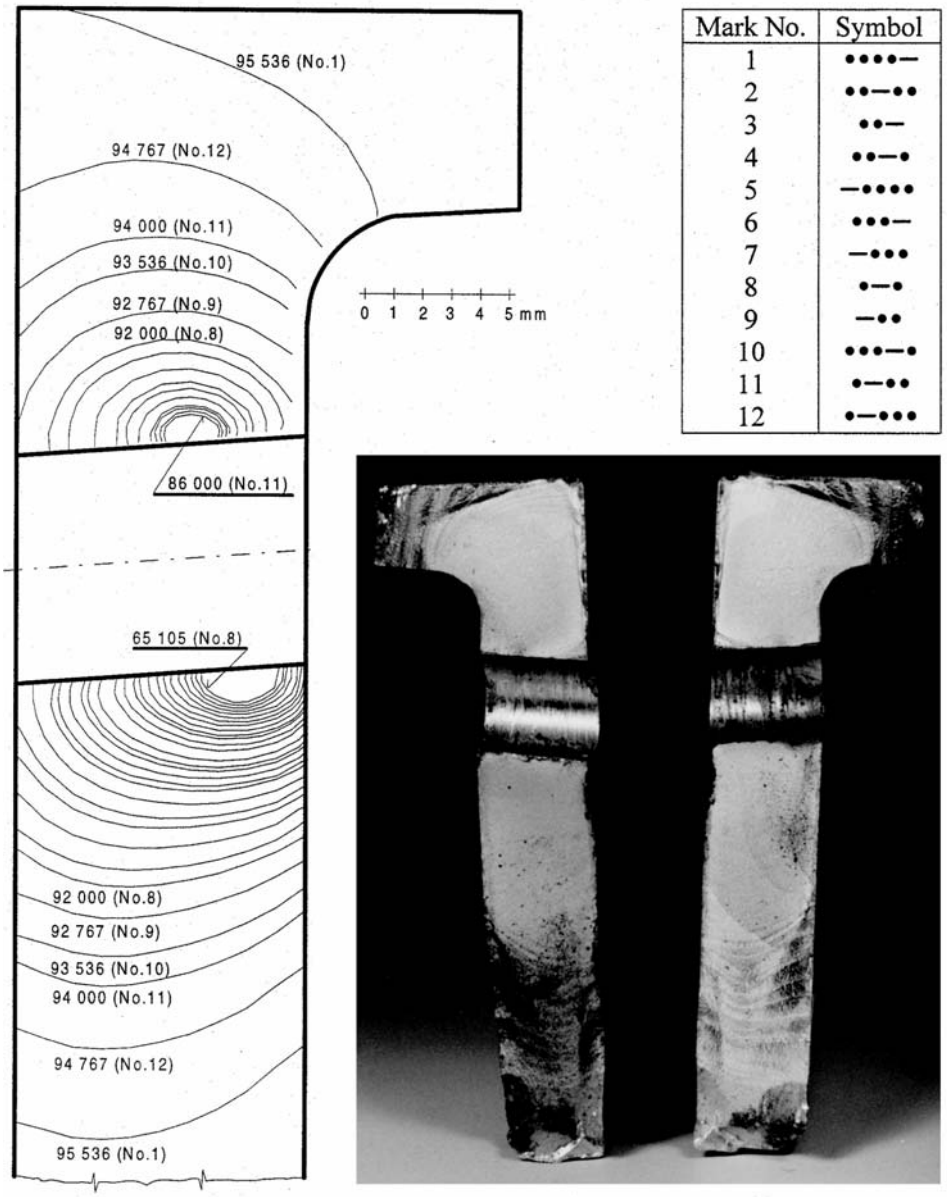

Fig. 6. Fractographic reconstitution of fatigue crack growth in a main beam based on the coded fracture marking introduced during the full-scale test of the fighter body. Results are presented as a function of SFH number.

a special cycle with a higher stress amplitude. In one marking set there is no problem with identifying individual marks; therefore, each mark differs from each other and thus it is unequivocal. Even in the case of difficulty with direct identification of some mark, there is a possibility to use a second level of information, i.e., to define it more precisely by means of identification of the neighbouring (i.e., the last before and next after) marks because the sequence of the individual marks is constant and known. The same marking set is repeatedly applied during the full-scale fatigue test.

The results of fractographic analysis of the main beam fracture are summarized in Fig. 6, where a two-dimensional description of fatigue process as a function of simulated flying hours (SFH) is presented. Both fatigue cracks under study initiated on the screw hole. The detailed fractographic analysis revealed the shape and position of the fatigue crack fronts corresponding to individual marks applied during the full-scale test in the time interval between 65 105 and 95 536 SFH. Examples of fractographic mark No. 1 on the fracture surface are presented in microfractograph in Fig. 7.

5. Conclusions

Methods of fractographic reconstitution of a fatigue crack growth are very useful especially in the failure analysis of struc-

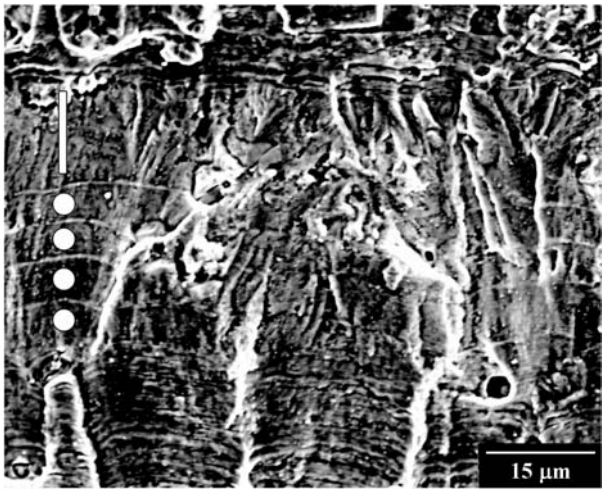

Fig. 7. Microfractograph of mark No.1 on the fighter main beam fracture.

tural components fatigued during the full scale tests or service. Methods of fractographic reconstitution are illustrated on three case studies focused on the area of aircraft structure testing and developments. In the first case, a model specimen of the aircraft wing spar was loaded at a constant stress amplitude and fractographic reconstitution was based on the striation spacing measurements. In the second one, during a full-scale test of the transport aircraft wing, the simple program block consists of 16 program cycles simulating 16 flights and one severe cycle simulating the gust was applied. Periodically repeated gust cycles resulted in beach marks on the fracture surfaces; fractographic reconstitution was based on the measuring of a beach mark spacing. In the third case study, the main beam of the fighter fuselage was tested under a complex (flight by flight) loading spectrum. In this fatigue test, special coded marking loading blocks were applied and fractographic reconstitution was based on the identification of corresponding marks on the fracture surface.

The results obtained represent a very reliable output to describe the fatigue process in time and/or in space, i.e., the invaluable information often unattainable by any other means.

This research has been supported by project MSM6840770021 "Diagnostic of Materials".

References

[1] PARRINGTON, R. J.: *Fractography of Metals and Plastics.* Practical Failure Analysis, 2, 2002, No.5, pp. 16–46.
[2] HULL, D.: *Fractography. Observing, Measuring and Interpreting Fracture Surface Topography.* Cambridge University Press 1999, 366 p.
[3] NEDBAL, I., SIEGL, J., KUNZ, J.: *Fractographic Study of Fatigue Crack Kinetics in Bodies and Structures.* In: Advances in Fracture Research 84 (Proc. ICF 6, New Delhi). Eds. S.R. Valluri et al. Vol. III. Oxford, Pergamon Press 1984, pp. 2033–2040.
[4] NEDBAL, I., KUNZ, J., SIEGL, J.: *Quantitative Fractography – Possibilities and Applications in Aircraft Research.* In: Basic Mechanisms in Fatigue of Materials (Proc. Int. Colloq., Brno). Materials Science Monographs, 46. Eds. P. Lukáš, and J. Polák. Amsterdam, Elsevier 1988, pp. 393–403.
[5] NEDBAL, I., SIEGL, J., KUNZ, J.: *Relation between Striation Spacing and Fatigue Crack Growth Rate in Al-Alloy Sheets.* In: Advances in Fracture Research (Proc. ICF 7, Houston). Eds. K. Salama et al. Vol.5. Oxford, Pergamon Press 1989, pp.3483–3491.
[6] NEDBAL, I., KUNZ, J., SIEGL, J.: *Microfractographic Aspects of Fatigue Crack Growth in 7010 Aluminium Alloy.* In: Fractography '97 (Proc. Int. Conf., Stará Lesná). Ed. L. Parilák. Košice, IMR SAS 1997, pp. 264–270.
[7] AUGUSTIN, P., PÍŠTĚK, A.: *Experimental Data Determination for the Damage Tolerance Analysis of the Wing Spar with Cracked Web.* In: Proc. EAN 2000 (38th Int. Conf. Experimental Stress Analysis, Třešť), 2000, pp. 9–14.
[8] KUNZ, J., SIEGL, J., NEDBAL, I., AUGUSTIN, P., PÍŠTĚK, A.: *Application of Quantitative Microfractography in Damage-Tolerance and Fatigue Evaluation of Wing Spar.* In: Proc. 24th International Congress of the Aeronautical Sciences (ICAS 2004, Yokohama). Ed. I. Grant. Edinburgh, Optimage Ltd., 2004, 10 p., CD-Rom.
[9] SIEGL, J., SCHIJVE, J., PADMADINATA, U. H.: *Comparison of Fractographic Observation Results and Predictions for MiniTWIST Flight Simulation Loading.* Int. J. Fatigue, 13, 1991, No.2, pp. 139–147.
[10] KUNZ, J., NEDBAL, I., SIEGL, J.: *Application of Fractography in Full-Scale Tests of Aircraft Structure Parts.* In: Fracture Behaviour and Design of Materials and Structures (Proc. ECF 8, Torino). Ed. D. Firrao. Vol. III. Cradley Heath, EMAS 1990, pp. 1662–1669.
[11] HRKAL, K., RŮŽIČKA, M.: *Life test of wing of aeroplane L 410 UVP – II. (in Czech),* [Technical report VZLÚ Z-2694/82.] Praha, VZLÚ 1982, 237 p.
[12] HRKAL, K., RŮŽIČKA, M.: *Life test of wing of aeroplane L 410 UVP – II. Annex 1. (in Czech)* [Technical report VZLÚ Z-2694/82.] Praha, VZLÚ 1983, 78 s.
[13] NEDBAL, I., KUNZ, J., SIEGL, J.: *Some Remarks on Fatigue Fracture Marking.* In: Fatigue '99 (Beijing). Vol. 4/4. Eds. X.R. Wu, and Z.G. Wang. Beijing - Cradley Heath, HEP - EMAS 1999, pp. 2373–2378.

https://doi.org/10.26552/com.C.2006.4.15-20

Zuzanka Trojanová – Pavel Lukáč *

THERMAL AND MECHANICAL FATIGUE IN A QE22 MAGNESIUM ALLOY REINFORCED WITH SHORT SAFFIL FIBRES

Using non-destructive methods changes in the microstructure of QE22 metal matrix composites (MMC) due to thermal and mechanical cycling have been investigated. Thermal stresses induced in composites due to a considerable difference between thermal expansion coefficients of the matrix and ceramic reinforcement may create new dislocations on cooling from elevated to ambient temperature. Thermal stresses can achieve the yield stress of the matrix and micro-glide of newly created dislocations as well as their annihilation can occur. Thermodynamic processes in the matrix influence these effects.

Keywords: Metal matrix composites, Squeeze casting, Dislocations, Internal friction, Acoustic properties, Thermal properties

1. Introduction

Commercial magnesium alloy QE22 was derived from Mg-RE-Zr alloys by the addition of silver, which improves mechanical properties of the alloy. Good creep resistance is attributed to both the strengthening effect of precipitates and the presence of the grain boundary phases that reduce the grain boundary sliding. Ageing causes precipitation within the grains. The precipitation process depends on silver content [1]. If the silver content is less than 2 wt.%, the precipitation process appears to be similar to that occurring in Mg-RE alloys, i.e. it starts with the GP zones (Mg-Nd, coherent) and finishes with $Mg_{12}Nd$ incoherent precipitates. For higher amounts of silver two independent precipitation processes have been reported; both started with Mg-Nd GP zones, rod-like or ellipsoidal, and leading ultimately to the formation of an equilibrium phase of probable composition $Mg_{12}Nd_2Ag$ [2]. A considerable improvement of the mechanical properties as well as the thermal stability of the alloy can be achieved by the reinforcement by ceramic fibres. Magnesium matrix composites possess good wear resistance, enhanced strength, good damping capacity and creep resistance and they keep low density and good machinability [3–5]. Benefits of the fibre reinforcement can be powered by precipitation hardening. Enhanced mechanical properties of commercial Mg-Ag-Nd-Zr alloy reinforced by short Saffil fibres have been reported elsewhere [3,6]. A difference between thermal expansion coefficients (CTEs) of the matrix and the reinforcement is a very important factor in composites with a metallic matrix. The coefficient of thermal expansion of a ceramic reinforcement is lower than that of most metallic matrices. This means that when a composite is subjected to temperature changes, thermal stresses arise at the interfaces between the matrix and the reinforcements. Thermal stresses resulting from a thermal mismatch can generally be expressed in the following form

$$\sigma_{TS} = f(C,r_i)\,\Delta\alpha\,\Delta T, \qquad (1)$$

where $f(C,r_i)$ is a function of the elastic constants, C, and geometrical parameters r_i, $\Delta\alpha$ is the difference in value of the thermal expansion coefficient of the two components and ΔT is the temperature change. The thermal stresses may relax and new dislocations are generated in the matrix. Therefore, there is a higher dislocation density in the matrix, especially near the interfaces. This high matrix dislocation density as well as the reinforcement/matrix interfaces can provide a high diffusivity path in metal matrix composites (MMC). The higher dislocation density would also affect precipitation kinetics in a precipitation hardenable matrix.

The aim of the present paper is to investigate QE22 magnesium alloy reinforced with δ-Al_2O_3 (Saffil) submitted to thermal and mechanical loading and to determine possible physical and thermodynamic processes occurring in the matrix. Non-destructive methods are used in this study.

2. Experimental procedures

2.1 Material

Composites were prepared by squeeze casting. Commercial QE22 alloy (nominal composition 2.5 wt.% Ag, 2 wt.% Nd rich Rare Earth, 0.6 wt.% Zr, balance Mg) was used as the matrix material. The alloy was reinforced with δ-Al_2O_3 short fibres (Saffil®) with a mean diameter of 3 μm and a mean length about 87 μm (measured after squeeze casting). The preforms consisting of the Al_2O_3 short fibres showing a planar isotropic fibre distribution and a binder system (containing Al_2O_3 and starch) were preheated to a temperature of 1000 °C that is higher than the temperature of the melt alloy and then inserted into a preheated die. The two-stage application of the pressure resulted in MMCs with a fibre volume fraction of 17.5 vol. %. The pressure required to force the melt into the die with the preform was 50 MPa for 30 s in the first step and 130 MPa for 90 s in the second step. The second step closes pores and

* **Zuzanka Trojanová, Pavel Lukáč**
Department of Metal Physics, Faculty of Mathematics and Physics, Charles University, Ke Karlovu 5, 12116 Praha 2, Czech Republic.
Tel.: +420 221911366; Fax +420 221911490; E-mail: ztrojan@met.mff.cuni.cz

shrinkage cavities. The short time of contact between the liquid alloy and the fibres leads to only slight reactions between the fibres and the matrix.

2.2 Damping measurements

Damping measurements were carried out on bending beams (80 mm long with thickness of 3 mm) in vacuum (about 30 Pa) at ambient temperature. The damping was obtained by the measurement of the logarithmic decrement of free decaying bending beam vibrations in an apparatus described elsewhere [7]. The bending beams fixed at one end and a permanent magnet attached at the free end dipping into a coil system were contactlessly excited to mechanical resonance of their fundamental vibration (clamped-free-bar with end loading) by an alternating magnetic field. This was realised by a closed feedback loop consisting of an excitation coil, an induction coil and a power AC amplifier. The free decaying vibration was determined via the effective alternating voltage induced by the moving permanent magnet into the induction coil. After reaching a certain (required) amplitude, the coil current was switched off by a PC and the declining mechanical vibration was stored in the PC via an ADC measuring the voltage induced by the moving permanent magnet [7,8]. Using these data, the logarithmic decrement δ of the free vibration was determined by the PC according to exponential law

$$A(t) = A_0 \exp(-\delta\, t/\tau)\,. \qquad (2)$$

In Eq.(2), A_0 is the required amplitude, t is time and τ is the period of vibrations.

2.3 Cycling of samples

Fatigue was realised by the controlled bending loading of the bending beam samples in the same apparatus as used for the damping measurements controlling the amplitude and number of vibrations. The samples were cycled for a certain time at a predefined amplitude. From the time and resonant frequency, the number of cycles was calculated. Immediately after cycling, the strain amplitude dependence of the decrement was measured. The resonant frequency of the system ranged from 71 to 73 Hz. The sample was cycled up to fracture, which was reached at $N = 2.19 \times 10^8$ cycles.

3 Experimental results and discussion

3.1 Thermal cycling

For many metallic materials, the strain dependence of the damping capacity can be divided into a strain independent and a strain dependent component. In the case of the logarithmic decrement, this experimental finding can be written as:

$$\delta = \delta_0 + \delta_H(\epsilon). \qquad (3)$$

δ_0 is the amplitude independent component, found at low amplitudes. The component δ_H depends on the strain amplitude ϵ and is usually caused by dislocation vibration in the material.

Figure 1a shows the plots of the logarithmic decrement against the logarithm of the strain amplitude for QE22+17.5vol.% Saffil composite before and after thermal cycling between the room temperature and increasing upper temperature up to 320 °C. Figure 1b shows the plots obtained at higher upper temperatures (320, 360 and 400 °C). From Figs. 1a and 1b, it can be seen that the strain dependences of the logarithmic decrement exhibit two regions in good accord with Eq. (3). The values of δ_H in the strain amplitude dependent region increase very strongly with increasing upper temperature of the cycle up to 360 °C and then, above 360 °C, the values of δ_H (at given strain amplitudes) decrease with the upper temperature. The critical strain ϵ_{cr} at which the logarithmic decrement becomes amplitude dependent may be used to calculate the effective critical stress amplitude corresponding to the micro-yield stress according to the equation

$$\sigma_c = E\,\epsilon_{\mathrm{cr}} \qquad (4)$$

where E is Young's modulus.

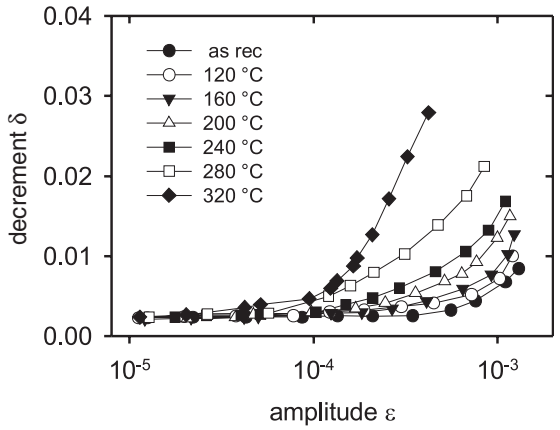

Fig. 1 (a) Amplitude dependence of decrement for QE22+17.5 vol.% Saffil obtained after thermal cycling between room temperature and various upper temperatures (up to 320 °C).

The experimental data indicate microstructure changes in specimens. An increase of internal stresses due to the difference in CTE is very probably responsible for these changes. The internal stresses produced by thermal loading of composites can be reduced by various relaxation mechanisms: creation of new dislocations and their glide, by decohesion or sliding of the matrix/reinforcement interface, by diffusion of solute atoms in the matrix. It is expected that the dislocation density near the reinforcements is significantly higher than that elsewhere inside of the matrix. The dislocations formed during cooling from an elevated temperature to a certain lower temperature can glide inducing plastic deformation in the matrix. An increase in the dislocation density near reinforcement fibres has been calculated as [9, 10]

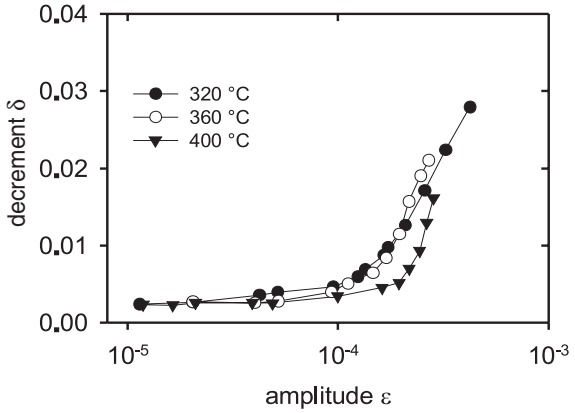

Fig. 1 (b) Amplitude dependence of decrement for QE22+17.5 vol.% Saffil obtained after thermal cycling between room temperatures and upper temperatures 320, 360 and 400 °C.

$$\Delta\rho = \frac{Bf\Delta\alpha\Delta T}{b(1-f)}\frac{1}{d}, \tag{5}$$

where f is the volume fraction of the reinforcing phase, d is its minimum size, b is the magnitude of the Burgers vector of dislocations and B is a geometrical constant. From Eq. (5) it follows that the dislocation density increases as the temperature difference increases. The residual thermal stresses are developed within the matrix during cooling. As QE22 matrix becomes softer with temperature, the internal thermal stresses in the matrix can exceed the matrix yield stress. Then, new dislocations are formed, they can glide and the matrix deforms. Highly strained zones, plastic zones, are formed. The zones with higher dislocation density are adjacent to reinforcements.

The strain amplitude dependence of the logarithmic decrement suggests dislocation unpinning processes. The differences in the damping behaviour of specimens thermally cycled to various upper temperatures can be attributed to the interaction between dislocations and point defects (solute atoms) including small clusters of foreign atoms and to changes in the dislocation density.

The strong strain dependence of the logarithmic decrement for QE22/Al_2O_3 composite specimens shown in Fig. 1 may be explained using the Granato-Luecke theory of the dislocation damping. In the Granato-Luecke theory [11, 12] the dislocation structure is assumed to consist of segments of L_N length along which weak pinning points are randomly distributed. The mean distance between two weak pinning points is ℓ, with $\ell \ll L_N$. The ends of the longer segments L_N are assumed to be unbreakable (strong) pinning points. The mean total density of dislocations is ρ. The periodic stress $\sigma = \sigma_0 \sin\omega t$ is applied. At $T = 0$, the dislocation loop is able to breakaway from the weak pinning points only at a sufficiently high stress. The stress necessary for breakaway of dislocations is determined by the largest double loop in a segment and it is strongly dependent on the statistic distribution of the pinning points. With increasing temperature (for $T > 0$ K), the stress is decreased because the breakaway process is thermally activated [13]. At higher temperatures the breakaway can occur at lower stresses than possible for double loop. However, higher activation energies are required because the breakaway is simultaneous from several neighbouring weak pinning points. At higher temperatures and low frequencies approximation, the stress dependence of the logarithmic decrement component δ_H can be expressed as [13]

$$\delta_H = \frac{\rho L_N^2}{6}\frac{v}{\omega}\left(\frac{3\pi kT}{2U_0}\right)^{1/2}\left(\frac{\ell^3\sigma_0^2}{U_0 G}\right)^{1/2} \exp\left[-\frac{4}{3}\frac{U_0}{kT}\left(\frac{U_0 G}{\ell^3}\right)^{1/2}\frac{1}{\sigma_0}\right] \tag{6}$$

where G is the shear modulus, σ_0 is the amplitude of the applied stress and ω is its frequency, v is the dislocation frequency, U_0 is the activation energy, k is the Boltzmann constant. With increasing upper temperature of the thermal cycle the decrement component δ_H increases, too. The observed behaviour may be explained if we consider that (a) during cooling and also during thermal cycling, new dislocations are created due to the difference in the CTE and/or (b) new pinning points on existing dislocations may be formed by thermodynamic processes in the matrix that can modify the number of free foreign atoms or their small clusters. Kiehn et al. [14] investigated the microstructure of QE22 with 26 vol.% Saffil fibres after the annealing step by step at increasing temperature using transmission electron microscopy. They observed incoherent matrix particles containing Zr, Nd and Al. During annealing step by step, the population of particles at the fibres did not change, but new (Al_xMg_{1-x})Nd cubic particles precipitate between 120 and 180 °C appeared. Above 180 °C, the hexagonal β-phase and/or tetragonal $Mg_{12}Nd$ substitute the former cubic phase. Between 240 and 300°C the β-phase transforms into semicoherent tetragonal $Mg_{12}Nd$, too. Kiehn et al. [14] have estimated that ceramic fibres and the reaction products of the inorganic binder (containing Al_2O_3) in the preform enhanced the Al concentration due to decomposition in the QE22 matrix. Contrary to the unreinforced alloy, Ag remains dissolved in the matrix of the composite and does not take part in the precipitation process. The main weak pinning points seem to be the solute atoms or their small clusters.

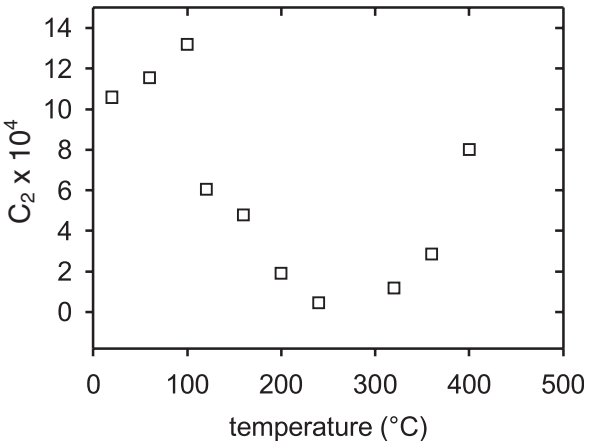

Fig. 2 Dependence of the C_2 parameter on upper temperature of thermal cycle.

The obtained experimental data may be analysed using Eq. (6) in the form $\delta = \delta_0 + C_1\epsilon\exp(-C_2/\epsilon)$. The values of C_2 parameter are plotted against the temperature of thermal treatment in Fig. 2. The C_2 parameter is proportional $C_2 \propto \ell^{-2/3}$ and, hence, the experimental results indicate that the mean distance between the weak pinning point increases with increasing temperature. This is reasonable because the dislocation density increases and the number of solute atoms (cluster) forming weak pinning points is constant. The C_2 parameter is practically constant at temperatures between 200 and 300 °C and then it slightly increases. This temperature variation of C_2 may be explained if the observations of Kiehn et al. [14] are taken into account. The plot of the C_1 parameter against the thermal treatment temperature is given in Fig. 3.

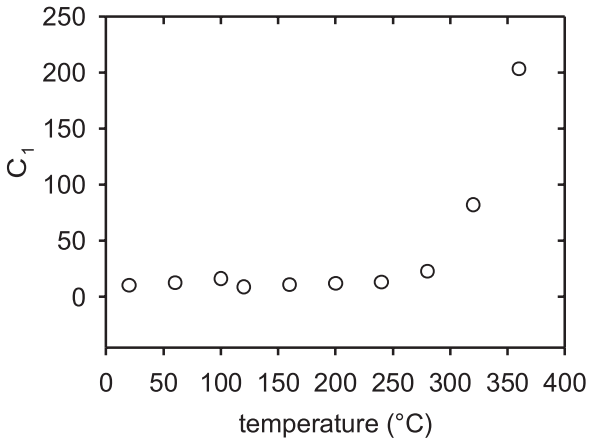

Fig. 3 Dependence of the C_1 parameter on upper temperature of thermal cycle.

The stress that is necessary for a thermal breakaway of dislocation loops σ_T at a certain temperature is given by [13]

$$\sigma_T = \sigma_M\left[1 - \left(\frac{kT}{U_1}\ln A\right)\right], \tag{6}$$

with

$$A = \frac{2}{3}\frac{\upsilon}{\omega}\frac{\sigma_M}{\sigma_0}\left(\frac{kT}{U_1}\right)^{\frac{3}{2}} \tag{8}$$

σ_M is assumed to be the breakaway stress in the pure mechanical process. For a double loop with the loop length ℓ_1 and ℓ_2, the breakaway occurs under the stress

$$\sigma_M = \frac{2F_m}{b(\ell_1 + \ell_2)}. \tag{9}$$

Here F_m is the maximum binding force between a dislocation and a pinning point. $U_1 = 4/3(F_m^3/\Phi)^{1/2}$, where Φ is a constant. All experiments were performed at ambient temperature; it is reasonable to consider that the influence of the thermal activation is, in the first approximation, the same. After thermal treatment, shorter dislocation segments (the mean distance between weak pinning points) become longer because of the enhanced dislocation density due to temperature cycling and due to the lower number of solute atoms. Then, the critical strain according to Eqs. (4) and (9) that is indirect proportional to ℓ should decrease with increasing upper temperature of the cycle. It is observed experimentally (Fig. 1); the critical strain ϵ_{cr} decreases with increasing upper temperature of the cycle. This tendency is stopped at a temperature of 360 °C where the decrement component δ_H decreases. The critical strain becomes higher, which corresponds to the shorter dislocation loops. Thermal stresses produced near the matrix/ceramic fibre interfaces are accommodated by the formation of plastic zones. The dislocation density can increase only up to the moment when the plastic zones formed in the matrix begin to overlap. Consequently, the dislocation loops formed in the vicinity of the matrix/fibre interfaces have the opposite sign on the both sides of the fibre. It should be mentioned that the yield stress in the matrix at higher temperatures is lower than the internal stresses and, at temperatures higher than 360 °C, the thermal tensile stresses change to compression ones.

3. 2 Mechanical cycling

The logarithmic decrements measured for a sample without prior mechanical cycling and for a sample after 4320 cycles are plotted against the maximum strain ϵ of the bending amplitude in Fig. 4. It is evident that the values of the logarithmic decrement (at selected strain amplitudes) in the sample after 4320 cycles are lower than those for the samples without mechanical cycling. It can be seen that the strain amplitude dependence of the logarithmic decrement can be expressed as a sum of two components, the same as the equation (3), i.e.

$$\delta = \delta_0 + \delta_H(\epsilon). \tag{3}$$

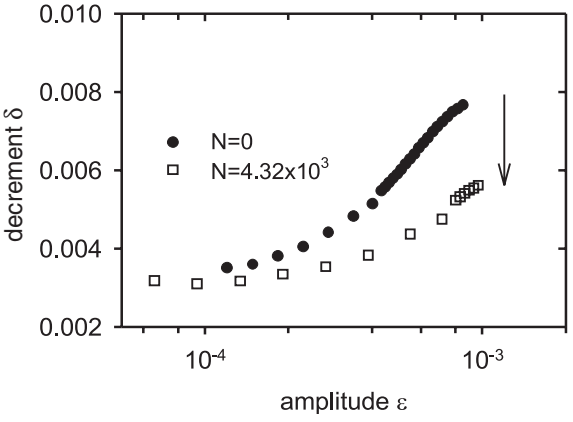

Fig. 4 Amplitude dependences of the logarithmic decrement for as received sample and after 4.32×10^3 cycles.

It is again assumed that dislocations are pinned by strong and weak pinning points. The mean distance between the strong pinning points is L_N and the mean distance between two weak pinning points is ℓ, with $\ell \ll L_N$. It is also assumed that the mean total dislocation density is ρ and that the periodic stress is applied. The logarithmic decrement in the strain amplitude independent region at low frequencies yields

$$\delta_0 = \frac{\pi\omega B_d}{36Gb^2}\rho\ell^4, \qquad (10)$$

where B_d is the damping force per unit length of dislocation per unit velocity.

The stress (strain) dependence of the decrement component δ_H can be expressed by equation (6). The microstructure changes in the composite samples upon mechanical cyclic loading are primarily induced by plastic deformation in the matrix [15].

The logarithmic decrement estimated at the strain amplitude $\epsilon_0 = 1.3 \times 10^{-4}$ depends on the number of cycles as shown in Fig. 5. It can be seen that after a decrease in the logarithmic decrement at the onset of the cycling process, the decrement is more or less constant with some fluctuation between 10^7 and 10^8 cycles. Cycling for $N > 10^8$ leads to an increase of the decrement (Fig. 5). The amplitude dependences of the logarithmic decrement component δ_H measured between 1.88×10^8 and 2.19×10^8 cycles

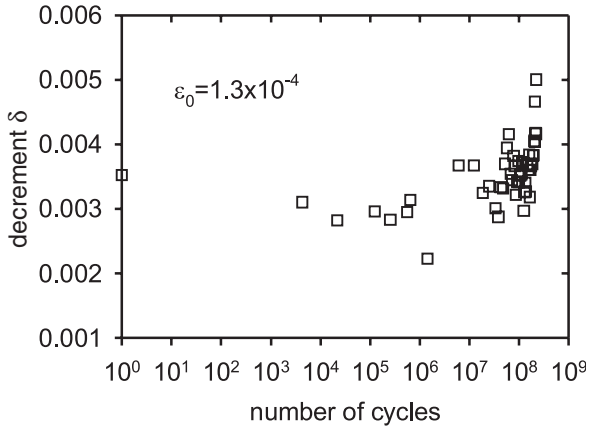

Fig. 5 Variation of the logarithmic decrement at $\epsilon_0 = 1.3 \times 10^{-4}$ with the number of cycles.

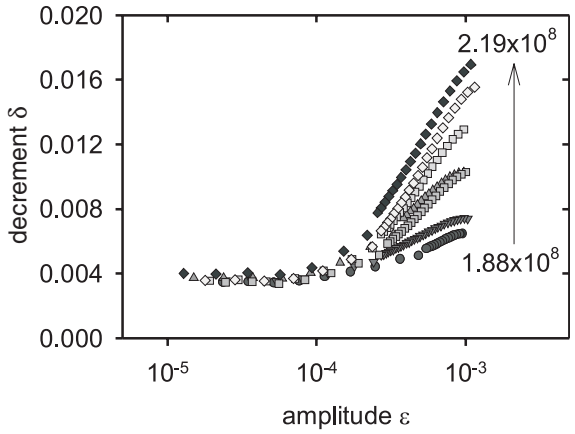

Fig. 6 Amplitude dependences of the logarithmic decrement for increasing number of cycles (at higher cycles).

are shown in Fig. 6. It can be seen that the decrement significantly increases with increasing number of cycles in the amplitude dependent part. This indicates a rapid increase of the dislocation density and also an increase in the distance between the weak pinning points (shorter dislocation segments) in the matrix. This increase of the decrement, on the other hand, is accompanied by a decrease of the resonant frequency (see Fig. 7). The comparison of our results with a similar investigation of magnesium alloy

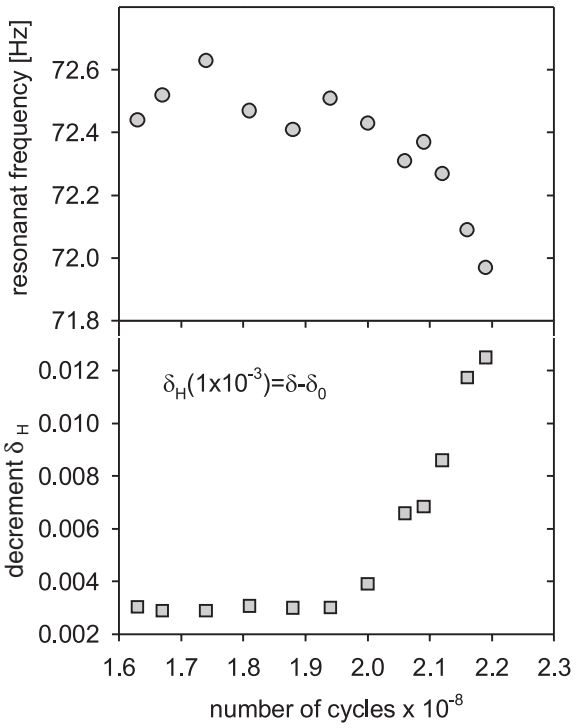

Fig. 7 Variation of the sample resonant frequency and decrement with the number of cycles. Decrement component δ_H is estimated at a maximum strain amplitude of 1×10^{-3}.

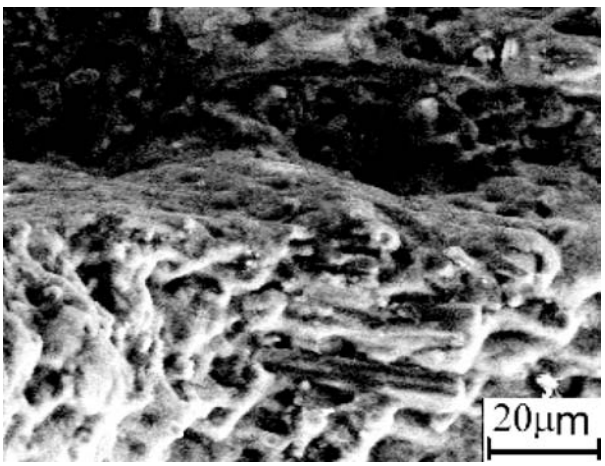

Fig. 8 Fibres pullout at the fracture surface.

AZ91 reinforced with 15 vol.% of short Saffil fibres [16] indicates that there is a substantial difference between the cycling loading behaviour of composites with AZ91 and QE22 matrix. While in the AZ91 composite cracks are formed during the cycling bending, such cracks were not observed in the composite with QE22 matrix [17]. We believe that this is due to the existence of the brittle intermetallic phase $Mg_{17}Al_{12}$ in the AZ91 alloy as well as in its composite. Small cracks are formed in this phase. Similar cracks were observed during thermal and mechanical loading of the AZ91 alloy [8,16]. The higher plasticity of the QE22 alloy without a brittle phase is very probably the reason for different fatigue behaviour of the QE22/Al_2O_3 composite. Plastic deformation is accumulated in the matrix. The observed decrease of the damping at the onset of the cycling process (see Fig. 5) is very probably caused by a decrease of the mobile dislocation density. Dislocation segments are inactive due to dislocation-dislocation interaction. The measured decrease of the resonant frequency at the end of the fatigue process indicates a stiffness loss due to cracks and maybe also by an increase of the number of bowable or moveable dislocations as a function of cycling. A rapid increase in the amplitude dependent component of the decrement at the end of the sample life is due to rapid nucleation or growth of cracks and a resulting strong local increase in the free dislocation density. Newly created dislocations at cracks tips accommodate these stresses. The dislocations can be also absorbed by interfaces. Crack deflection along an interface is followed by the separation of the fibre/matrix interface. The pull out of fibres was observed at the fracture surface. Holes after fibres are visible in Fig. 8. No fibre fracture was observed.

4. Conclusions

The microstructure of QE22/Al_2O_3 composites is stable up to 200 °C. From the internal friction measurements, it can be concluded that changes in the microstructure occur at temperatures above about 200 °C. These changes are very probably connected with migration of solute atoms and precipitation processes. The dislocation density slightly increases, which is very probably reflected by a small increase in the logarithmic decrement. Tensile internal stresses generated at temperatures higher than 220–240 °C are high enough to invoke motion of newly formed dislocations. Thermal cycling at temperatures higher than ~ 360 °C causes a new situation: motion and annihilation of newly formed dislocations in the matrix under appearing compressive internal stresses leads to and the decrease of the decrement. And accumulation of the plastic deformation in the matrix presumably mainly due to crack nucleation or growth increased the amplitude independent as well as amplitude dependent components of the logarithmic decrement. Pull out of fibres during fracture of the composite was observed.

Acknowledgement

The work is part of the Research Project CZ-88/2006 (Scientific and Technical Co-operation between the Czech Republic and the Slovak Republic) financed by the Ministry of Education of the Czech Republic.

References

[1] SVOBODA, M., PAHUTOVÁ, M., MOLL, F., BŘEZINA, J., SKLENIČKA, V.: *In: Magnesium Alloys and Their Applications.* Ed.: Kainer, K.U. Weinheim, Wiley-VCH 2000, p. 234.
[2] POLMEAR, I. J.: *Mater. Sci. Techn.*, 10, 1994, p. 1.
[3] KAINER, K. U.: *In: Magnesium Alloys and Their Applications.* Eds.: Mordike, B.L., Hehmann, F. Oberursel, DGM 1992, p. 415.
[4] OAKLEY, R., COCHRANE, R. F., STEVENS, R.: *Key Engn. Mater.,* 104-107, 1995, p. 387.
[5] WILKS, T. E., KING, J. F.: *In: Magnesium Alloys and Their Applications.* Eds.: Mordike, B.L., Hehmann, F. Oberursel, DGM 1992, p. 431.
[6] KAINER, K. U.: *Mater. Sci. Eng.* A, 135, 1991, p. 243.
[7] GÖKEN, J., RIEHEMANN, W.: *Mater. Sci. Eng.* A, 324, 2002, p. 134.
[8] GÖKEN, J., RIEHEMANN, W.: *Mater. Sci. Eng.* A, 370, 2004, p. 417.
[9] ARSENAULT, J. R., SHI, N.: *Mater. Sci. Eng.,* 81, 1986, p. 175.
[10] DUNAND, D. C., MORTENSEN, A.: *Acta Metall*. Mater., 39, 1991, p. 127.
[11] GRANATO, A. V., LUECKE, K.: *J. Appl. Phys.,* 27, 1956, p. 583.
[12] DE BATIST, R.: *In: Materials Science and Technology.* Vol. 2B. Eds. Cahn, R.W., Haasen, P., Kramer, J. Weinheim, VCH 1994, p. 159.
[13] GRANATO, A. V., LUECKE, K.: *J. Appl. Phys.,* 52, 1981, p. 7136.
[14] KIEHN, J., SMOLA, B., VOSTRÝ, P., STULÍKOVÁ, I., KAINER, K. U.: *phys. stat. sol.* (a), 164, 1997, p. 709.
[15] LLORCA, J.: *Progr. Mater. Sci.*, 47, 2002, p. 283.
[16] TROJANOVÁ, Z., MIELCZAREK, A., RIEHEMANN, W., LUKÁČ, P.: *Comp. Sci. Tech*., 66, 2006, p. 585
[17] MIELCZAREK, A., RIEHEMANN, W., TROJANOVÁ, Z., LUKÁČ, P.: *Mater. Sci. Eng.* A, In press.

https://doi.org/10.26552/com.C.2006.4.21-24

Ivo Černý – Rayner M. Mayer – Ivan Fürbacher *

AN EFFECT OF MICROSTRUCTURE DEFECTS ON FATIGUE RESISTANCE OF GLASS FIBRE REINFORCED POLYMER COMPOSITES USED FOR SPRINGS OF FREIGHT VEHICLES

Fatigue properties of glass reinforced polymer (GRP) composite materials and advanced components manufactured using GRP are discussed with an emphasis on scale and microstructure effects. Results of an experimental investigation of fatigue damage mechanisms under bending and shear cyclic loading and effects of microstructural defects resulting from an insufficient resin wet out are presented and analysed. It was shown that if microstructural defects are present in the component, initiation of fatigue damage is localised into these areas, resulting in sudden, premature failure. Fatigue life can be then reduced by more than three orders in comparison with the perfect material. The presence of defects is affected particularly by properties of the constituents and moulding parameters. Suitable changes of the process parameters resulted in a significant improvement of fatigue resistance.

1. Introduction

Characteristic properties of long fibre glass reinforced polymers (GRP) composites like low specific weight, high strength and generally very good fatigue resistance enable one to use these materials in heavy-duty light-weight structures, like aircraft components or wind turbine blades. In additions, low E-modulus together with internal damping and low dynamic stiffness make GRP composites suitable for the manufacture of road-friendly leaf springs and suspensions including those for high capacity trailers and railway freight vehicles. The low E-modulus in comparison with steel is a very important characteristic enabling the introduction of a new design philosophy for springs, suspensions and bogies. In case of springs, it is possible to use just one or two leaves with stable damping properties and other characteristics during the whole service life. In addition, due to the low specific weight, a 60% reduction of the whole suspension weight can be obtained by replacing steel spring with composite springs with the same function. This is particularly important because springs represent unsprung mass. An efficient noise damping is an additional, but very important feature of GRP materials making suspensions more environmentally friendly. All these properties are the reason, why the design and characterisation of glass fibre reinforced composites have received recently a great amount of interest [1–3].

In comparison with metals, the use of GRP composites has specific difficulties. Due to the material heterogenity, any change of shape and size of a component can affect its mechanical properties and so, changes have to be experimentally verified. If process parameters are not correctly or other characteristics of the constituents like glass preforms are not perfectly maintained or incorrectly selected, various kinds of defects can arise, like bubbles, voids, porosity or insufficient wet out. These defects can fundamentally reduce static and fatigue strength [4–5].

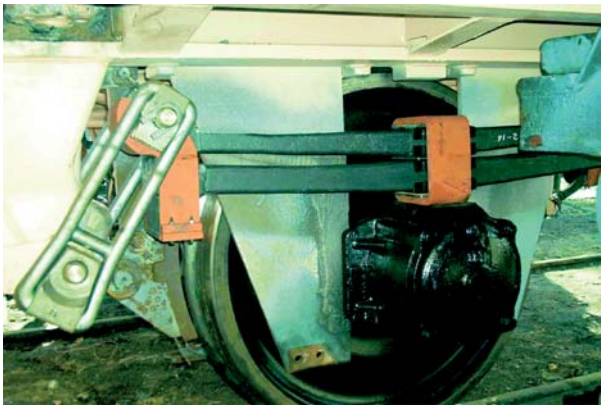

Fig. 1 GRP spring with new type of shackles on a new Czech wagon during fit test

Within an on-going European research and development EUREKA project Eurobogie, significant progress has been reached in the field of an innovative design and manufacture of GRP springs for railway freight vehicles to replace traditional multi-leaf steel springs. The prototype of GRP railway spring together with a new type of shackles Niesky I during a fit test on a new Czech wagon is shown in Fig. 1.

To ensure the requested high reliability and safety of springs, a large number of static and fatigue tests on components besides a detailed material characterisation was carried out. In the paper, results of fatigue tests of the full-scale components are described, analysed and compared with the results obtained on small laboratory specimens with particular emphasis on the material microstructure and presence of defects.

* **Ivo Černý[1], Rayner M. Mayer[2], Ivan Fürbacher[1]**
[1]SVÚM a.s., Areál VÚ 565, CZ-19011 Praha 9, Czech Republic, E-mail: strenght@svum.cz, Ivo.Cerný@seznam.cz
[2]Sciotech Ltd., 9 Heathwood Close, Yateley, GU46 7TP, U.K.

2. Experiments

Fatigue tests were performed on completely assembled two-leaf springs. Both the leaves were made from glass fibre reinforced polyester (Scott Bader Crystic PD9229) and manufactured by a vacuum assisted resin transfer technology by EM Fiberglas. The reinforcing E-glass rovings (Vetrotex P192) are assembled using knitting machinery to form a unidirectional glass tape of constant width (Culzean Textile Solutions). This consists of 97% glass in the longitudinal direction and 3% in the transverse direction. The top leaf has parabolic thickness characteristic by a constant bending stress. The parabolic shape is achieved by cutting suitable core layers to length. These are then heat set to produce a preform glass tape pack. The glass fibre volume fraction of the springs is about 65 %. The total mass of the two GRP leaves is 26 kg giving a total suspension mass of 38 kg, compared with 120 kg for the UIC 22.5 tones parabolic steel suspension. The material properties of the unidirectional composites were measured at RISØ National Laboratory [6]. Basic mechanical properties are: bending stiffness and strength about 35 GPa and 1000 MPa, respectively, static interlaminar shear strength 50 MPa. The experimental programme included fatigue tests performed on 3PB specimens, too. All the tests carried out in [6] were performed on specimens taken from a bottom leaf section without defects, which was checked using ultrasonic non-destructive testing.

Fatigue load amplitude during full-scale spring tests corresponded to the recommendations of railway standard UIC 517 or to the requirements of Czech Railways, respectively. The former case defines the static load to correspond to the maximum static operation loading, which is 105 kN for the 22.5 tones axle, and load amplitude ±25% of the static load. In the latter case, the static load is the same, but load amplitude is ± 30%. The requested number of cycles to failure should not be less than one million. In both the cases, springs have to be attached by pins going through eye ends on carriages enabling free horizontal motion. Load frequency was 1.2 Hz.

From the material point of view, the full-scale spring tests can be evaluated as tests of single large bending specimens of the maximum thickness 52 mm, width 115 mm and test span 1190 mm. It was calculated that actual stress in the top leaf, if loaded separately without the bottom leaf, corresponds almost exactly to 50% of the loading used for the whole component within the precision better than 2%. This calculation was also experimentally verified [7].

An additional group of fatigue tests to study scale effects was performed on small 3PB specimens taken and manufactured from two randomly selected leaves, top and bottom, without any non destructive (NDE) testing, unlike the fatigue material characterisation tests in [6]. Dimensions of 3PB specimens were selected to ensure the same type of loading as in actual leaves representing the large specimens, namely thickness 5.2 mm and test span 120 mm. These dimensions resulted in the same ratio of bending and interlaminar shear cyclic stresses, respectively. Width of these specimens was 25 mm, load frequency was between 35 and 40 Hz.

3. Results and discussion

Results of all fatigue tests are summarised and mutually compared in Fig. 2. There are four different groups of data: (i) full-scale tests of complete springs evaluated and recalculated as fatigue tests of individual top leaves representing large specimens, (ii) tests of small 3PB specimens taken from randomly selected top and bottom leaves without non-destructive inspection, (iii) results of fatigue tests of small 3PB specimens cut from a bottom leaf with an almost perfect microstructure as examined by ultrasonic method [6], recalculated in terms of stress amplitude and (iv) two experimental points of fatigue tests of GRP trailer springs made from a similar material and by a similar process, with a good microstructure [8, 9].

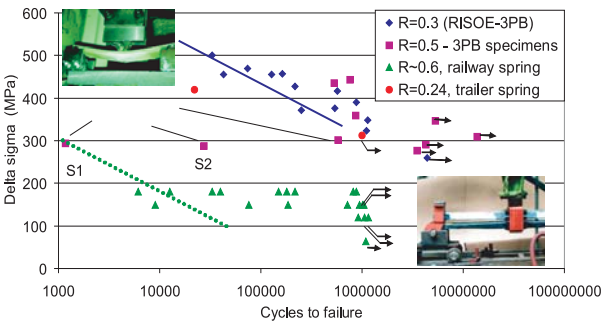

Fig. 2 Comparison of bending fatigue tests results of material coupons and springs

The results of fatigue tests of full-scale GRP railway springs look to have a large scatter. Actually, it is not a scatter but a systematic dependence corresponding to the process of gradual improvement of numerous manufacturing parameters like changes of preform tool, preform lay-up, number and position of injection channels in the mould, catalyst, accelerator, inhibitor, time of vacuum operation and injection time. Unlike the first tested group of GRP springs with fatigue life bellow 100000 cycles, when the parameters were not optimised, and springs with just partially optimised parameters with a medium fatigue life between 100000 and 200000 cycles, springs manufactured with quite optimum parameters have acceptable fatigue life of more than 1 million cycles. However, the general potential of the excellent fatigue resistance of GRP material still has not been fully reached.

When the first group of full-scale tests of the railway springs was performed, premature failures bellow 100000 cycles were rather surprising, considering the very good fatigue resistance results obtained on small 3PB specimens tested at the RISØ National Laboratory. To find causes of the premature failure, detailed microstructure analyses of central areas of broken top leaves were carried out. It followed from the failure mode that interlaminar shear fatigue resistance was particularly poor as all railway springs broke suddenly by one or two interlaminar shear cracks passing along the length of the leaf near its neutral axis, near the centre plane with zero bending stress but maximum shear stress. Examining the microstructure, large areas of very poor wet out were found

in all leaves with the premature failure. An example of an insufficiently wetted area with quite large voids is in Fig. 3.

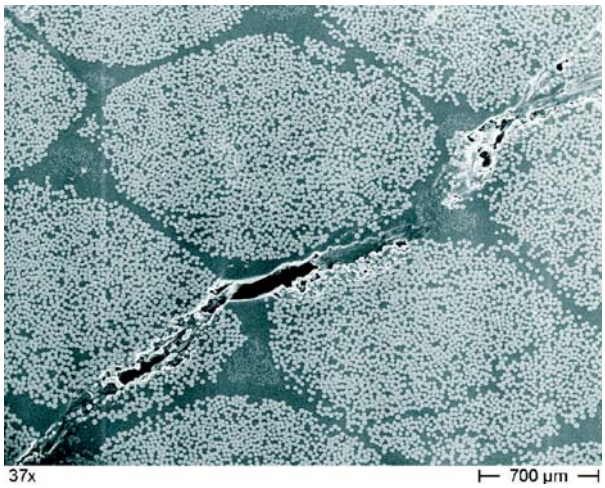

Fig. 3 Voids arisen from insufficient wet out initiating shear fatigue cracks in resin between yarns

As regards the third group of fatigue tests, namely 3PB specimens tested at SVÚM a.s., taken from a top and bottom leaf, respectively, randomly selected, not checked by NDT methods, it is clear that most of fatigue results of this group (Fig. 2) correspond quite well to the results obtained at RISØ National Laboratory on 3PB specimens with a perfect microstructure. On the other hand, two specimens, marked S1 and S2 in Fig. 2, had a significantly reduced fatigue life. The reason was the microstructure. In the central areas of specimens S1 and S2, voids and poor wet out was found, unlike the other specimens of this group, where the microstructure was quite good. Not only fatigue life, but also failure mode was different. Specimen S1 broke suddenly, along the central plane of maximum shear but zero bending stress, unlike the specimens with the good fatigue resistance, when failure occurred by a gradual progressive reduction of bending stiffness (Fig. 4) connected with a continuous damage development in a significant volume of the specimen material in the area of tension stresses (Fig. 5).

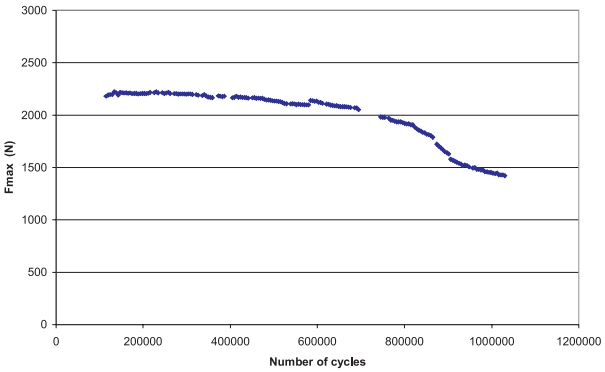

Fig. 4 Example of continuous stiffness changes during 3PB fatigue loading of specimens with good fatigue resistance

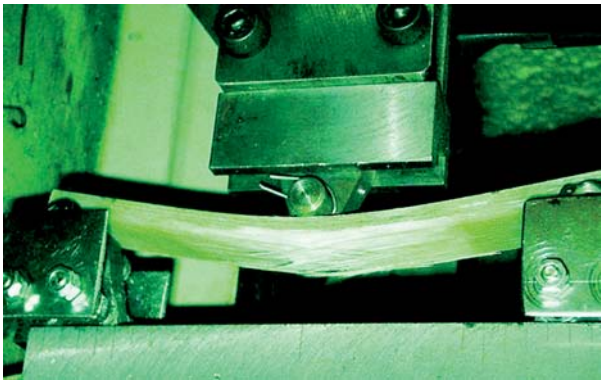

Fig.5 Typical damage development in area of tensile stresses in big material volume of 3PB specimens with good fatigue resistance

It follows from Fig.2 that fatigue resistance of the worst specimen S1 corresponds almost exactly to the worst results obtained during full-scale testing of actual springs. If a regression line parallel to that of 3PB specimens with a good microstructure is drawn, passing through the S1 point, this line corresponds to the worst results of actual spring tests. This effect can be explained by a different probability of an occurrence of harmful voids in full-scale leaves and in small specimens made from them, respectively. Most of the 3PB specimens of the third group were evidently taken from areas of the leaves with a good microstructure. Then the fatigue life corresponded to the results obtained at RISØ [6]. Just two specimens were randomly taken from areas with the insufficient wet out. Their fatigue resistance was lower by two or three orders in comparison with the specimens with perfect microstructure.

As regards full-scale leaves, the probability of an occurrence of microstructure defects is small, if the manufacturing process allows all air to be excluded and sufficient time for all the glass filaments inside the bundles (4800 tex) to be wet out. High cycle fatigue damage of GRP composites, unlike metals, is quite a global process, connected with gradual changes of stiffness. However, in case of a defect occurrence, fatigue cracking starts in the weakest points of the microstructure and is therefore strongly localised. Then the global stiffness remains almost constant. When the fatigue

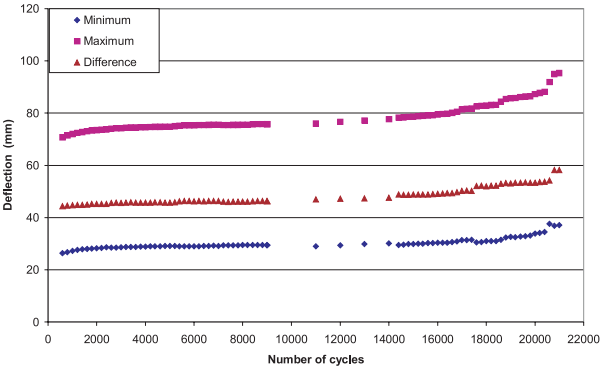

Fig.6 Sigmoidal change of deflection typical for GRP composites with good microstructure during fatigue test of trailer spring in bending.

crack is locally initiated, it causes a sudden break by interlaminar shear.

In comparison with railway springs, the fatigue resistance of GRP trailer springs in Fig. 2 was very high. Hereat, dimensions of the trailer springs affecting shear stresses, namely maximum thickness and span distance, 58 mm and 1040 mm, respectively, were very similar to those of railway springs. With the load range of 15–65 kN corresponding to the maximum bending stress range of 312 MPa, fatigue life was more than 1 million cycles without failure, which is fully comparable with fatigue tests of the small 3PB specimens. When the load amplitude was subsequently raised to the value 22–89 kN, corresponding to the bending stress range 420 MPa, fatigue life was 22000 cycles to failure. This very good fatigue resistance was connected with a different failure mode – no sudden break, but continuous damage accumulation in a big material volume (Fig. 6).

4. Conclusions

An experimental programme was carried out with the aim to characterise fatigue properties of advanced leaf springs for railway freight vehicles made from long-fibre glass reinforced polyester composite. The programme comprised (i) bending fatigue tests of small specimens taken from a good quality spring to characterise the material, (ii) fatigue tests of whole springs representing large samples and (iii) bending fatigue tests of small specimens randomly taken from actual spring leaves, where the quality was not checked by any NDE method. A comparison with trailer springs manufactured by a similar technology within a previous project was made. The results can be summarised as follows:

- Fatigue strength of the first series of full-scale railway springs was quite poor and did not correspond to the excellent fatigue resistance of small specimens with a good microstructure. Fatigue life of components was lower by more than three orders.
- Most specimens randomly taken from the actually manufactured springs of rather low quality had very good fatigue resistance, corresponding to those specimens used for the basic fatigue material characterisation. However, fatigue life of several specimens of this group corresponded to the premature failure of the worst group of components.
- The main reason for the insufficient fatigue life of components was a presence of voids and bubbles resulting from an insufficient wet out. If small specimens were taken from areas with no defects, their fatigue life was excellent. On the contrary, small specimens with the poor fatigue properties contained microstructural defects as they were taken from insufficiently wetted areas.
- After improving the processing and lay up of the constituents, fatigue resistance was significantly increased and satisfied conditions of railway standards. On the other hand, a comparison with fatigue strength of trailer springs evaluated in the past indicated that there still may be additional fatigue strength to be attained and some further improvements may be reached resulting in negligible differences between fatigue strength of good specimens and full-scale components.

Acknowledgements

The work has been carried out within the project EUREKA E! 1841 Eurobogie, supported by the Czech Eureka grants OE 148 and OE 44/2 and by UK Department of Trade and Industry. The authors appreciate discussions with many colleagues including Aage Lystrup of RISØ National Laboratory.

References

[1] HARRIS, L. R.: *Composite leaf spring design.* GKM Technology report, August, 1990.
[2] CHAPLIN, C. R., MAYER, R. M., REZAKHANLOU, R.: *A new approach to composite leaf springs.* Proc. of the conf. Autotech, Birmingham, 1995.
[3] CHIANUMBA, A., JERONIMIDIS, G., MAYER, R. M.: *Advanced vehicle suspensions using glass reinforced plastics.* Proc. 6th European Congress on Lightweight and Small Cars: The Answer to Future Needs, Cernobbio, Italy; 1997, A2.11108: 549–558.
[4] STONE, D. E. W., CLARKE, B.: *Non-destructive determination of the void content in carbon fibre reinforced plastics by measurement of ultrasonic attenuation.* RAE Tech. Report 74172, 1974
[5] RHEILÄNDER, J. T., NIELSEN, S. A., BORUM, K. K., GUNDTOFT, H. E.: *NDE of polymeric composites: A comparison of techniques.* Proc of the 18th Risoe Int. Symposium on Materials Science, Ed. Andersen S.I. et. al., RISØ National Laboratory, Roskilde, Denmark, 1997, pp. 101–125.
[6] LYSTRUP, A., BORUM, K., BRØNDSTED, P.: *Mechanical properties and characterisation of GFRP material from train bottom spring No. 01-02-I6.* Eureka Eurobogie project E!1841 report RISØ-I-2094(EN), November 2003, Roskilde, Denmark
[7] JARRIER, E., MAYER, R. M.: *Manufacturing improvements and testing of leaf springs.* Eureka Eurobogie project E!1841 report, Sciotech Projects, Reading University, August 2005
[8] ČERNÝ, I., FÜRBACHER, I., MAYER, R. M.: *Possibilities of use of springs made from long-fiber glass reinforced composites in the suspensions of road and rail freight vehicles.* Key Engng. Materials, Vols. 230–232, pp.251–254.
[9] ČERNÝ, I., FÜRBACHER, I., MAYER, R. M.: *Possibilities of use of springs from composite materials in suspensions of railway freight wagons.* Proc. of the 14th Int. Conf. "Current Problems in Rail Vehicles – PRORAIL", Žilina, 6.–8. 10. 1999, Vol. 1, pp.49–56

https://doi.org/10.26552/com.C.2006.4.25-28

Zdeněk Knésl – Pavel Hutař – Stanislav Seitl *

CONSTRAINT ASPECTS OF THE EVALUATION OF FATIGUE TEST RESULTS IN PARIS REGION

The growth of the fatigue crack is dependent on the crack growth resistance of the material as a bulk property. The fatigue crack growth properties of a material are usually described by the correlation between a crack propagation rate, and a corresponding range of the stress intensity factor (Paris-Erdogan law). Formulated modified Paris-Erdogan law estimates quantitatively the changes of the fatigue crack propagation rate due to different level of constraint. In-plain constraint was described by T-stress value. The validity of the approach suggested has been proved by the comparison of measured and calculated values of the crack propagation rate and it was found that experimental values correspond well with those numerically predicted. The results presented makes it possible to relate experimentally measured data obtained from specimens with different geometries and thus contribute to more reliable estimates of residual fatigue life of structures.

1. Introduction

The fatigue life of structures can be divided into two parts. The first one corresponds to a crack initiation period and the second one corresponds to a crack growth period until a complete failure. Crack initiation and growth are different phenomena and their influence on the total service life of structures depends on many circumstances.

The fatigue life of an unnotched specimen in high cycle fatigue regime is largely covered by the crack initiation period. The crack growth period could almost be disregarded and often neglected. Nevertheless there are situations where the fatigue crack propagation period plays a decisive role and has to be carefully analysed. Let us mention two such examples. The crack initiation period might be shorter due to the existence of stress concentrators (such as existing cracks, notches, material discontinuities...). In this case the fatigue crack propagation in components can start practically even without a crack initiation period. Another category of problems connected directly with fatigue crack propagation is related to a fatigue crack growth monitored by periodic inspections. The purpose of the inspections is to discover fatigue cracks before they become dangerous and to do this it is necessary to know how fast a crack is growing in order to set timely inspection periods. In this situation is the knowledge of the fatigue crack propagation rate of paramount importance.

The growth of the fatigue crack is then dependent on the crack growth resistance of the material as a bulk property. The fatigue crack growth properties of a material are usually described by the correlation between a crack propagation rate, da/dN, and a corresponding range of the stress intensity factor ΔK. The correlation is usually expressed by an empirical function based on test data. The most popular relation between da/dN and ΔK can be described by a power function (Paris-Erdogan law), see e.g. [1], [3].

$$da/dN = C\,\Delta K^m \tag{1}$$

with C and the exponent m as material constants. The fact that C and m are material parameters means that for a given material and set of test conditions, the growth rate should depend only on ΔK, i.e. the eq. (1) represents a material curve. Eq. (1) does not account for R-effect on crack growth, neither for the asymptotic behavior near the threshold and the final failure regions. In order to apply eq. (1) to predict the lifetime of structures, the corresponding material data, C and m, must be known. The methods for conducting fatigue crack growth testing and evaluation of parameters C and m are specified in standards (e.g. ASTM E 647 [2]). The testing can be conducted on any type of a test specimen or structural component. Usually a compact tension specimen (CT), center cracked tension specimen (CCT) or three point bend specimen (3PB) are used for generating material da/dN data. Some results of the fatigue crack propagation tests using several different specimens showed significant dependence on specimen geometry, e.g. [4], [8], [9]. Thus the C, m values cannot be considered as material constants, in all cases and their values can depend on geometry of the specimen used for their determination. This fact makes questionable the transferability of the laboratory data to real structural components. The aim of the contribution is to suggest an approach how to quantify the effect of specimen geometry on the fatigue crack propagation rate.

2. Experimental observations

The influence of the specimen geometry on the fatigue crack propagation rate (FCPR) taken from paper [9] is presented on Fig.1.

As a result, the fatigue crack propagation rate was found to be greater for CCT specimen than for the CT one. In our laboratory

* **Zdeněk Knésl, Pavel Hutař, Stanislav Seitl**
Institute of Physics of Materials, Žižkova 22, 616 62 Brno, E-mail: knesl@ipm.cz

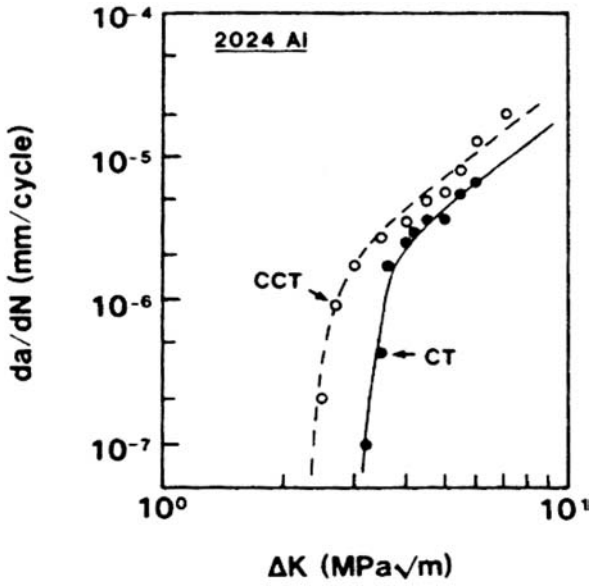

Fig.1 Effect of specimen geometry on crack behavior near threshold of 2024 aluminum alloy at $R = 0.1$. Taken from reference [9].

0.45% carbon steel was used for similar experiments, see Fig. 2. The measurements are in agreement with previous authors. All experiments were performed at the same conditions – room temperature and loading stress ratio $R \sim 0.1$ (i.e. $\Delta K_I \sim K_I$). The crack length was measured optically with a resolution of 0.01 mm.

Discrepancies in the fatigue crack growth rate in the Paris region can be explained by constraint based fracture mechanics. In conventional one parameter fracture mechanics the stress field around the crack tip is described by one parameter. In two parameter constraint based fracture mechanic the stress field is expressed by means of the two parameters, the stress intensity factor K_I and the T-stress. The T-stress quantifies the effect of the crack tip constraint, which depends on the outer geometry of structure. Both these parameters are related to the first and second term of Williams expansion [10]. The stress field near the crack tip for a normal mode of loading can then be expressed as

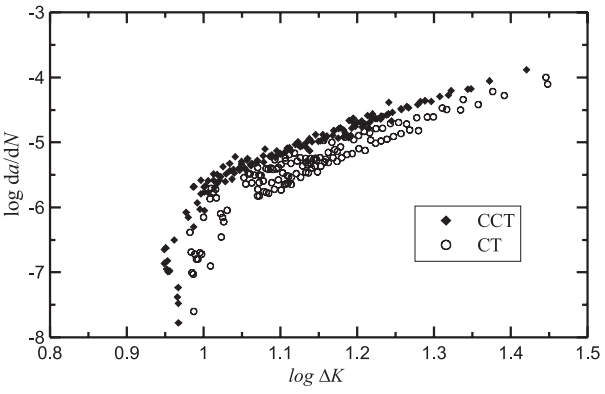

Fig. 2 Influence of the constraint on the threshold values and fatigue crack propagation rate of 0.45% carbon steel at $R = 0.1$ [4].

$$\sigma_{ij} = \frac{K_I}{\sqrt{2\pi r}} f_{ij}(\theta) + T\delta_{1i}\,\delta_{1j}, \qquad (2)$$

where K_I is the stress intensity factor, T is T-stress and f_{ij} is a known function of the polar angle θ.

The center cracked plate tension specimen (CCT) represents geometry with negative values of the T-stress (loss of constraint), which is practically independent of the crack length [7]. On the other hand the compact tension (CT) specimen corresponds to geometry where the T-stress values are positive and depend more significantly on the crack length [7]. Therefore, the fatigue crack propagation rate was found to be higher for a structure with a negative value of T-stress (CCT specimen) than for a structure with a positive value of T-stress (CT specimen).

3. Constraint based description of fatigue crack behavior

During cyclic loading the monotonic and cyclic (or reversed) plastic zone is created ahead of the growing crack. The size and the properties of the plastic zone are decisive for the propagation of a fatigue crack and control its behaviour [3].

The results of finite element computations in Fig.3 show that for the same value of K_I (we assumed the normal mode of loading only), the crack tip plastic zone size and shape are different for different values of the T-stress. Typically, a negative value of the T-stress, $T < 0$, causes enlargement of the plastic zone as compared to the case where $T = 0$. Moreover, for plane strain conditions, the plastic zone is rotated to the region ahead of the crack tip for negative values of T. The size of the plastic zone decreases for positive values of the T-stress, but the dependence is not so pronounced. Note that $T = 0$ corresponds to the assumptions of one parameter fracture mechanics.

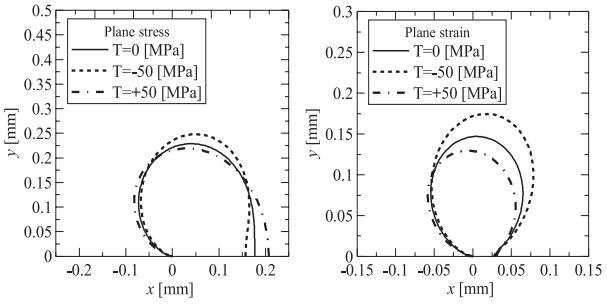

Fig.3 Dependence of the size and shape of the crack tip plastic zone on the T-stress value (a) plane stress conditions (b) plane strain conditions.

Accepting the assumption that the size of the plastic zone is dominant for the propagation of a fatigue crack, it is possible to estimate quantitatively the changes of the fatigue crack propagation rate due to different constraint level [4].

Under small scale yielding (SSY) conditions there is a single valued relation between the size of the plastic zone at the crack tip and the value of the corresponding stress intensity factor controlling the fatigue crack propagation rate. Following this, one of the parameter, say $S_P = S_P(K_I)$, which characterizes the area of the plastic zone, can be used as the controlling variable. Paris law can be then rewritten as a function of S_P in the form:

$$da/dN = C\left(\sigma_0 \sqrt[4]{\frac{S_P}{\Psi(v)}}\right)^m , \quad (3)$$

where $\Psi(v)$ is a known function of the Poisson ratio v. Under the framework of one parameter linear-elastic fracture mechanics, equations (1) and (3) are equivalent. The assumption of a unique relationship between da/dN vs. K_I independent of the geometry and the fact that the area of the plastic zone depends on the geometry of the specimen are contradictory. If the constraint expressed by the T-stress influences the size of the plastic zone, it may also influence the fatigue crack propagation rate da/dN, and the da/dN vs. ΔK curve may depend on the geometry of the specimen. Thus eq. (3) considers the effect of the stress field at the tip of the crack, including the non-singular T-term, on the fatigue crack propagation rate.

The influence of the T-stress on the size of the plastic zone $S_p(K, T)$ was assessed using a modified boundary layer analysis, see, e.g., [5]. As a result of the numerical simulations, it can be seen that the relation between $S_p(K, T)$ and $S_p^0(K, T = 0)$ depends on the hardening coefficient n only very slightly and can be expressed in the form:

$$S_p(K, T) = \lambda(T/\sigma_0)^4 \, S_p(K, T = 0), \quad (4)$$

where

$$\lambda(T/\sigma_0) = 1 - 0.85\left(\frac{T}{\sigma_0}\right)^3 + 0.52\left(\frac{T}{\sigma_0}\right)^2 - 0.3\left(\frac{T}{\sigma_0}\right), \quad (5)$$

Using the Paris-Erdogan equation (1) and (5) we get the following form:

$$da/dN = C\,[\lambda(T/\sigma_0)]^m \, K^m. \quad (6)$$

Eq. (6) represents a modified form of the Paris-Erdogan equation and makes it possible to account the constraint effect on the fatigue crack propagation rate. C and m are material constants obtained for conditions corresponding to $T = 0$. The value of the T-stress in (5) represents the level of constraint corresponding to the given specimen geometry. Eq. (6) can be expressed in the form corresponding to standard Paris – Erdogan equation.

$$da/dN = C^* \, (K)^m, \quad (7)$$

where $C^* = C_0\,[\lambda(T/\sigma_0)]^m$. It follows from eq.(7) that da/dN vs. K_I curves corresponding to different specimens geometry with different values of T-stress create a set of parallel straight lines on a log-log scale. This corresponds to experimental results presented in the paper. The "constraint based" material parameter C^* can be expressed in form:

$$C^* = C^0\left(1 - 0.85\left(\frac{T}{\sigma_0}\right)^3 + 0.52\left(\frac{T}{\sigma_0}\right)^2 - 0.3\left(\frac{T}{\sigma_0}\right)\right)^m , \quad (8)$$

where C^0 is the experimentally obtained material constant for ($T = 0$), T is a T-stress and σ_0 is a yield stress of controlled structure.

4. Conclusions

The influence of in-plane constraint on the propagation rate of the fatigue crack in the Paris region has been investigated. After assumption that the size of the plastic zone is dominant for the propagation of the fatigue crack modified Paris-Erdogan equation has been introduced. The results of the paper can be summarized in the following way:

The effect of the specimen geometry on the relationship between the propagation rate of a fatigue crack and the range of the stress intensity factor amplitude might make questionable the uniqueness of the da/dN vs. ΔK curve for different geometries, which is essential if laboratory data are to be transferred to engineering applications.

Formulated modified Paris-Erdogan law estimates quantitatively the changes of the fatigue crack propagation rate due to different level of constraint. In-plain constraint was described by T-stress value. The validity of the approach suggested has been proved by the comparison of measured and calculated values of the crack propagation rate and it was found that experimental values correspond well with those numerically predicted.

Under small scale yielding conditions, the specimens with negative values of the T-stress exhibit a higher fatigue crack propagation rate than the specimens with positive values of T-stress at the same value of stress intensity factor range ΔK. It was found that, depending on the material properties, geometry and loading of the specimen difference in da/dN due to constraint can reach 100 % for extreme values of T, see eqs. (5, 6).

To overcome problems connected with influence of the specimen geometry on the fatigue crack propagation rate and to increase the reliability of the transferability of basic fatigue crack propagation data from laboratory specimen to engineering structures, the level of constraint of the specimen and the structure should be the same. If the constraint levels are different it is necessary to use eq. (8) and recalculate the value of C parameter in Paris law.

Acknowledgements

This investigation was supported by grants 1QS200410502, 101/04/P001 and 106/06/P239.

References

[1] ANDERSON, T. L.: *Fracture mechanics,* CRC Press, Boca Raton, Florida, 1995
[2] *Annual Book of ASTM Standards 1999*, Standard Test Method for Measurement of Fatigue Crack Growth Rates, E647-99, 1999
[3] DUGGAN, T. V.: *A theory for fatigue crack propagation,* Engineering Fracture Mechanics, Vol. 9, 1977, pp. 735–747
[4] HUTAŘ, P., SEITL, S., KNÉSL, Z.: *Quantification of the effect of specimen geometry on the fatigue crack growth response by two-parameter fracture mechanics,* Material Science & Engineering A, 387–389, 491–494, 2004
[5] HUTAŘ, P., SEITL, S., KNÉSL, Z.: *Effect of constraint on fatigue crack propagation near threshold in medium carbon steel,* Computational Materials Science, Volume 37, Issues 1–2, 51–57, 2006
[6] KNÉSL, Z., SEITL, S., HUTAŘ, P.: *Accounting for effects of constraint on propagation of fatigue crack,* Damage & Fracture mechanics VII, WIT press, 245–253, 2002
[7] KNÉSL, Z., BEDNÁŘ K., *Two parameter fracture mechanics: calculation of parameters and their values (in Czech)*, Institute of Physics of Materials, Brno, 1998
[8] TONG J.: *T-stress and its implications for crack growth,* Engineering Fracture Mechanics, 69, 1325-1337, 2002
[9] VECCHIO, R. S., CROMPTON, J. S., HARTZBERG, R. W.: *The influence of specimen geometry on near threshold fatigue crack growth,* Fatigue Fract. Engng. Mater. Struct., 10, 333–342, 1987
[10] WILLIAMS, M. L.: *On the Stress Distribution at the Base of Stationary Crack,* Journal of Applied Mechanics, 24, 109–114, 1957

https://doi.org/10.26552/com.C.2006.4.29-33

Jan Kohout – Stanislav Věchet – Vojtěch Hrubý *

COMPARISON OF A NEW EQUATION DESCRIBING FATIGUE CRACK GROWTH CURVES WITH THE NASGRO EQUATION

The so-called NASGRO equation allows a very good description of fatigue crack growth curves, i.e. the dependence of crack length increase per one fatigue cycle da/dN on the stress intensity factor range ΔK. In 1999 the first author of this paper published quite similar equation, which written for given loading cycle asymmetry with positive stress ratio R contains the same parameters having similar meaning as in the NASGRO equation. In most cases studied by the authors this equation leads to a better fit than the NASGRO equation, above all when the experimental curve contains relatively long Paris straight line and/or relatively sharp bend from this line to the threshold stress intensity factor range. The generalization of the NASGRO equation for various values of stress ratio R was made in a quite complicated way. The new equation was generalized using the Walker model based on the relation $\Delta K(R) = \Delta K(0)(1 - R)^{-m}$ which is valid also for threshold value ΔK_{th} but not for critical stress intensity K_c being a constant independent of R. Then the shift of the growth curves with the change of R ratio is described only by one parameter m ($0 < m < 1$) both for positive and for negative values of R. It means that the crack closure models are very important for explanation and deep study of fatigue crack growth mainly in negative R region but play no crucial role in a phenomenological description of the growth in the case of short-term tests in non-aggressive media.

1. Introduction

The NASGRO is a commercial complex of very sophisticated and deeply developed computer programs covering all necessary procedures dealing with the growth of long fatigue cracks, including extensive database of experimentally determined fatigue crack growth curves for various structural materials. Some of the parts of the NASGRO program are freely accessible as a demoversion including reference manual [1]. Here so-called NASGRO equation can be found, which describes fatigue crack growth curves, i.e. the dependence of crack length increase per one fatigue cycle da/dN on stress intensity factor range ΔK. For special case of repeating tension (i.e. for stress intensity parameter $R = 0$) it can be written in the form

$$\frac{da}{dN}(\Delta K) = C\Delta K^n \frac{\left(1 - \frac{\Delta K_{th}}{\Delta K}\right)^p}{\left(1 - \frac{\Delta K}{K_c}\right)^q} . \qquad (1)$$

It contains six parameters: C and n are connected with the Paris straight line, ΔK_{th} is threshold stress intensity factor range, K_c is critical stress intensity, and p, q are exponents describing the bends of the curve from the Paris straight line to ΔK_{th} and K_c, respectively.

In 1999 one of authors of this contribution published an equation for the description of fatigue crack growth curves [2] which can be rewritten into the form

$$\frac{da}{dN}(\Delta K) = C\Delta K^n \frac{1 - \left(\frac{\Delta K_{th}}{\Delta K}\right)^p}{1 - \left(\frac{\Delta K}{K_c}\right)^q} . \qquad (2)$$

This form is very similar to the NASGRO equation and includes the same parameters having nearly the same meaning as in the NASGRO equation. Both equations describe all three regions of a fatigue crack growth curve: region I – initiation, region II – stable propagation, and region III – unstable fracture. The equations (1) and (2) are written in very useful forms in which the description of single regions is separated: the term before the fraction describes the Paris straight line (if the log-log fit is considered) typical for the stable propagation region, the numerator of the fraction describes the bend of a curve in the initiation region to the threshold stress intensity factor range, and the denominator of the fraction describes the region of unstable fracture where the growth rate increases over all limits. These special forms of the equations can be used as a *building kit*, because they allow simple adjustment for the cases when only two of all three regions are covered with experimental results and thus only the terms corresponding to the mentioned regions are included into the equations. E.g., the equations only for regions II and III are

* **Jan Kohout[1], Stanislav Věchet[2], Vojtěch Hrubý[3]**
[1]Department of Mathematics and Physics, Military Technology Faculty, University of Defence, 612 00 Brno, Czech Republic, E-mail: Jan.Kohout@unob.cz
[2]Institute of Materials Science and Engineering, Faculty of Mechanical Engineering, Brno University of Technology, 616 69 Brno, Czech Republic
[3]Department of Mechanical Engineering, Military Technology Faculty, University of Defence, 612 00 Brno, Czech Republic

$$\frac{da}{dN}(\Delta K) = C\Delta K^n \frac{1}{\left(1-\frac{\Delta K}{K_c}\right)^q} \quad \text{or} \quad \frac{da}{dN}(\Delta K) = C\Delta K^n \frac{1}{1-\left(\frac{\Delta K}{K_c}\right)^q}. \tag{3}$$

For various values of parameter R the NASGRO equation is written in the form [1]

$$\frac{da}{dN}(\Delta K, R) = C\left[\frac{1-f(R)}{1-R}\right]^n \Delta K^n \frac{\left(1-\frac{\Delta K_{th}}{\Delta K}\right)^p}{\left[1-\frac{\Delta K}{K_c(1-R)}\right]^q}, \tag{4}$$

where $f(R) = K_{op}/K_{max}$ is crack opening function generally expressed by a polynomial of R with rather complicated coefficients. Only in special cases it is the linear function of R or directly equals to R (see [1]). Generalization of Eq. (2) was based on the Walker approach [3]. Walker introduced so-called effective value of stress intensity factor range $\Delta\overline{K}$ given by the relation

$$\Delta\overline{K} = K_{max}(1-R)^{\gamma} = \Delta K(1-R)^{\gamma-1} \tag{5}$$

from which the stress intensity factor range ΔK for various values of parameter R can be recalculated according to the relation

$$\Delta K(R) = \Delta K(0)(1-R)^{\gamma-1} = \Delta K(0)(1-R)^m. \tag{6}$$

The exponents γ and m used in the recalculations can gain values between 0 and 1. The generalization of Eq. (2) for various loading cycle asymmetry can be made replacing $\Delta K = \Delta K(0)$ by the term $\Delta K(R) = \Delta K(1-R)^{-m}$ with the exception of the denominator of the fraction where ΔK must be replaced by $K_{max} = \Delta K/(1-R)$ similarly to the generalization of the NASGRO equation (unstable fracture appears when the maximum stress intensity K_{max} increases close to the critical stress intensity K_c). The threshold stress intensity factor range $\Delta K_{th0} = \Delta K_{th}(0)$ for $R = 0$ and critical stress intensity Kc are independent of R and therefore they remain without any change. Thus the following equation

$$\frac{da}{dN}(\Delta K, R) = C\left[\frac{\Delta K}{(1-R)^m}\right]^n \frac{1-\left[\frac{\Delta K_{th0}(1-R)^m}{\Delta K}\right]^p}{1-\left[\frac{\Delta K}{K_c(1-R)}\right]^q} \tag{7}$$

was obtained, see [2]. Considering the rather complicated expression of $f(R)$ function, this equation is considerably simpler than the corresponding NASGRO equation (4). On the other hand, Eq. (4) could have a little wider ability to fit various courses of fatigue crack growth curves.

The curves of fatigue crack growth are usually plotted in a log-log coordinates in which the Paris-Erdogan equation is presented as a straight line. In one curve the crack growth rate changes by many orders (up to 10^6 times or even more) and it is usually determined with approximately constant variation (i.e. relative uncertainty). For this reason it is better to use not crack growth rate but its logarithm in regression.

2. Comparison of both equations for given loading cycle asymmetry

Eqs (1) and (2) should be compared with respect to their ability to fit real experimentally measured fatigue crack growth curves. For comparison of Eqs (1) and (2) the curve published in [1] (Fig. 14 on p. 27) was used. The results of regression are presented in Fig. 1. Both regression curves are nearly indistinguishable in the interval of stress intensity factor range covered by the results of experimental measurements. The sum of squares of deviations for the NASGRO equation is higher by 5.3 % than for the new equation. It means that Eq. (2) is more suitable for regression but in fact this difference is not conclusive. A more substantial difference between both curves appears to be above the interval of the stress intensity factor range covered by the experimental results where the curves substantially diverge. This divergence can be presented by the values of critical stress intensity K_c determined by regression, i.e. (75.8 ± 48.6) MPa m$^{1/2}$ and (60.2 ± 6.2) MPa m$^{1/2}$ using Eq. (1) and Eq. (2), respectively. The standard deviations of K_c values differ by an order, which is a very conclusive argument. It can be concluded that the extrapolation behaviour of the new equation is substantially better than that one of the NASGRO equation.

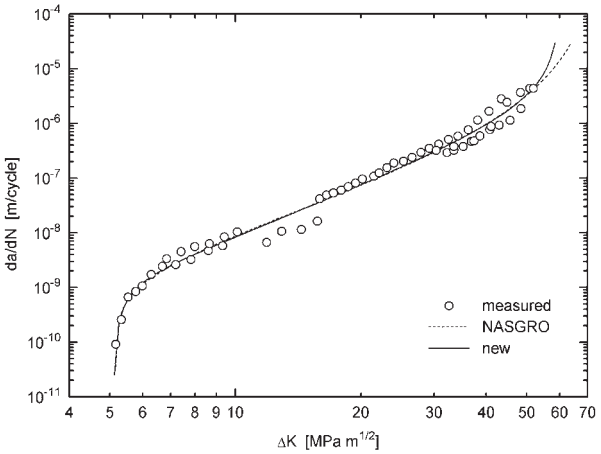

Fig. 1 Fatigue crack growth curve from [1] fitted using Eqs (1) and (2)

3. New equation for various loading cycle asymmetries

Direct comparison of Eqs (4) and (7) describing the fatigue crack growth curves for different loading cycle asymmetries is dif-

ficult just to the complexity of $f(R)$ function. Therefore, only the ability of Eq. (7) to fit the curves for different R will be verified. For this reason, the curves for the values of loading cycle asymmetry parameter $R = 0.1$ and 0.5 published by Forman and Hu [4] were used. The result of regression is presented in Fig. 2. It can be seen that the experimental points are successfully fitted by the curves and their shift can be described by the only parameter $m = (0.52 \pm 0.03)$.

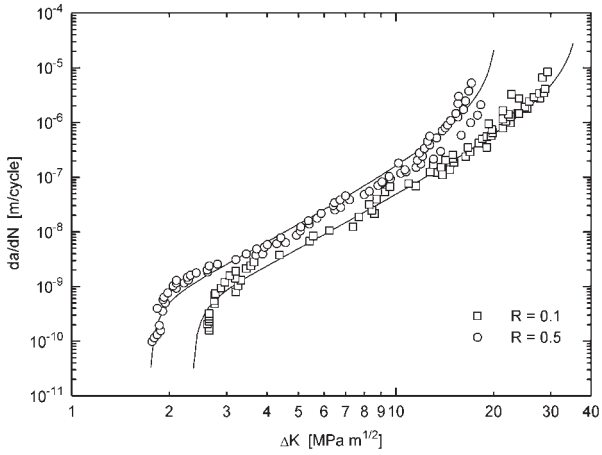

Fig. 2 Fatigue crack growth curves for different R values from [4] fitted using Eq. (7)

Validity of Eq. (7) can be questionable mainly in the case of negative values of loading cycle asymmetry parameter R when the closure of fatigue crack plays a crucial role. Fig. 3, presenting fatigue crack growth curves determined for values $R = 0, -0.43, -1$, and -2.33 by Klesnil and Lukáš [5, 6], however shows that the Walker approach expressed by Eq. (6) is very well applicable also for negative R values. For regression shown in Fig. 3 Eq. (7) was used in its simplified form

$$\frac{da}{dN}(\Delta K, R) = C\left\{\left[\frac{\Delta K}{(1-R)^m}\right]^n - \Delta K_{th0}^n\right\} \qquad (8)$$

which can be obtained from Eq. (7) using following simplifications: (i) the region III of unstable fraction is not considered (denominator in Eq. (7) is not used) and (ii) the equality $n = p$ is considered. For $R = 0$ Eq. (8) is identical with the Klesnil-Lukáš equation [7], which was originally derived for $R = -1$ and the stress intensity factor amplitude K_a. The fit based on Eq. (8) is presented in Fig. 3 by the dashed lines.

4. Exchange of variables in regression

The fatigue crack growth curve covering the whole interval of stress intensity factor range has two asymptotes $\Delta K = \Delta K_{th}(R)$ and $\Delta K = K_c(1 - R)$. The consequence of these vertical asymptotes is that $\Delta K_{th}(R)$ must be less than all values of ΔK and $K_c(1 - R)$ has to be greater than all values of ΔK. It means that, e.g., the minimum value of ΔK has unacceptably strong influence on $\Delta K_{th}(R)$ while the influence of all others can be negligible. This unpleasant feature of the $da/dN = f(\Delta K)$ regression can be avoided by the exchange of variables leading to the $\Delta K = f^{-1}(da/dN)$ regression. In the case of Eq. (8) the inverse function can be simply expressed in the form

$$\Delta K\left(\frac{da}{dN}, R\right) = (1 - R^{)m}\left[\frac{1}{C}\frac{da}{dN} + \Delta K_{th0}^n\right]^{1/n}. \qquad (9)$$

The fit based on Eq. (9) is presented in Fig. 3 by the full lines.

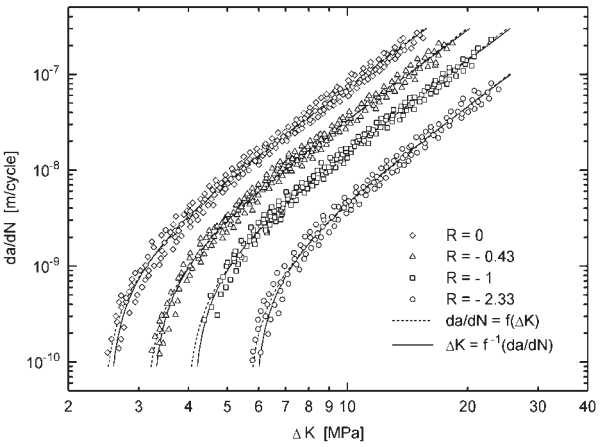

Fig. 3 Fatigue crack growth curves for different R values from [5, 6] fitted using Eqs (8) and (9)

Generally, however the inverse function is not always possible to express explicitly (see, e.g., Eqs (1), (2), (4), and (7)). Then, the inverse function should be calculated numerically using, e.g., the Newton method or the *regula falsi* method which can be simply implemented into a regression procedure. Unfortunately, some of the simple regression procedures use only explicitly expressible regression functions as a standard and implicitly given functions cannot be used or substantial complications are connected with their application. The comparison of regressions using the regression function $da/dN = f(\Delta K)$, see Eq. (7), and corresponding inverse function $\Delta K = f^{-1}(da/dN)$ is shown in Fig. 4 for the same set of experimental data as shown in Fig. 1. The *regula falsi* method was used for numerical calculation of inverse function because in comparison with the Newton method the derivative of the primary function is not required. Again, as the values of the stress intensity factor range change by more than one order and they are usually determined with an approximately constant variation, the logarithm of ΔK should be used in regression.

The difference between the curves in Fig. 4 is evident near the asymptotes, especially in the region of unstable fracture. From the point of view of regression the $\Delta K = f^{-1}(da/dN)$ fit is a little better (so-called *corrected index of determination* is equal to 0.9854 in this case compared with 0.9843 for the primary function). Unfortunately, the measurements were not performed sufficiently close to the upper asymptote and in such case the underestimation of K_c value is impending for the inverse function, cf. $K_c = (50.8 \pm \pm 4.2)$ MPa m$^{1/2}$ with $K_c = (60.2 \pm 6.2)$ MPa m$^{1/2}$ obtained for

the primary function. On the other hand, the accuracy in ΔK_{th} value determination is substantially decreased when the inverse function is used for regression (cf. $\Delta K_{th} = (5.22 \pm 0.39)$ MPa $m^{1/2}$ for the inverse function and $\Delta K_{th} = (5.11 \pm 0.03)$ MPa $m^{1/2}$ for the primary function in light of standard deviations).

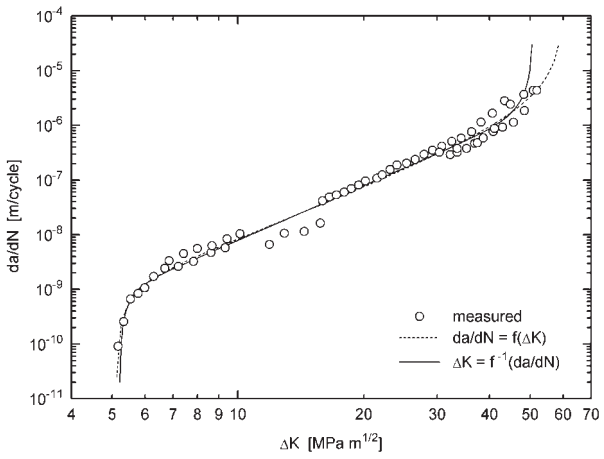

Fig. 4 Fatigue crack growth curves from [1] fitted using primary and inverse function, see Eq. (7)

5. Discussion

New equations for fit of fatigue crack growth curves, i.e. Eq. (2) for a given loading cycle asymmetry and Eq. (7) for various loading cycle asymmetries, cannot be compared with the NASGRO complex of computer programs, only with the NASGRO equations themselves. With regard to the fitting ability the new equations mostly led to slightly lower sum of squares in comparison with the NASGRO equation, at least in not very large set of growth curves studied up to now. It seems that the new functions can fit better the bends between the Paris straight line and vertical asymptotes. It is probably the reason why the new functions have better extrapolation behaviour.

The new equations can be used also for negative values of loading cycle asymmetry parameter, when the closure of fatigue crack appears. It means that the closure effects are not important for a phenomenological description of fatigue crack growth curves, their role is crucial only when the mechanisms of crack growth at crack closure are studied or modelled. On the other hand, the new equations cannot be probably used when the loaded sample is exposed in aggressive media or when long interruptions of loading are applied, but in such cases also the NASGRO equations can hardly be used universally.

The new and the NASGRO equations describing fatigue crack growth can be compared also from the viewpoint of standard deviations of the regression parameters. The parameter deviations corresponding to the new equations are mostly lower than deviations corresponding to the NASGRO equations. The only exception are parameters p and q describing the bends between the Paris straight line and asymptotes whose deviations are generally high. As an example of comparison the values of slope n of the Paris straight line in Fig. 1 were evaluated as follows: (3.09 ± 0.38) and $(2.20 \pm \pm 0.64)$ for the new and the NASGRO functions, respectively. This slope can also be determined in Fig. 1 graphically (using a tangent to the curve in the point of inflexion) with the result $n \approx 3.1$. It is apparent that n parameter of the new function corresponds very well to the slope of the Paris straight line. Similar conclusion cannot be however drawn for n parameter of the NASGRO function. It seems to be the most important advantage of the new function.

Parameter C in all equations describing the growth rate da/dN represents an extrapolated value of this rate for $\Delta K = 1$ MPa $m^{1/2}$ on the Paris straight line characterized by the Paris-Erdogan power law $da/dN = C\Delta K^n$. For most materials the value of 1 MPa $m^{1/2}$ lies rather far from the interval covered by experimental points and therefore parameter C is determined with a high standard deviation. Also in the case of parameter C the standard deviation corresponding to the NASGRO equation is higher than the deviation corresponding to the new equation. The modification of the Paris-Erdogan equation in the form

$$\frac{da}{dN}(\Delta K) = C_0\left(\frac{\Delta K}{\Delta K_0}\right)^n \qquad (10)$$

enables a substantial decrease of the standard deviation of parameter C_0 by a suitable choice of constant ΔK_0 ($C_0 = C$ for $\Delta K_0 = = 1$ MPa $m^{1/2}$) but also illusory correlation between parameters C and n discussed, e.g., in papers [8, 9] disappears. For the curve presented in Fig. 1 the lowest variation of parameter C_0 (i.e. the quotient of standard deviation and average value) 10.21 % was obtained for $\Delta K_0 \approx 9.68$ MPa $m^{1/2}$ in the case of the new function and 22.21 % for $\Delta K_0 \approx 8.60$ MPa $m^{1/2}$ in the case of the NASGRO function. Generally, for usual metal materials the value $\Delta K_0 \approx 10$ MPa $m^{1/2}$ can be recommended. The suitable value of ΔK_0 chosen from the interval of stress intensity factor range covered by experimental points decreases not only the variation of parameter C_0 but also the corresponding covariance coefficients, which simplifies non-linear regression calculations (at least it decreases the number of necessary iterations).

Existence of vertical asymptotes can lead to abnormal fits especially when the dispersion of experimental points closely to the asymptotes is larger. This problem can be solved by exchanging the variables (independent $\longleftrightarrow$ dependent). The inversion function can be explicitly written only for simplified equations; in other cases the numerical calculation of inverse function has to be implemented into a regression procedure using iterative numerical methods, e.g., using the Newton method or the regula falsi method. Derivative of the primary function necessary for the Newton method can be performed analytically (it is rather complicated for Eq. (7)) or calculated numerically when the choice of step length is important.

The application of the inverse function is useful when the dispersion of experimental points close to the asymptotes is large.

On the other hand, when the bend between the Paris straight line and the $K_c(1 - R)$ asymptote is not sufficiently covered with experimental points, the K_c value determined from regression using the inverse function can underestimate the *real* K_c value. Therefore, the choice between the primary and inverse functions should be performed responsibly and individually in each individual case.

Non-linear regression can be performed also using MS Excel software, which is part of Microsoft Office accessible in the majority of PCs all over the world. For this reason the Solver application is allocated, which contains a very effective minimization procedure giving directly the values of regression parameters. Standard deviations and regression using the numerically calculated inverse function are not directly available but they can be programmed using the Visual Basic implemented in MS Excel.

6. Conclusions

1. The new equations (for given loading cycle asymmetry as well as for various asymmetries) allow a slightly better fit of measured fatigue crack growth curves than the corresponding NASGRO equations. They have also better so-called extrapolation behaviour.
2. Parameter n in the new function is numerically equal to the slope of the Paris straight line. It is not valid for parameter n in the NASGRO function.
3. The shift of the curves with changing loading cycle asymmetry can be described by the single parameter m with values from the interval (0, 1). This Walker approach is successful for positive as well as for negative values of loading cycle asymmetry parameter R (probably only for non-aggressive media). It means that crack closure effects are not too important for a purely phenomenological description of fatigue crack growth curves.
4. In the case of large dispersion of experimental data close to asymptotes an abnormal fit can be obtained. In this case the exchange of variables can lead to a better fit.

Acknowledgments

Financial support of the Ministry of Defence of the Czech Republic within the research project MO0FVT0000404 is gratefully acknowledged. Moreover, the authors are grateful to all the authors (see [1, 4–6]) whose original experimental results were used in their considerations and calculations.

References

[1] FORMAN, R. G., SHIVAKUMAR, V., METTU, S. R., NEWMAN, J. C.: *Fatigue Crack Growth Computer Program "NASGRO" Version 3.0.* Reference Manual. NASA, Houston 2000 (see also www.nasgro.com).
[2] KOHOUT, J.: *International Journal of Fatigue 21*, 1999, p. 813.
[3] WALKER, K.: *ASTM STP 462*, 1970, p. 1.
[4] FORMAN, R.G., HU, T.: *ASTM STP 842,* 1984, p. 108.
[5] KLESNIL, M., LUKÁŠ, P.: *Engineering 22*, 1972, p. 269 (in Czech).
[6] KLESNIL, M., LUKÁŠ, P.: *Engineering 23*, 1973, p. 34 (in Czech).
[7] KLESNIL, M., LUKÁŠ, P.: *Engineering Fracture Mechanics 4*, 1972, p. 77.
[8] ROMVÁRI, P., TÓTH, L., NAGY, D.: *Strength Problems,* 1980, No 12, p. 18 (in Russian).
[9] BERGER, F., ZOUHAR, G., TEMPUS, G.: *International Journal of Fatigue 23,* 2001, p. 383.

https://doi.org/10.26552/com.C.2006.4.34-37

kamUNikácie
COMMUNICATIONS

Marián Buršák – Otakar Bokůvka *

INFLUENCE OF TECHNOLOGICAL FACTORS ON FATIGUE PROPERTIES OF STEEL SHEETS

Treatment technology can influence the fatigue process positively or negatively. The paper analyzes the influence of cold levelling of strips from coils of steel grade E 700 TS (R_e = 700 MPa) on the fatigue crack initiation and the fatigue limit under one-sided bending (R = 0.1). It indicates a positive effect on the above-mentioned characteristics if strips are loaded under one-sided bending from the side where residual compressive stress is formed during levelling.

By blasting a sheet made of steel grade 11 375.1, the fatigue limit under symmetrical flat bending was increased due to the hardening and formation of residual compressive stress. The paper also indicates risks connected with blasting, influencing the fatigue life.

Key words: *Internal stress, steel sheets, levelling, blasting, mechanical properties, fatigue limit.*

1. Introduction

The steel fatigue process is a function of a great number of external and internal factors, and their superposition significantly changes the fatigue resistance of material. The internal factors mainly include the structural state of material, which is given by the chemical composition and production technology of a product [1, 2, 11]. The relationship between the structure and mechanical properties have attracted a great attention, and the yield point R_e, at which macroscopic plastic deformation takes place, is often considered as a macroscopic characteristic of the structure [3, 4]. From the practical point of view, the fatigue limit of steels is expressed using the yield point or the tensile stress of material, $\sigma_C = k.R_m$, while the material constant k usually decreases with the growing steel strength, i.e., generally said, it is again a function of the steel structure [2, 5].

The treatment technology of a product usually results in a change of the properties given by the original structure of steel. During the cold levelling of strips from coils, on the upper side of the coil tensile stress and on the lower side compressive stress are formed, which significantly influence the initiation of fatigue damage and hence the service life of a product [6, 7]. During the surface treatment of a steel strip by blasting, compressive stress is also formed in the surface layer and tensile stress below this layer, while the deformation hardening of the surface layer and a change of the surface roughness take place. Some of the mentioned changes of the state decelerate (compressive stress, strain hardening) and others accelerate (increased roughness, tension stress below the strain-hardened layer) the fatigue process [8, 9]. It results from the above-mentioned that from the viewpoint of the fatigue life it is necessary to utilize their favourable effect in the production technology.

The paper aims to analyse the influence of residual stress after the cold levelling of steel strips, as well as the influence of blasting on the fatigue life, since flat products are mainly loaded by variable loading, during which material fatigue takes place.

2. Experiments and their analysis

Residual stress influences the fatigue properties of steel strips with higher yield points more intensively. Therefore the experiments were carried out on a strip, 8 mm thick, made of microalloyed steel E 7000TS. The surface treatment by blasting is usually carried out on steel sheets with higher plasticity, and for experiments was used 3 mm thick steel sheet made of 11 375.1 steel.

The structure of the microalloyed steel strip (C = 0.08%, Mn = 1.80%, Si = 0.41%, Al = 0.016%, Mo = 0.16%, Nb = 0.46%, Ti = 0.16%, V = 0.012%, Zr = 0.057% – wt.%) after controlled rolling is non-polyedric, formed by acicular ferrite, bainite and precipitates of microalloying elements. The structure of the steel strip made of 11 375.1 steel was ferritic-pearlitic, with the ferrite grain size of cca 0.012 mm, corresponding to the carbon content of 0.15%. The basic mechanical properties of the tested sheets are shown in Tab. 1.

Basic mechanical properties of tested steel strips Table 1.

Steel	Thickness [mm]	R_e [MPa]	R_m [MPa]	A_5 [%]
E 7000TS	8	703	832	20.4
11 375.1	3	208	400	32.0

After the cold levelling of the coil, residual tensile stress is formed on the upper side of the strip and residual compressive stress is formed on its lower side, as shown in Fig. 1. Using the tensometric residual stress measuring method, stress in the amount

* **Marián Buršák[1], Otakar Bokůvka[2]**
[1]Faculty of Metallurgy, Technical University of Košice, Letná 9, 042 00 Košice, Slovakia, E-mail: Marian.Bursak@tuke.sk
[2]Faculty of Mechanical Engineering, University of Zilina, Univerzitná 1, 010 26 Zilina, E-mail: Otakar.Bokuvka@fstroj.utc.sk

of cca 120 MPa was measured in the depth of 0.5 mm on the upper side of the strip and cca 70 MPa in the depth of 4 mm [10]. Test samples were taken from the strips in the rolling direction and notched test bars were made for fatigue tests (Fig. 2). The influence of residual stress on the fatigue crack initiation and the fatigue limit was tested under one-sided bending, with the asymmetry coefficient $R = 0.1$.

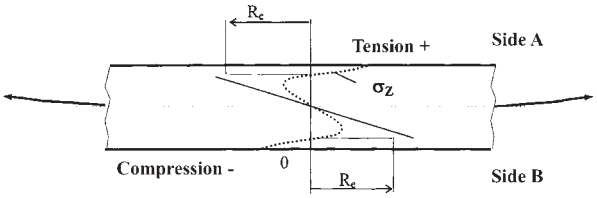

Fig. 1 Distribution of residual stress σ_z after levelling a coil

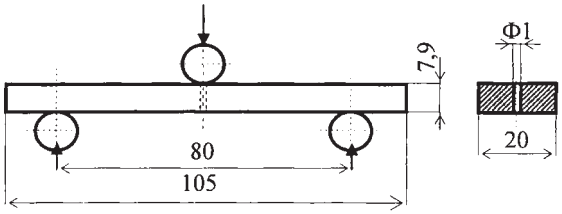

Fig. 2 Fatigue test bars made of E 700 TS steel strip

Test samples were taken in the rolling direction from the strips made of 11 375.1 steel and test bars were made for fatigue bending tests (Fig. 3). Some of these test bars were blasted on all the sides with steel granulate with the size of 0.9 mm under the impact angle of 75° and the pressure of 0.5 MPa. The result of blasting was surface strain hardening to the depth of 0.05 mm, while the microhardness close to the surface (0.01 mm) increased by 45 HV 0.01, when compared with the hardness of the basic material. Because of the thickness of the hardened layer, the X-ray diffraction method was used to determine residual stress in this layer. Using this method it was found out that before blasting the sample had tension stress on the surface (cca 79 MPa) and after blasting it had residual compressive stress of as many as 293 MPa. The blasting resulted in an increased roughness of the test bars. The ground test bars had the mean arithmetic deviation $R_a = 0.27$ μm and the highest profile height $R_z = 1.56$ μm, and the blasted test bars had $R_a = 9$ μm and $R_z = 45$ μm. Such prepared test bars

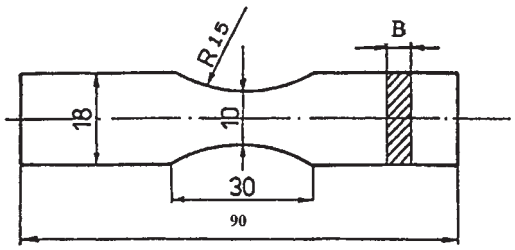

Fig. 3 Fatigue test bars made of 11 375.1 steel strip

were fatigue-tested under flat bending with the symmetric cycle ($R = -1$).

The results of the fatigue crack initiation and growth tests on notched bars (Fig. 2) are shown in Fig. 4. The bars were loaded under one-sided bending, with the upper stress levels from 700 to 550 MPa. The documented results indicate that when the test bar was loaded under one-sided bending on the upper side (designation A), the crack initiation period was significantly shorter comparing to the test bar loaded on the lower side (designation B). For example, at the stress of 700 MPa a crack 1 mm long is formed under loading on the side A after 54.000 cycles and on the side B after 107.000 cycles. This indicates an adverse effect of residual tension stress on the fatigue crack initiation.

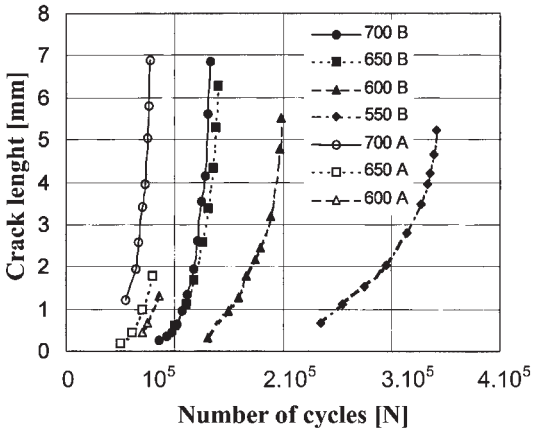

Fig. 4 Fatigue crack growth dependence on the number of cycles in E 700 TS steel at the stress of 700, 650, 600 and 550 MPa. A - Bending on the upper strip side, B - Bending on the lower strip side

Residual stress also influences the fatigue limit values, similarly as the fatigue crack initiation. Fig. 5 presents Wöhler curves, obtained on notched bars under one-sided bending on the upper

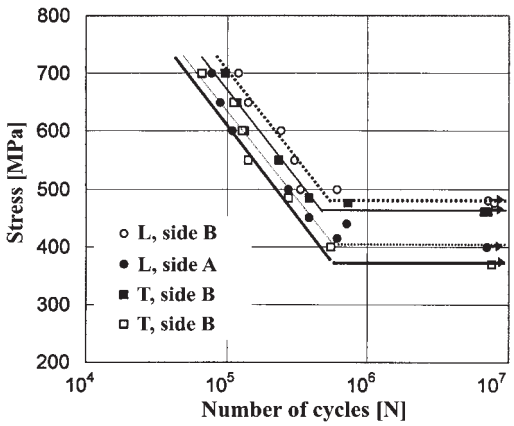

Fig. 5 Wöhler curves of E 700 TS steel for notched bars under one-sided bending (R = 0.1), L - rolling direction, T - transversal direction, A - Bending on the upper strip side, B - Bending on the lower strip side

side (A) and the lower side (B). The number of cycles to failure in the oblique section of the curve, as well as the value of the fatigue limit under bending σ_{Co} for 7.10^6 cycles, are lower in case of loading the bars on the upper side of the strip (A). The orientation of the bar with regard to the rolling direction has also a slight effect. The values of the fatigue limit under bending are lower in the transversal direction (T) than in the rolling (longitudinal) direction (L). This is, besides the structure, also caused by different values of residual stress in the L and T directions; residual stress is lower in the T direction. These facts could be utilized in practice, for example in the manufacture of flat products and their expected loading (containers, vehicles, etc.).

The experimental results of the influence of the blasted layer on the fatigue properties of the tested steel sheet are shown as Wöhler curves in Fig. 6. The fatigue limit of the blasted bars ($\sigma_{Co} = \pm 196$ MPa) is higher than the fatigue limit of the ground bars ($\sigma_{Co} = \pm 176$ MPa) by 11%, which generally applies in the area of the time fatigue limit under bending. The above-mentioned indicates a clear positive effect of blasting on the fatigue properties, which is a result of strain hardening and residual compressive stress in the blasted layer.

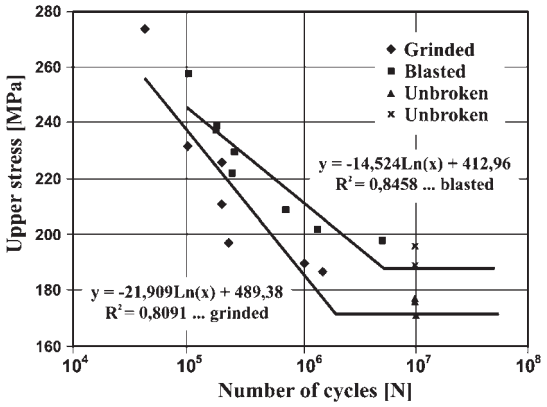

Fig. 6 Wöhler curves of steel grade 11 375.1 under flat bending ($R = -1$)

The analysis of the distribution of residual stress in the blasted layer (Fig. 7) also indicates certain risks, arising from the positive influence of blasting on the fatigue properties. Below the strain-hardened layer, residual tension stress is formed, which negatively influences the fatigue properties. Significantly increased surface roughness has also an adverse effect. In case of overloading (Fig. 6 at 260 MPa), the favourable effect of blasting is lost and French defect band of the blasted bars is obviously extended, which may result in a fatigue fracture at a lower stress than the experimentally determined σ_{Co} of the blasted bars.

Another risk of the decrease of fatigue resistance of blasted bars is shown by the results of the σ–N relationship, processed using non-linear regression, which also takes into account fatigue tests where the test bar did not fail [11]. Such results processed as the σ–N relationship are shown in Fig. 8. The fatigue limits at 10^7 cycles are comparable with the results obtained from Wöhler curve

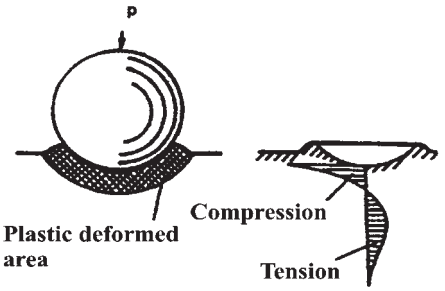

Fig. 7 Scheme of distribution of residual stress after blasting

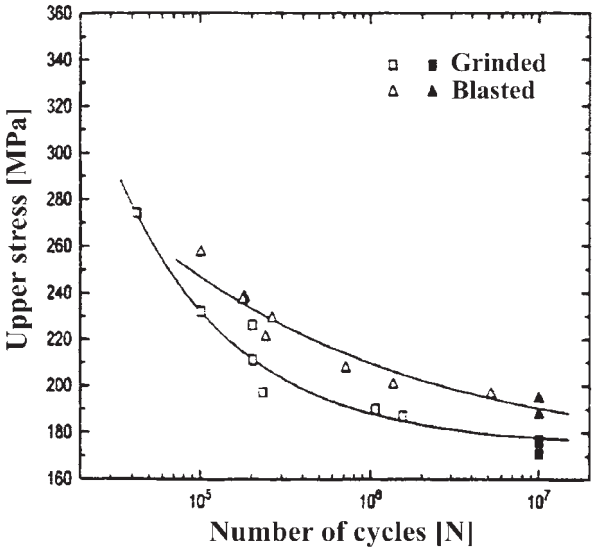

Fig. 8. Wöhler curves of 11 375.1 steel under flat bending, determined by non-linear regression analysis

(Fig. 6). For the ground bars $\sigma_C = \pm 178 \pm 3$ MPa, and for the blasted bars $\sigma_C = \pm 192 \pm 3$ MPa. It results from Fig. 8 that in the ground bars at 10^7 cycles the saturation of fatigue damage takes place, but in the blasted bars a damage accumulation takes place even after this number of cycles, and a decrease of the fatigue limit can be expected at a higher number of cycles. The non-linear regression also enabled us to determine the fatigue limit at an infinite number of cycles, σ_∞, and this theoretic value is 175 ± 3 MPa for ground bars, hence it practically does not differ from the σ_{Co} value, but for blasted bars it is 169 ± 15 MPa and is lower than σ_{Co}, and has also a significant dispersion variance. In accordance with the pieces of knowledge from [9], can be assume that the initiation of the fatigue failure was not on the surface, but below the blasted layer, where residual tension stress occurs. Its propagation towards the surface is also supported by unevenness of the blasted sheet surface. This creates conditions for fatigue failures at stress lower than σ_{Co}.

Figs. 9 and 10 document the fracture surfaces of ground bars and blasted bars at different stress values, and hence cycles to failure. The fatigue fracture of ground bars is initiated and propagates on the whole surface of the bar, while in blasted bars the

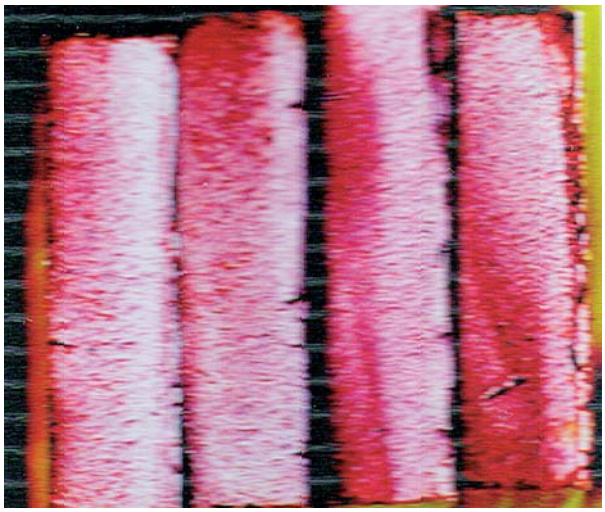

a) b) c) d)

Fig. 9 Fracture surfaces of ground bars of made of steel grade 11 375.1 under flat bending:
a) σ = 211 MPa, N = 202.600 cycles, b) σ = 197 MPa, N = 232.900 cycles, c) σ = 192 MPa, N = 944.000 cycles, d) σ = 190 MPa, N = 1.070.600 cycles

a) b) c) d)

Fig. 10. Fracture surfaces of blasted bars made of steel 11 375.1 under flat bending:
a) σ = 222 MPa, N = 246.200 cycles, b) σ = 230 MPa, N = 268.600 cycles, c) σ = 209 MPa, N = 733.100 cycles, d) σ = 202 MPa, N = 1.405.400 cycles

fatigue fracture is initiated preferably in certain points of the surface, which indicates an adverse influence of roughness on the fatigue process. These pieces of knowledge should be considered in calculations of the fatigue life of components with a strain-hardened functional surface.

3. Conclusion

The paper analyses the influence of residual stress and surface strain hardening of steel sheets on fatigue properties under bending. After the cold levelling of 8 mm thick steel made of E 700TS steel, residual tension stress is formed on one side of the sheet and residual compressive stress on the other side. These types of stress influence the fatigue process in such a way that on the side of residual tension stress under one-sided bending (R = 0.1) the fatigue crack initiation starts at a significantly lower number of cycles and the fatigue limit is also lower than in case of one-sided bending on the side with residual compressive stress.

The blasting of a 3 mm thick strip made of 11 375.1 steel results in the strain hardening of the surface layer with the thickness of about 0.5 mm, the formation of residual compressive stress, but also an increased surface roughness. The fatigue limit under symmetric bending at the number of cycles 10^7 (σ_{Co}) is higher for blasted surfaces (by about 11%) than for ground surfaces. It results from the analysis of fatigue tests that the theoretic fatigue limit (at an infinite number of cycles) of blasted sheets can also be at the same level or lower than that of ground sheets.

The presented results can be applied in practice when designing the production technology of flat products (orientation of the strip with regard to the loading method) and determining the fatigue life of strain hardened products.

References

[1] PUŠKÁR, A.: *Limit States of Materials and Components (in Slovak),* VEDA Bratislava, 1989
[2] TREBUŇA, F., BURŠÁK, M.: *Limit States, Fractures (in Slovak)*, Grafotlač Prešov, 2002, ISBN 80-7165-362-4
[3] PARILÁK, Ľ.: *Structure Matter of Mechanical and Fracture Properties (in Slovak)*, HP, HF TU Košice, 1992
[4] ŠTEFAN, B.: *Sheets Steel (in Slovak)*, 20, 1993, 16
[5] MICHEĽ, J., ČIŽMÁROVÁ, E., ORUŽINSKÁ, S.: *Metallic Materials (in Slovak)*, 3, 1999, 191
[6] MACKINNON, J. A., POOK, L. P.: *Experimental Techniques,* September, 1987, 15
[7] PEŠEK, L.: Kovine, Zlitine, Technologije, 3, 1996, No 3-4, 185
[8] MIHALÍKOVÁ, M., KOVALOVÁ, K., MICHEĽ, J.: *Materials Engineering (in Slovak)*, 11, 2004, 3, 13
[9] KOVALOVÁ, K., MAMUZIČ, I, BURŠÁK, M.: *Metallurgy (in English)*, 43, 2004, 4, 335
[10] HIDVÉGHY, J., BURŠÁK, M., VRCHOVINSKÝ, V.: *Acta Metallurgica Slovaca,* 5, 1, 1999, 165
[11] HÍREŠ, O.: *Physical Metallurgy of Steels and their Heat Treatment (in Slovak)*, GC TECH, Trenčín, 2006, ISBN 80-8075-099-8.

https://doi.org/10.26552/com.C.2006.4.38-41

kamUNikácie
COMMUNICATIONS

Marián Buršák – Ján Micheľ *

INFLUENCE OF ATMOSPHERIC CORROSION ON THE SERVICE LIFE OF STEEL SHEETS

The paper analyses the influence of the duration of atmospheric corrosion on basic mechanical and fatigue properties of steel sheet 2.16–4.46 mm thick, made of low-carbon steel with higher atmospheric corrosion resistance. A decrease of mechanical properties as a function of the exposure time is mainly due to a weight loss and the fatigue limit decrease under flat bending is due to increased surface roughness weathering steel too. The fatigue limit is a crucial characteristic for the service life of products, since after 5 years of exposure it decreased by 36%, while the ultimate tensile strength decreased by as little as 8%.

Key words: *Low-carbon steel, corrosion resistance, surface roughness, mechanical properties, fatigue limit.*

1. Introduction

Most metal structures and equipment (80%) work under atmospheric corrosion conditions. The atmospheric corrosion rate depends to a great extent on the presence of gaseous or dissolved solid impurities, mainly SO_2, H_2S, HCl, chlorides, etc. The chemical composition of steel also plays a significant role in assessing the atmospheric corrosion processes [1]. Therefore, low-carbon steels with increased atmospheric corrosion resistance of COR-TEN type were developed, which are currently manufactured under various trademarks. These steels are generally characterized as complex low-alloyed steels of Cu-Cr-Ni-P chemical concept, with an ability to create, under certain atmospheric conditions, a continuous and very adhesive layer of corrosion products on their surface. This layer effectively slows down the further corrosion process and has an aesthetic appearance [2, 3, 4].

As a result of corrosion, degradation of chemical properties of steels takes place. Under atmospheric corrosion conditions, degradation of mechanical properties is mainly caused by a weight loss (thickness) and a change of the surface relief (increased roughness). Literature shows that these changes are the most intensive at the beginning of the service life and with the exposure time the degradation intensity decreases and in steels with increased corrosion resistance it approaches to zero [3, 5, 6]. The loss of weight mainly decreases the calculated values of strength properties and the change of roughness mainly decreases plastic properties, but particularly the fatigue life [6, 7, 8, 9, 10]. The fatigue life of surface-damaged products is very susceptible to the method of variable loading [9]. For flat products, flat bending is the most frequent method of variable loading, where surface unevenness plays an important role, where fatigue failure is initiated.

The aim of the paper is to analyze the influence of atmospheric corrosion on basic mechanical properties and fatigue characteristics of hot rolled sheets made of low-carbon steel with higher atmospheric corrosion resistance.

2. Experiments and their analysis

Experiments were made on steel strips 2.16–4.46 mm thick, made of low-carbon steel with increased atmospheric corrosion resistance KONOX 345 T. Their orientation chemical composition is: C_{max} = 0.12%, Mn = 0.20–0.44%, Si = 0.25–0.55%, P = = 0.07–0.15%, S_{max} = 0.015%, Al_{min} = 0.02%, Cu = 0.25–0.60%, Cr = 0.50–1.2%, Ni_{max} = 0.65%. The microstructure of tested sheets is fine-grained, ferritic-pearlitic.

For experiments, tensile and fatigue test bars were made of the tested steel strips (Fig. 1). Some of these test bars were exposed to atmospheric corrosion for a period up to 5 years. On such prepared test bars, the surface roughness was measured and the metallographic analysis of the surface layer was made. The influence of the exposure time on mechanical and fatigue properties was investigated using tensile tests and fatigue tests under flat bending ($R = -1$) at the frequency of 35 Hz. The fatigue limit was determined for the number of cycles to failure 10^7.

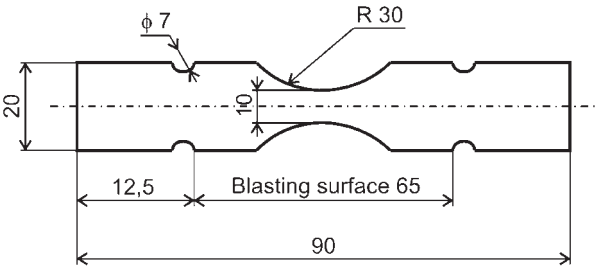

Fig. 1 Test bars for fatigue tests under flat bending

* **Marián Buršák, Ján Micheľ**
Faculty of Metallurgy, Technical University of Kosice, Letná 9, 042 00 Košice, Slovakia,E-mail: Marian.Bursak@tuke.sk

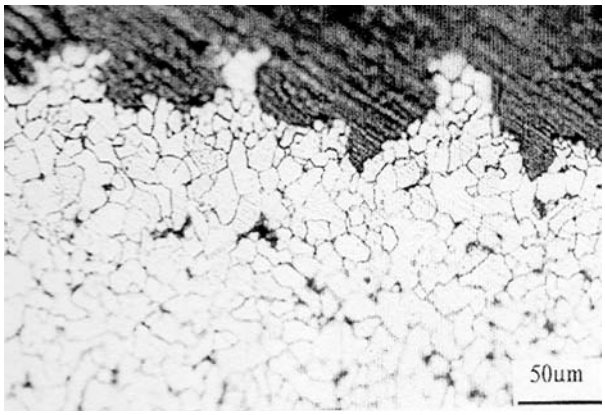

Fig. 2 Microstructure of a surface layer after 5 years exposure to atmospheric corrosion

As a result of atmospheric corrosion, a loss in weight and a change in the surface morphology take place. Figure 2 documents the surface morphology after 5 years of exposure to atmospheric corrosion and Fig. 3 documents the relationship between the change of surface roughness and the time of exposure of tested sheets to atmospheric corrosion, represented by the mean arithmetic deviation of the profile R_a and the highest height of the profile R_y, A significant change of the profile takes place within the first 2 years of exposure and then this change is mitigated, even saturation takes place. The above-mentioned analysis also resulted in the program of mechanical tests. Basic mechanical and fatigue properties were investigated on the initial state, after 2 years and after 5 years of exposure to atmospheric corrosion.

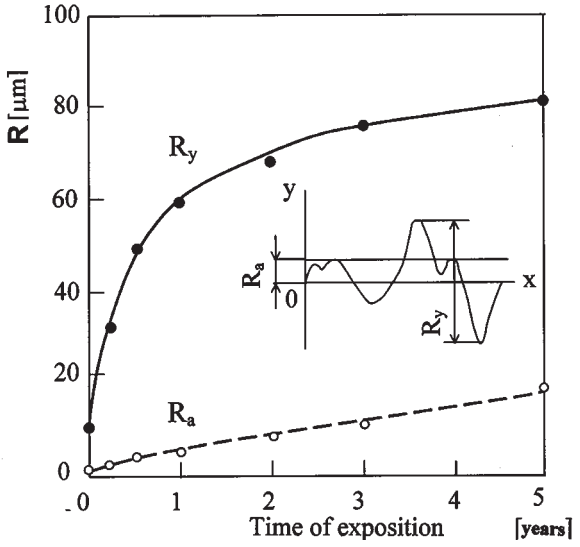

Fig. 3 Influence of the exposition time to atmospheric corrosion on surface roughness R_a, R_y

Figure 4 shows the relationships between the basic mechanical properties and the time of exposure to atmospheric corrosion, and Fig. 5 shows the relative decrease of the yield point R_{eCOR}/R_e and the elongation A_{80COR}/A_{80}, respectively, after exposure. The

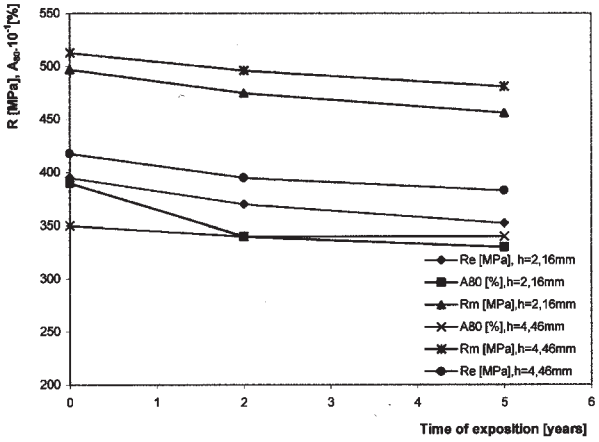

Fig. 4 Influence of the exposition time to atmospheric corrosion on basic mechanical properties

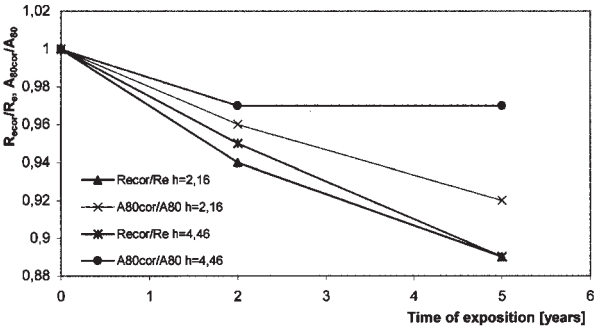

Fig. 5 Influence of the exposition time to atmospheric corrosion and the sheet thickness on the relative decrease of the yield point R_{eCOR}/R_e and the elongation A_{80COR}/A_{80}

results show that the basic mechanical properties decrease significantly during the first 2 years and then their decrease is less significant. The decrease of mechanical properties of the tested steel due to atmospheric corrosion is also influenced by the sheet thick-

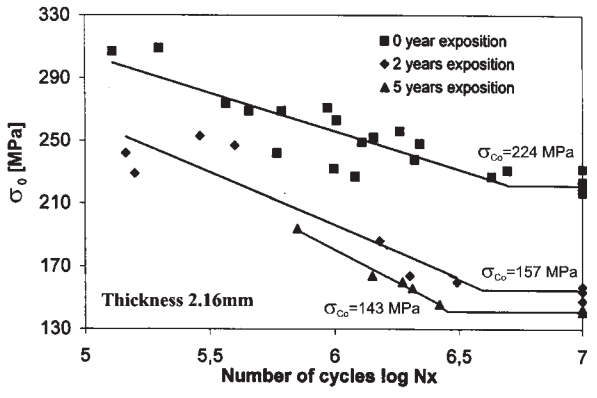

Fig. 6 Wöhler curves of the sheet 2.16 mm thick after 0 - 2 and 5-year exposition to atmospheric corrosion

ness; the less the thickness, the more significant the corrosion influence.

The results of the fatigue tests under flat bending at a symmetrical cycle are shown in Fig. 6 and Fig. 7. A decrease of the fatigue limit under flat bending after exposure to atmospheric corrosion when compared with the fatigue limit under bending of sheets in the initial state is shown in Fig. 8.

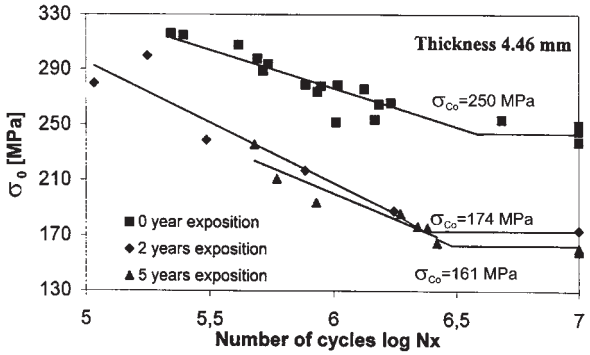

Fig. 7 Wöhler curves of the sheet 4.46 mm thick after 0 - 2 and 5-year exposition to atmospheric corrosion

The analysis of the results of fatigue tests under bending at a symmetrical cycle indicates that within the first 2 years of exposure to atmospheric corrosion the fatigue limit of tested sheets significantly decreases, and when this exposure time is exceeded, the decrease of the fatigue limit is less significant or the fatigue limit is stabilized. The experiments show (Fig. 8) that the sheet thickness, in fact, does not influence the decrease of σ_{Co} due to the time of exposure to atmospheric corrosion.

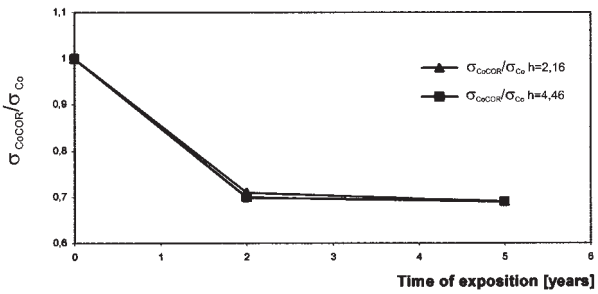

Fig. 8 Influence of the exposition time to atmospheric corrosion on the relative decrease of the fatigue limit under bending $\sigma_{CoCOR}/\sigma_{Co}$

The results of the influence of the atmospheric corrosion exposure time on the basic mechanical and fatigue properties of the tested sheets are in accordance with theoretical and practical knowledge. It is necessary to discuss factors that degrade the structural strength or the service life of flat products to a great extent. Under static loading conditions, a weight loss (sheet thickness) is a crucial factor. Since this loss under atmospheric corrosion conditions, regardless of the sheet thickness, is constant, the intensity of decrease of the structural strength of thinner flat products will be higher (the thickness dependence is exponential); for the tested sheet 2.16 mm thick the decrease of R_m due to atmospheric corrosion is 8% and for the sheet 4.46 mm thick this decrease is 6%. From this point of view, the elimination of atmospheric corrosion by an addition to the thickness is effective. Considering the high plasticity of the tested sheets, but also other sheets intended for the manufacture of flat products, a decrease of the elongation due to increased surface roughness by atmospheric corrosion does not have a significant practical importance.

The experimental results and literary knowledge indicate that under variable loading conditions the surface roughness is a crucial factor of degradation of properties due to atmospheric corrosion, which significantly increases during the first two years of exposure and is not dependent on the sheet thickness. The decrease of the fatigue limit of the tested sheets after two years of exposure by 30%, or after 5 years by 36%, is significant. The loss in weight is practically negligible from the viewpoint of its effect on the fatigue limit. The work [6] shows that the loss in weight after 5 years of exposure participated in a decrease of the fatigue limit by as little as 4%.

It results from the above-mentioned that the solution of the influence of atmospheric corrosion on the fatigue life by an addition to the sheet thickness is of a little effect. The solution consists in reducing the surface roughness of sheet (flat product), particularly its Ry value. From the viewpoint of the material design of a product, this means that we should choose a steel sheet grade that guarantees the formation of a uniform, continuous layer of corrosion products. Low-carbon steels with increased atmospheric corrosion resistance, and hence the tested steel KONOX 345 T, meet this condition to a certain degree. As a result of their complex alloying, under atmospheric corrosion conditions within two-three years a protective layer is formed, which, in fact, stops the corrosion process. The work [6] compares the degradation of the tensile fatigue limit at the max-to-zero cycle ($R = 0$) of steel with increased resistance to atmospheric corrosion 15 127.1 and unalloyed steel 11523.1. After 5 years of exposure, the fatigue limit for the number of cycles 10^7 decreased by 34% for steel 15 127.1 and by 40% for steel 11523.1. Under flat bending conditions, this difference is even higher.

Conclusion

The paper analyses the influence of the time of exposure to atmospheric corrosion (2–5 years) on the basic mechanical and fatigue properties of complex low-alloyed steel with increased resistance to atmospheric corrosion KONOX 345 T. The analysis of experimental results and literary knowledge gave the following conclusions:

- The tested steel, besides advantageous mechanical properties, also meets the condition of increased resistance to atmospheric corrosion. After 2 years of exposure, the loss in weight and the increase of surface roughness of sheet are stabilized, even stopped.
- The decrease of mechanical properties (R_e, R_m) as a function of the time of exposure to atmospheric corrosion is identical to

the course of the loss in weight; hence, the loss in weight is a crucial degradation factor. Since this loss in weight is not dependent on the sheet thickness, the decrease of mechanical properties decreases with a growing thickness.

- The decrease of the fatigue limit under flat bending ($R = -1$) as a function of the time of exposure to atmospheric corrosion is comparable with the course of the roughness profile height Ry. The roughness of the sheet surface is a crucial degradation factor, and hence the sheet thickness has only a slight effect on the decrease of the fatigue limit.

The decrease of the ultimate tensile strength due to atmospheric corrosion after five years of exposure was 8% for the sheet 2.16 mm thick and 6% for the sheet 4.46 mm thick, but the decrease of the fatigue limit under bending was as many as 36%. Since flat products (e.g. parts of vehicles, containers, etc.) work under variable loading conditions, when calculating their service life the degradation of the fatigue limit will be a crucial factor. From this point of view, the use of steels with increased resistance to atmospheric corrosion for products with a long service life has high economic gains in terms of cost of surface protection and its renewal. Also, higher mechanical properties of these steels make it possible to reduce the product weight.

References

[1] KOCICH, J., TULEJA, S.: *Corrosion of Metals (in Slovak)*, Alfa Bratislava, 1980
[2] KOLLÁR, J., ŠIMON, Á.: *Steel Sheets (in Slovak)*, 25, 1, 1996, 19
[3] LAPČÍKOVÁ, E.: *Metallurgical Letters (in Slovak)*, 19, 11, 1976, 815
[4] KOCICH, J., TULEJA, S.: *Korózna ochrana kovov Corrosive protection of Metals (in Slovak)*, Alfa Bratislava, 1989
[5] ŠEVČÍKOVÁ, J.: *METALLURGIST (in Czech),* 33, 6, 1983, 228
[6] MICHEĽ, J., MIHALIKOVÁ, M.: *Influence of corrosive enviroment on fatigue properties of steels,(in Slovak)*, In.: Letná škola únavy 2004, Zuberec-Roháče, sept. 2004, 62
[7] BURŠÁK, M. et al.: *Influence of rolling conditions and atmospheric corrosion on mechanical and fatigue properties of KONOX grade steel (in Slovak)*, In.: Valcovanie plechov za tepla, Stará Lesná, okt. 2000, P34-1
[8] MIHALÍKOVÁ, M., KOVALOVÁ, K., MICHEĽ, J.: *Material Engineering (in Slovak)*, 11, 3, 2004, 13
[9] KOVALOVÁ, K., MICHEĽ, J.: *Acta Mechanica Slovaca*, 8, 2004, 3, 113
[10] MAMUZIČ, I.: *Metallurgy (in English)*, 44, 2005, 4, 305

https://doi.org/10.26552/com.C.2006.4.42-46

kamUNikácie
COMMUNICATIONS

Stanislav Věchet – Jan Kohout – Klára Hanzlíková – Vojtěch Hrubý *

FATIGUE BEHAVIOUR OF NODULAR CAST IRON AT VARIOUS LOADING CYCLE ASYMMETRY

Fatigue behaviour of nodular cast irons is described in specialized literature quite well but the majority of fatigue tests in high cycle region has been made at symmetrical bending or at symmetrical tension-compression loading. The role of loading cycle asymmetry is very important because the fatigue limit of nodular cast irons is substantially influenced by mean static stress. Unfortunately, the number of papers describing the influence of mean static stress is quite low. The aim of the presented paper consists in presenting the results of long-term research of nodular cast irons at high cycle region at different loading cycle asymmetry. Several heats with various heat treatments leading to various structures of matrix were used for fatigue tests performed mainly at symmetrical tension-compression loading and at repeating tensile loading. From S–N curves the fatigue limits for 10^7 cycles were determined and then used for the calculation and construction of the Haigh and the Smith diagrams. Nodular cast irons seem to be more sensitive to mean static stress than structural steels. It was found that, in contrast to many papers, the dependence of upper stress on mean stress is not linear but parabolic with the exponent lower than 1 whose value is linear function of UTS.

1. Introduction

1.1. Nodular cast iron

Nodular cast iron and particularly its high-strength type called ADI (austempered cast iron) is very prospective structural material with worldwide increasing production. In European industrially developed countries its production increases by 5 to 10 % every year, to the detriment of production of grey and tempered iron, cast steels, weldments, forgings etc. [1,2]. Besides excellent technological properties its advantage consists in favourable shape of graphite particles which, in comparison with other cast irons, does not decrease substantially the mechanical properties of metal matrix. Accordingly, various heat treatments are applied for nodular cast iron similarly as for usual structural steels and thus its mechanical properties can be changed in a wide range of strength and plasticity. Variability in the microstructure of cast iron matrix is even substantially wider than in the microstructure of steels because the graphite particles can work as *stocks* of carbon and, therefore, in one heat of cast iron wide range of ferritic-pearlitic mixtures can be obtained from purely ferritic to nearly purely pearlitic matrix.

Nodular cast iron can be used for many industrial components as e.g. gear wheels, valve levers of diesel engines, crankshafts, piston rods etc. Considerable part of its production is applied in military industry, above all for the details of military vehicles and some types of armour. Most of these products are loaded statically as well as dynamically and, therefore, the crucial role in degradation processes is played by mechanical fatigue. Relatively high number of data dealing with fatigue behaviour of nodular cast iron, which have been published, can be used only in a limited extent because they are neither complete nor uniform, sometimes they are even contradictory. It is a consequence of the fact that various test devices and various test bars have been used for fatigue tests performed according to different test procedures. Also different data processing of fatigue results has been applied, e.g. fit procedures of S–N curves including various numbers of cycles to fracture defining fatigue limit. Moreover, most high-cycle fatigue tests leading to determination of S–N curves and fatigue limits have been performed at symmetrical bending or at symmetrical push-pull loading. The influence of various asymmetry of loading cycle on fatigue behaviour of nodular cast iron has not been studied sufficiently widely in spite of the fact that fatigue limit of nodular cast iron depends very strongly on a static tensile stress component of the total loading stress.

1.2. Influence of loading cycle asymmetry

The value of fatigue limit is a function of loading cycle asymmetry and it increases or decreases according to the sign of mean stress. This fact is usually presented by the Smith or the Haigh diagram. While the Smith diagram expresses the dependence of extreme stresses of loading cycle (i.e. upper stress σ_h and lower stress σ_n) on mean stress σ_m of loading cycle, the simpler Haigh diagram determines the relation between the stress amplitude σ_a and the mean stress σ_m. Both diagrams are mostly drawn for the number of cycles to fracture corresponding to the fatigue limit (usually 10^7 cycles), but also the families of curves for various cycle numbers are presented.

For a simple estimation of the shape of both diagrams several relations were proposed describing the dependence of the maximum

* **Stanislav Věchet[1], Jan Kohout[2], Klára Hanzlíková[1], Vojtěch Hrubý[3]**
[1]Institute of Materials Science and Engineering, Faculty of Mechanical Engineering, Brno University of Technology, 616 69 Brno, Czech Republic, E-mail: vechet@umi.fme.vutbr.cz
[2]Department of Mathematics and Physics, Military Technology Faculty, University of Defence, 612 00 Brno, Czech Republic
[3]Department of Mechanical Engineering, Military Technology Faculty, University of Defence, 612 00 Brno, Czech Republic

stress amplitude on the mean stress of loading cycle. A very often used type is

$$\sigma_a = \sigma_C \left[1 - \left(\frac{\sigma_m}{R_m} \right)^{\alpha} \right] \quad (1)$$

with various values of exponent α, which cover the range from 1 to 2 for most structural materials [6]. For $\alpha = 1$ typical for high-strength steels and some types of cast irons with lamellar and nodular graphite the linear Goodman relation is obtained. The Gerber quadratic parabola for $\alpha = 2$ is valid for low carbon, unalloyed or low alloyed steels.

The contribution presents the results of long-term research of high-cycle fatigue behaviour of several types of nodular cast iron with emphasis on various asymmetry of a loading cycle.

2. Experiments

Three heats of nodular cast iron marked 0, 13 and 15 were used for fatigue tests [3]. Heats 0 and 15 were not alloyed, heat 13 was alloyed with Cu. Chemical composition of all three heats is given in Table 1. Heats 13 and 15 were heat treated in various ways and thus eight different matrices were obtained. Their marks consist of letters meaning heat treatment and of numbers meaning basic heat, e.g. BU13 means ADI with upper bainite matrix made of heat 13.

Chemical composition of studied nodular cast irons (in wt %) — Table 1

Heat	C	Si	Mn	P	S	Mg	Cu
0	3.26	2.06	0.11	0.020	0.008	0.057	-
13	3.43	2.55	0.56	0.055	0.016	0.093	0.61
15	3.46	2.10	0.25	0.047	0.002	0.058	-

Feritization annealing was applied to heat 0 to obtain purely ferritic microstructure marked F0. Heats 13 and 15 were used as cast and marked as P13 (nearly purely pearlitic structure) and FP15 (ferritic-pearlitic structure). Isothermal transformation of heat 13 led to upper bainite BU13. Four matrices were obtained by heat treatment of heat 15: pearlite P15 by normalization annealing and upper bainite BU15, transient bainite BT15, and lower bainite BL15 by isothermal transformation.

Ferritization and normalization annealing was performed in electric muffle furnace. Heat treatment conditions are presented in Table 2. Austempering of ADI was performed in electric crucible furnaces. Austenitization was made at 900 °C during 1 hour in GS530+C3 salt bath, isothermal transformation was made at 400 (BU), 350 (BT) and 300 °C (BL) in AS140 salt bath. The dwells at transformation temperatures were chosen from a very wide temporal range 2 minutes to 25 hours to obtain the structure with maximum elongation to fracture [4]. Transformation conditions are given in Table 3.

Structures and heat treatment conditions of ferritic-pearlitic nodular cast irons — Table 2

Material	Graphite particles		Matrix	Heat treatment
	shape	size [μm]	ferrite/pearlite [%]	conditions
F0	VI	30 - 60	100/0	ferritization annealing 870 °C, 11 hours, furnace
P13	VI, V	30 - 60	4/96	as cast
FP15	VI, V	30 - 120	55/45	as cast
P15	VI, V	30 - 120	0/100	normalization annealing 900 °C, 1 hour, air

Metallographic samples were prepared by standard procedure using heads of test bars after mechanical tests. The shape and size of graphite particles were determined using cuts before etching (VI means perfectly globular and V imperfectly globular grains). After etching in so called Nital 2% (solution of nitric acid in ethanol) the content of ferrite and pearlite in structure was evaluated. For observation of structure the Zeiss-Neophot 21 light microscope was used. Retained austenite in austempered matrix was determined using X-ray quantitative phase analysis in heads of cylindrical test bars, which were not deformed and their original structure was not changed by possible transformation of retained austenite due to tensile loading. Resulting structures are described in Table 2 (ferritic and pearlitic structures) and in Table 3 (austempered structures). Microstructure of ADI transformed at 400 °C is presented in various magnifications in Fig. 1 to 3.

For the determination of basic mechanical properties (yield stress $R_{p0.2}$, ultimate tensile strength R_m, elongation to fracture A_5 and reduction of area Z) at static tensile loading three or four

Structures and heat treatment conditions of austempered nodular cast irons — Table 3

Material	Graphite particles		Matrix	Transformation	Transformation
	shape	size [μm]	austenite [%]	temperature [°C]	dwell [min]
BH13	VI, V	30 - 60	41.9	400	50
BH15	VI, V	30 - 120	34.4	400	40
BP15	VI, V	30 - 120	19.9	350	100
BD15	VI, V	30 - 120	9.5	300	60

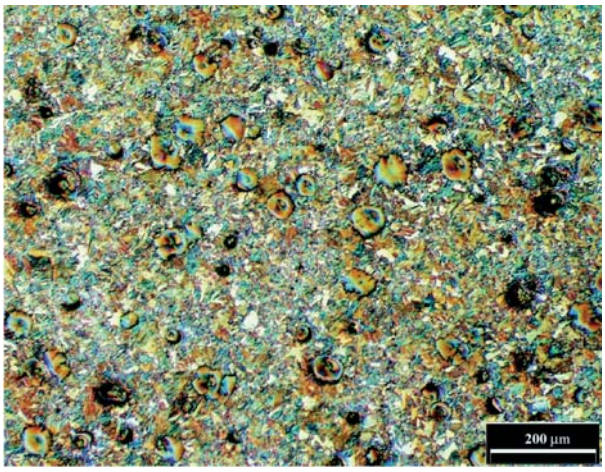

Fig. 1 Structure of ADI transformed during 40 minutes at 400 °C. (Nital etching, the Nomarski method, actual magnification 100 x)

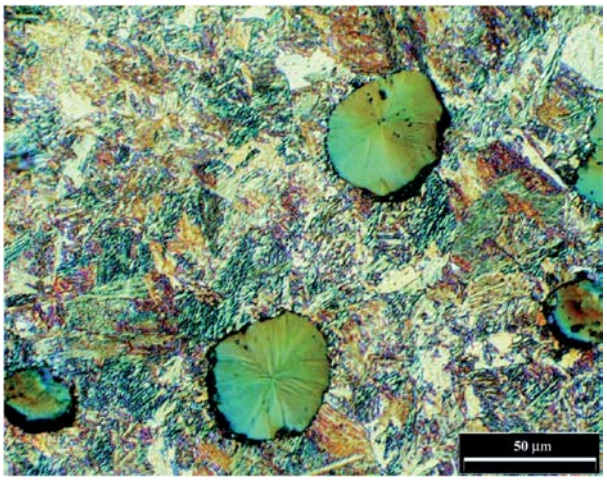

Fig. 2 Structure of ADI transformed during 40 minutes at 400 °C. (Nital etching, the Nomarski method, actual magnification 500 x)

cylindrical test bars with a diameter of 6 mm and length of 30 mm were used, see Fig. 4. The tests were performed using Zwick 1478 testing device at room temperature, with crosshead velocity of 1 mm/min (corresponding strain rate is about $5 \cdot 10^{-4}\ \mathrm{s}^{-1}$).

Fatigue properties were evaluated by determination of S–N curves and fatigue limits. Fatigue tests were performed on the Amsler high-frequency pulsator (frequency of 180 Hz, room temperature) at symmetrical push-pull loading ($R = -1$) and repeating tension ($R = 0$, stress ratio R is equal to quotient of lower stress and upper stress of loading cycle). Each of S–N curves was determined using 12 to 15 test bars with a diameter of 7 mm, which were ground to surface roughness $Ra = 0.4\ \mu$m, see Fig. 5. S–N curves were fitted using nonlinear least square method with three-parameter regression function

$$\sigma(N) = aN^b + \sigma_\infty \qquad (2)$$

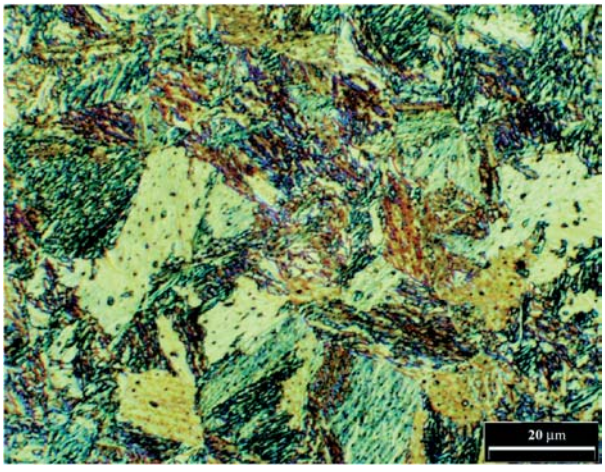

Fig. 3 Structure of ADI transformed during 40 minutes at 400 °C. (Nital etching, the Nomarski method, actual magnification 1000 x)

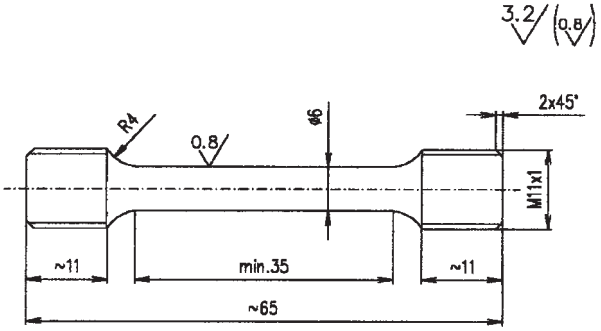

Fig. 4 Test bar for static tensile test (real size)

proposed by Stromeyer and recommended by Weibull [5], which describes very well fatigue behaviour of metals in high-cycle region. The fatigue limits $\sigma_C\,(R = -1)$ and $\sigma_{hC}\,(R = 0)$ for a basic number of cycles to fracture $N_C = 10^7$ were determined directly using the equation obtained by modification of Eq. (2)

$$\sigma(N) = (\sigma_C - \sigma_\infty) \cdot (10^{-7}\ N)^b + \sigma_\infty \qquad (3)$$

which contains fatigue limits as one of regression parameters.

3. Results

The results of static tensile tests together with fatigue limits for symmetrical push-pull loading and repeating tensile loading are presented in Table 4. Also the values of parameter α calculated according to the relation

$$\alpha = \frac{\log \dfrac{2\sigma_C - \sigma_{hC}}{2\sigma_C}}{\log \dfrac{\sigma_{hC}}{2R_m}} \qquad (4)$$

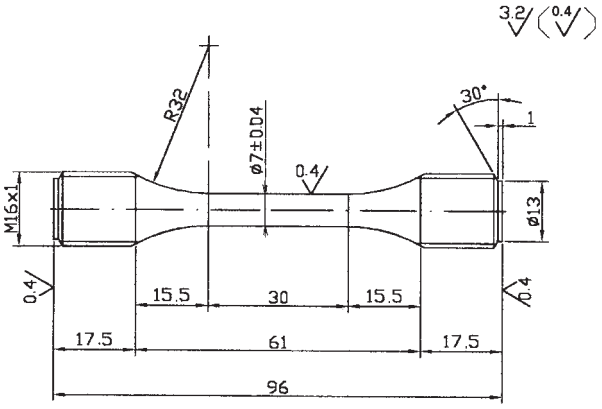

Fig. 5 Test bar for fatigue test (real size)

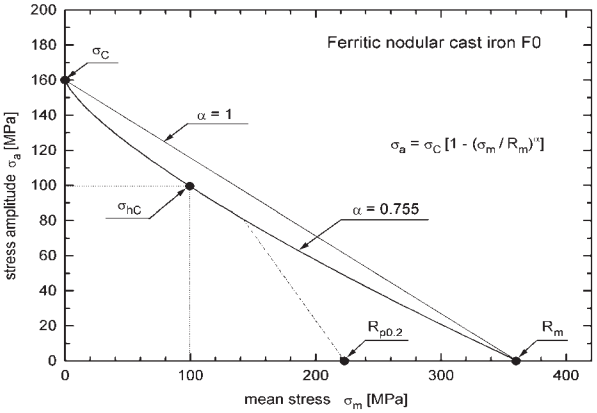

Fig. 6 The Haigh diagram for ferritic nodular cast iron F0

derived from Eq. (1) are added (natural as well as common logarithms can be used). Individual S--N curves are not presented due to the limited extent of paper. Only some examples of the Haigh diagram and only one example of the Smith diagram are shown, see Figs. 6 to 9.

4. Discussion

In papers [7–9] the Smith diagrams for various types of ferritic-pearlitic nodular cast iron are presented. Their straight-line shapes correspond to the linear Goodman relation. The results of our studies showed that for all 8 studied materials the general relation (1) must be used, see Figs. 6 to 8. The shape of all the Haigh diagrams is convex because the value of exponent α is lower than 1 ($0 < \alpha < 1$), see Table 4. This behaviour is common for all the studied irons with either ferritic-pearlitic or bainitic structure (in the last years called also ausferrite). The obtained results clearly show that it can be very inaccurate to use the linear Goodman relation for nodular cast irons, especially for ADI. This finding is inconsistent with the mentioned papers [7–9].

Static tensile and fatigue properties of nodular cast irons — Table 4

Mater.	$R_{p0.2}$ [MPa]	R_m [MPa]	A_5 [%]	Z [%]	σ_C [MPa]	σ_{hC} [MPa]	α [1]
F0	223	361	23.7	28.6	160	199	0.755
P13	417	654	3.2	2.0	236	317	0.786
BH13	645	881	5.4	3.4	236	290	0.528
FP15	316	505	16.3	13.5	186	248	0.782
P15	702	1030	4.6	3.5	231	333	0.700
BH15	809	1032	7.2	4.9	253	370	0.764
BP15	1036	1203	3.4	1.4	241	304	0.482
BD15	1348	1531	1.1	1.0	229	275	0.381

The values of exponent α significantly depend on the matrix of nodular cast iron. The highest values were found for ferritic-pearlitic irons in the range 0.700 to 0.786, in which also the value 0.764 for BU15 lies. The values for other types of ADI are lower; the lowest value 0.381 was obtained for BL15. The approximate dependence of this exponent on UTS as one of most important characteristics of the matrices was determined in the form valid for UTS expressed in MPa

$$\alpha(R_m) = 0.943 - 0.329 \cdot 10^{-3} R_m \quad \text{(for } R_m \text{ in MPa)}, \quad (5)$$

see Fig. 10. This relation explicitly shows that the value of exponent α is always lower than 1 and significantly decreases with the increasing UTS [10, 11]. Low α value means that the material is extremely sensitive to the increase of mean stress, especially in the range of small mean stresses.

5. Conclusions

On the basis of the study of fatigue behaviour of nodular cast iron with ferritic-pearlitic as well as bainitic matrices (ADI) obtained at various temperatures of isothermal transformation the following conclusions can be formulated:

1. The dependence of the loading cycle amplitude on the mean stress at push-pull loading has a convex shape for all types of nodular cast iron (ferritic-pearlitic as well as ADI).
2. The shape of the Smith and the Haigh diagrams cannot be approximated using the linear Goodman relation, but a general relation containing exponent α lower than 1 must be used.
3. The highest values of exponent α were obtained for ferritic nodular cast iron and for ADI transformed at 400 °C. The lowest value of exponent α was obtained for ADI transformed at 300 °C.
4. The value of exponent α decreases with the increasing UTS not only for ferritic-pearlitic nodular iron, but also for ADI. This relation can be approximately expressed by a linear equation.

Acknowledgments

Financial supports of the Ministry of Defence of the Czech Republic within the research project MO0FVT0000404 are gratefully acknowledged.

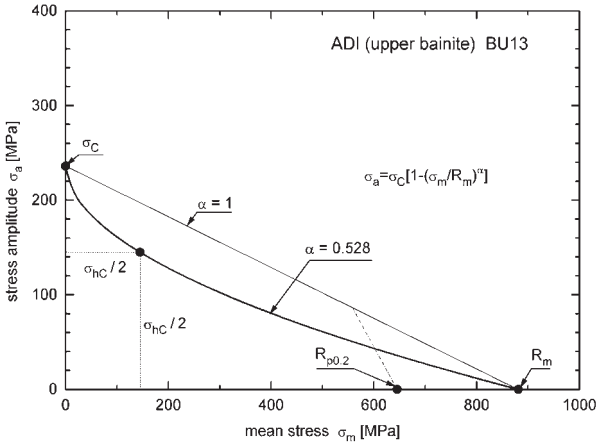

Fig. 8 The Haigh diagram for ADI BU13

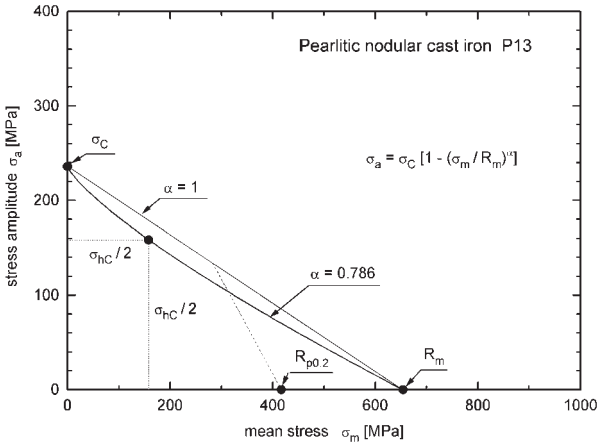

Fig. 7 The Haigh diagram for pearlitic nodular cast iron P13

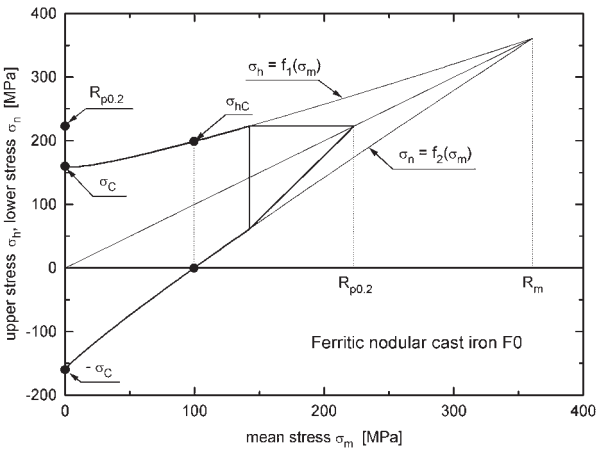

Fig. 9 The Smith diagram for ferritic nodular cast iron F0

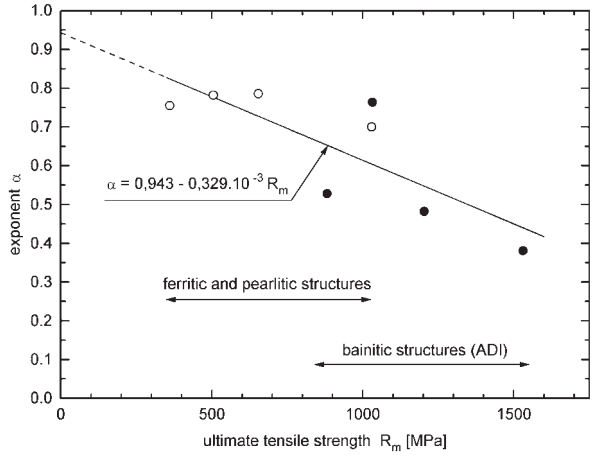

Fig. 10 Dependence of exponent α on ultimate tensile strength (○ - ferritic and pearlitic structures, ● - bainitic structures)

References

[1] KEOUGH, J. R.: *Foundry Management and Technology 123*, 1995, No. 11, p. 27.
[2] HARDING, R. A.: *Foundryman 86*, 1993, p. 197.
[3] VĚCHET, S.: *PhD Thesis, Brno University of Technology*, Brno 1989, (in Czech).
[4] DORAZIL, E.: *High Strength Austempered Ductile Cast Iron.* Academia and Horwood, Praha and Chichester 1991.
[5] WEIBULL, W.: *Fatigue Testing and Analysing of Results.* Pergamon Press, Oxford etc. 1961.
[6] DYLĄG, Z., ORŁOŚ, Z.: *Materials Fatigue and its Testing. SNTL*, Praha 1968 (in Czech).
[7] TAUSCHER, H.: *Dauerfestigkeit von Stahl und Gusseisen (4th edition).* VEB Fachbuchverlag, Leipzig 1982.
[8] NIETH, F., WIEGAND, H.: *Giesserei-Forschung 29*, 1977, p. 131.
[9] JAHN, J. *Giessereitechnik 30*, 1984, p. 71.
[10] VĚCHET, S., KOHOUT, J.: *Foundry Industry 48*, 2000, p. 37 (in Czech).
[11] VĚCHET, S., KOHOUT, J., BOKŮVKA, O.: *Fatigue Properties of Nodular Cast Iron*. EDIS, Žilina 2001 (in Czech).

https://doi.org/10.26552/com.C.2006.4.47-50

Klára Hanzlíková – Stanislav Věchet – Jan Kohout *

THE RELATION BETWEEN MICROSTRUCTURE COMPOSITION AND FATIGUE PROPERTIES OF ADI

The presented work deals with a high-strength variant of nodular cast iron, so-called ADI (austempered ductile iron). This material ranks among prospective structural materials and is more and more applied in all important branches of machine industry. Recently it has even been applied to castings for cyclically loaded components, i.e. gears and traversing wheels, crankshafts of motor-cars, vans and trucks, swivel pins, rail brakes, pressure pipes in oil industry etc. The microstructure composition of an ADI matrix consists especially of bainitic ferrite and stabilized austenite. However, in dependence on transformation dwell some amount of martensite can appear as well.

In this work the relation between mechanical properties and microstructure composition of the matrix mixture was studied in detail for the case of ADI transformed at 380 °C, with emphasis on fatigue properties.

1. Introduction

Austempered ductile iron used in an increasing measure for various cyclically loaded components [1, 2] is obtained by isothermal heat treatment of nodular cast iron. This way of heat treatment includes austenitization, isothermal transformation and final cooling usually in water. Heat treatment conditions influence the microstructure and mechanical properties of ADI differently: whereas the austenitization conditions (at usual temperatures in the range of 850 to 900 °C and typical dwell from 1 to 3 hours) play only a marginal role, the conditions of isothermal transformation (i.e. temperature and the length of isothermal transformation dwell) influence the matrix microstructure composition and, consequently, mechanical properties of ADI substantially [3, 4].

This work is focused on the relation between the matrix mixture composition and mechanical properties of ADI in dependence on isothermal transformation dwell. For the study an ADI obtained by isothermal transformation at the temperature of 380 °C was chosen. For determining the relation between the matrix mixture composition and mechanical properties of ADI the transformation dwells in the range of 2 to 540 minutes were used.

2. Experimental material and techniques

For the study an unalloyed nodular cast iron with chemical composition 3.56 wt. % C, 2.24 wt. % Si, 0.25 wt. % Mn, 0.02 wt. % P, 0.004 wt. % S and 0.054 wt. % Mg was selected.

Cylindrical testing bars for static tensile tests (with the initial diameter of 6 mm and gauge length of 30 mm) and for fatigue tests (with the initial diameter of 7 mm and effective length of 10 mm) were made from this material. Isothermal heat treatment was performed in the following steps: austenitization took 1 hour in NaCl salt bath at the temperature of 900 °C, isothermal transformation was performed at the temperature of 380 °C in AS 140 salt bath, final cooling was done in water. For studying the relation between the obtained matrix mixture composition and mechanical properties of ADI the isothermal dwells of 2, 5, 10, 25, 60, 120, 270 and 540 minutes were used.

For the microstructure evaluation, the metallographic cuts were prepared using the front faces of screw heads. Etched and not etched microstructures were observed by an OLYMPUS GX 71 light microscope with an Olympus DP 11 digital camera. The content of stabilized austenite and the analysis of graphite nodules were determined by an image analysis using LUCIA software of the Laboratory Imaging Company and ACC software of the SOFO Company.

The tensile tests were performed at the usual room temperature (i.e. 20 to 25 °C) on the testing device TIRATEST 2300 with a force range of 100 kN. The crosshead speed was 2 mm/min corresponding to the loading strain rate of 10^{-3} s^{-1}. Fatigue tests were performed at the room temperature as well, at symmetrical loading cycle, using an AMSLER 10 FHP 1478 high-frequency resonance pulsator at the test frequency of 201 Hz. Each of S–N curves was determined by the tests of 12 to 15 test bars. For the data regression by the least square method, the three-parametrical non-linear function (1) proposed by Stromeyer and recommended by Weibull [5] was used

$$\sigma(N) = aN^b + \sigma_\infty \,, \tag{1}$$

where as σ stress amplitude can be considered, a, b, and are parameters of the regression curve, and N is the number of cycles to the fracture.

* **Klára Hanzlíková[1], Stanislav Věchet[1] and Jan Kohout[2]**
[1]Institute of Materials Engineering, Faculty of Mechanical Engineering, Brno University of Technology, Technická St 2, CZ-616 69 Brno, Czech Republic
[2]Department of Mathematics and Physics, Military Technology Faculty, University of Defence, Kounicova St 65, CZ-612 00 Brno, Czech Republic

3. Results

The determined content of microstructure components, average values of static mechanical characteristics and fatigue limits for a reference number to the failure $N_C = 10^7$ are presented in Table 1 for all the transformation dwells.

Static mechanical properties, fatigue limits, fatigue ratio and content of stabilized austenite or martensite (if any) of ADI transformed at 380 °C in dependence on transformation dwell. Table 1

τ_t [min]	$R_p0.2$ [MPa]	R_m [MPa]	A_5 [%]	δ_C [MPa]	δ_C/R_m [-]	AS [%]	M [%]
2	-	138	0.1	-	-	18.3	66.8
5	562	698	0.3	-	-	28.5	34.3
10	739	885	0.6	-	-	31.6	4.8
25	773	1003	2.7	226	0.225	33.8	0
60	830	1051	5.2	249	0.236	34.8	0
120	853	1040	4.8	235	0.225	31.9	0
270	872	1091	4.6	234	0.214	25.4	0
540	899	1109	2.3	-	-	17.7	0

As Table 1 and Fig. 1 show, the composition of the microstructure mixture in the matrix of ADI transformed at 380 °C is substantially influenced by the isothermal transformation dwell. The microstructure consists especially of bainitic ferrite and stabilized austenite. However, for short transformation dwells also some amount of martensite appears. In the case of the shortest dwell, i.e. 2 minutes, it is even a dominant structural component (see Figs 1, 2).

During the transformation of austenite into bainitic ferrite, the surrounding non-transformed austenite is being enriched by carbon, which increases its stability. It leads to a gradual increase in the amount of this phase in the matrix with an increasing transformation dwell, which is to the detriment of martensite creation. For the transformation dwell of 25 minutes the stability of non-transformed austenite is sufficient and so the martenzitic transformation during subsequent cooling is wholly suppressed. Stabilized austenite reaches its maximum content for the transformation dwell of 60 minutes (Fig. 3). With further prolongation of the transformation dwell its amount starts to decrease and for the longest dwell only about half of the maximum content was determined in the matrix microstructure (Fig. 1). The results of the mechanical properties testing show that their values are substantially influenced by the isothermal transformation dwell (see Table 1 and Figs 4, 5, 6).

UTS values Rm and yield stress $R_p0,2$ increase in the whole range of studied dwells and reach their maxima for the longest dwells (see Fig. 4). The dependence of elongation to the fracture A_5 on the transformation dwell is different. Its value increases at first and reaches its maximum for the transformation dwell of 60 minutes. When this dwell length is exceeded, the value of A_5 changes

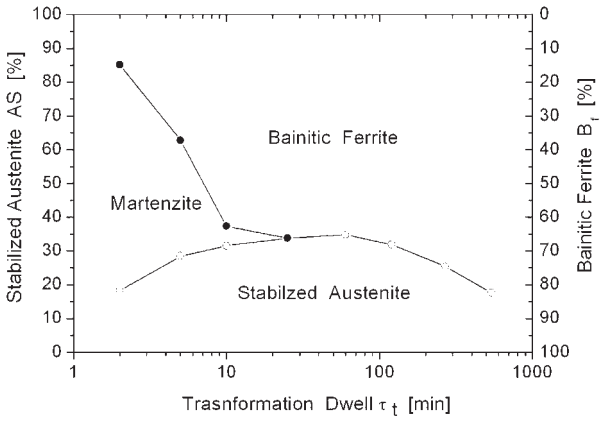

Fig. 1: The composition of the ADI microstructure in dependence on the transformation dwell.

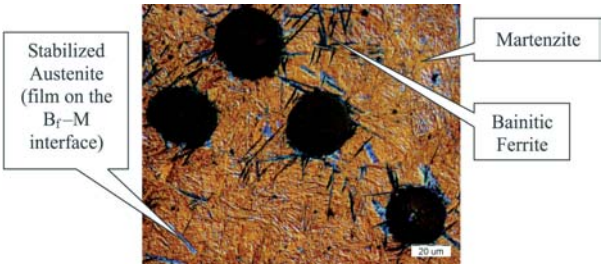

Fig. 2: The matrix microstructure of ADI for the transformation dwell of 2 minutes.

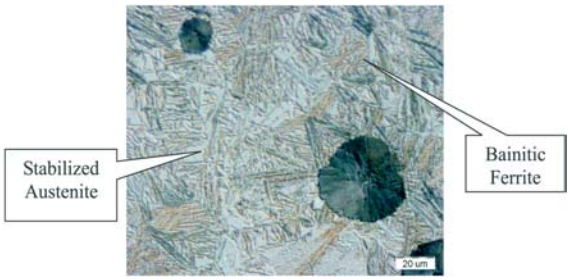

Fig. 3: The matrix microstructure of ADI for the transformation dwell of 60 minutes.

only slightly up to the dwell of 270 minutes, when it starts to decrease substantially (see Fig. 4).

In the previous work [4] as well as in the work [6], fatigue properties of nearly identical material changing with increasing transformation dwells were already studied. It was found out that the dependence of the fatigue limit σ_C on the transformation dwell is similar to the dependence of A_5. In the range of short dwells, the value of the fatigue limit σ_C gradually increases. After reaching its maximum, σ_C decreases but still remains in the interval of sufficient values. Then the substantial decrease was observed till the longest dwells were achieved. Because of time-consuming

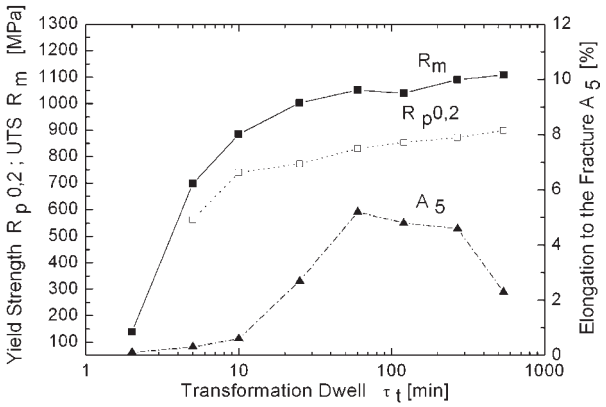

Fig. 4: Static mechanical properties of ADI in dependence on the transformation dwell.

fatigue tests, in this work only the range of transformation dwells from 25 to 270 minutes was tested, which was chosen pursuant to the previous studies. As Table 1 and Fig. 5 show, in the studied range of transformation dwells the value of fatigue limit σ_C increases at first. Optimum fatigue properties were reached for the transformation dwell of 60 minutes, which is also evident in Fig. 6. After reaching its maximum, σ_C slightly decreases but still remains in the range of sufficient values.

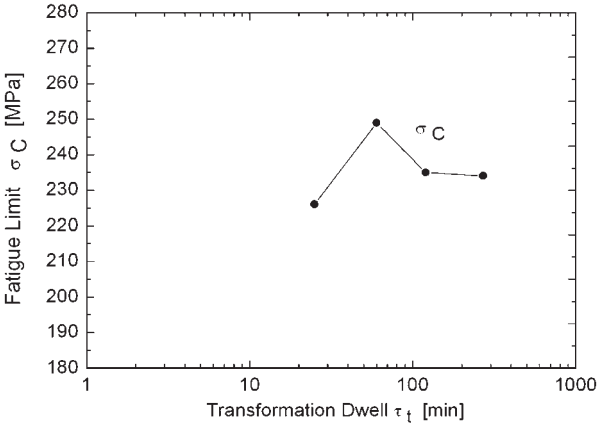

Fig. 5: The fatigue limit of studied ADI in dependence the transformation dwell.

Because of the similarity in the chemical composition of the studied material to the materials in previous studies, also the similarity in dependence of fatigue limit on the whole studied range of transformation dwells could be assumed. It follows from this similarity that in the range of 2 to 25 minutes fatigue limit will probably gradually increase with a transformation dwell prolongation and when the transformation dwell of 270 minutes is extended, the value of the fatigue limit will probably substantially decrease (approximately according to the Fig. 7).

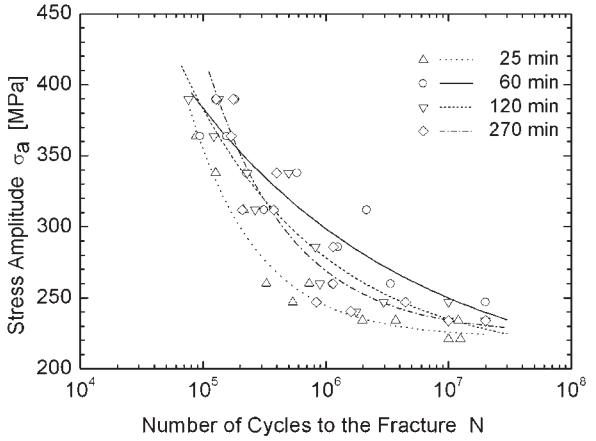

Fig. 6: The comparison of S-N curves for studied transformation dwells

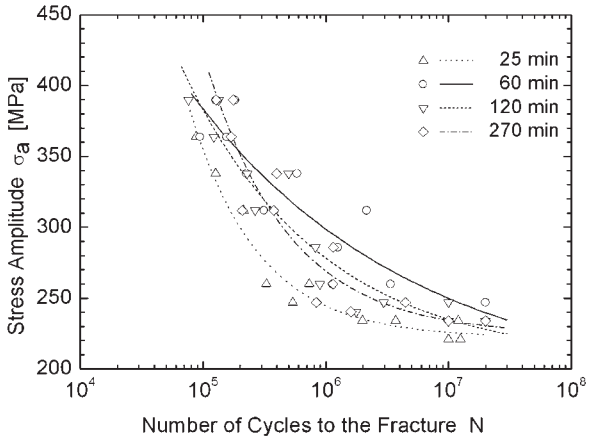

Fig. 7: The dependence of fatigue limit on the dwell at isothermal transformation of ADI obtained in previous study [4].

4. Discussion

Regarding the results of this study, it can be said that the values of mechanical properties depend on the structural matrix mixture. The ADI matrix consists especially of bainitic ferrite and stabilized austenite (Fig. 1). Bainitic ferrite is the carrier of strength in the ADI matrix, thus the UTS and yield stress reach their maxima when bainitic ferrite is a strongly prevalent structure component of the matrix (see dwells of 270 and 540 minutes in Fig. 4). Stabilized austenite is, on the contrary, the carrier of plasticity in the ADI matrix, thus the elongation to the fracture reaches its maximum for the transformation dwell when the matrix contains the maximum amount of stabilized austenite, i.e. for 60 minutes (see Fig. 8a). For longer dwells the elongation starts to decrease again as consequence of stabilized austenite decreasing due to its further transformation into bainitic ferrite.

The dependence of the fatigue limit on the transformation dwell coincides with the dependence of elongation to the fracture.

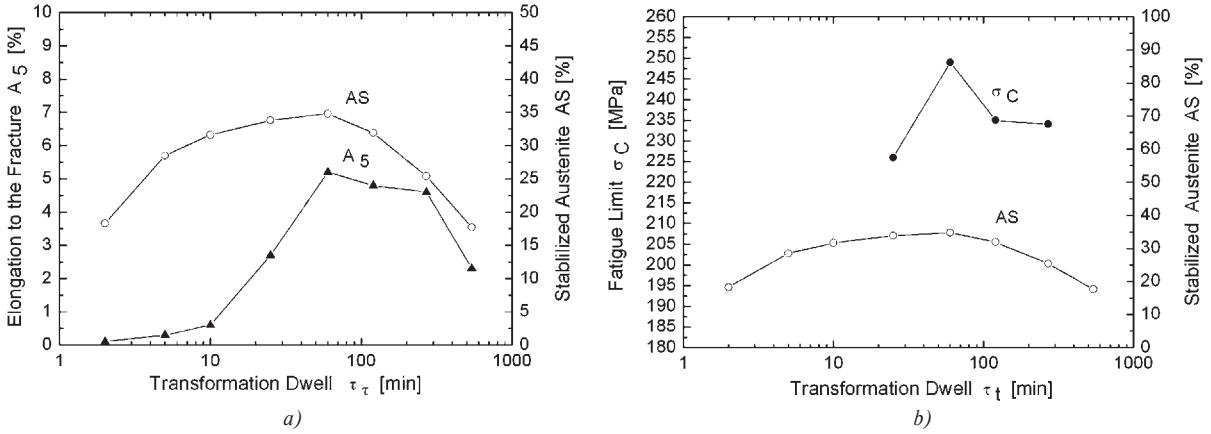

Fig. 8: The comparison of dependences of elongation to the fracture (a) and of fatigue limit (b) with the amount of stabilized austenite on the transformation dwell.

Thus its maximum value is also reached when the matrix contains the maximum amount of stabilized austenite, i.e. for the transformation dwell of 60 minutes (Fig. 8b). A high level of the fatigue limit appears also when austenite content starts to decrease. The reason of this effect is probably an increasing deformability of bainitic ferrite with a transformation dwell prolongation.

In the case of short dwells, i.e. in the range of 2 to 25 minutes, lower values of strength, plasticity and fatigue limit are caused by the presence of martenzite in the ADI matrix, which is a brittle and very hard phase and cause premature cracks of the testing bars.

5. Conclusions

The microstructure matrix composition and, consequently, mechanical properties are very substantially influenced by the dwell at temperature of isothermal transformation. In the case of ADI obtained by isothermal transformation at temperature of 380 °C, the optimum static mechanical properties were achieved for the transformation dwells in the range of 60 to 270 minutes. In the case of fatigue properties, the optimum range of transformation dwells is from 40 to 270 minutes approximately. To achieve the optimum combination of static and fatigue properties, the transformation dwell of 60 minutes should be used.

The results of the study show that in dependence on the transformation dwell, the ADI with high variety of mechanical properties can be obtained, thus ADI with combination of mechanical properties corresponding to a given application is possible to produce.

Acknowledgement

Financial supports of the Ministry of Defence of the Czech Republic within the research project MO0FVT0000404 are gratefully acknowledged.

References:

[1] HUGES, I. C. H.: *Brit. Foundryman,* vol. 74, 1981, p. 229
[2] KEOUCH, J. R.: *Foundry Management and Technology,* vol. 123, 1995, Nr. 11, p. 27
[3] VĚCHET, S., KOHOUT, J., HANZLÍKOVÁ, K.: *Fatigue Properties of ADI in Dependence on Isothermal Transformation Dwell.* Komunikácie, Žilinská univerzita v Žiline, 2/2004, p. 12–15. ISSN 1335-4205.
[4] VĚCHET, S., KOHOUT, J., HANZLÍKOVÁ, K.: *Influence of Isothermal Dwell on Tensile and Fatigue Properties of Austempered* Ductile Iron. Material Science Forum, volume 482/2005, ISSN 0255-5476, p. 371–374.
[5] WEIBULL, W.: *Fatigue Testing and Analysis of Results.* Pergamon Press, 1961.
[6] KOPAS, P., NOVÝ, F., BOKŮVKA, O.: *High-cycle Fatigue of High-strength Graphitic Cast Irons (in Slovak).* In Proceedings of Letná škola únavy materiálov 2004, VII. ročník. Zuberec-Roháče, Slovenská republika 6.–10. 9. 2004. Žilinská Univerzita v Žilině, p. 198–206. ISBN 80-80-70-283-7.

https://doi.org/10.26552/com.C.2006.4.51-56

Gejza Rosenberg *

INFLUENCE OF ANNEALING ON STRUCTURE AND FATIGUE PROPERTIES OF MICROALLOYED STEEL

Advanced microalloyed steels (HSLA steels) contain microstructural components whose mechanical properties can be altered by exposure to elevated temperatures, for example, in application of welding cycles. The objective of this paper is to identify the relative influence of annealing (annealing at 650°C for 25 min) on microstructure and fatigue properties variability of HSLA steels. The results obtained in this work suggest that in spite of no or very small positive effect of annealing on the fatigue limit of HSLA steels with no stress concentrator in its presence it can be expected that the annealing has a negative influence either on fatigue crack initiation or fatigue crack growth.

Key words: *fatigue strength; crack initiation; fatigue crack growth, low-temperature annealing; pipeline steel; microstructure;*

1. Introduction

Hot rolled steel strips are the most frequently used structural materials. Microalloyed steels (usually named as high strength low alloyed steels) have an indisputable position among them representing about 10 per cent of the world steel production. The principal advantage of these steels is the possibility to achieve high strength levels without increasing the amount of alloying elements. The required mechanical properties are achieved by means of controlled rolling where the mastering of precipitation processes (of the elements Al, Ti, Nb, V, Zr) during deformation and cooling from finishing temperature is of primordial importance. This process enables to use the four basic strengthening mechanisms – solid solution strengthening, dislocation strengthening, microstructural strengthening and precipitation strengthening. Usually 70 percent of the yield stress value is due to grain refinement (the finishing rolling temperatures play here a deciding role) and precipitation (the coiling temperatures play here a deciding role). Using of all four strengthening mechanisms at the same composition it is possible to obtain twofold to threefold higher values of yield stress when compared to conventional steels. This enables a significant weight reduction of the projected structures at a cost reduction of about 25 per cent [1–3]. HSLA steels are world-wide used for such structural applications as tubes, boilers, pressures vessels, bridges, ships, automotive industry, for welded machine parts. Structural materials are often exposed to cyclical changes of temperature or stress (eventually of both) being the primary cause of failure in structural applications.

The selection of a material with optimal properties is significantly influenced by its resistance to cyclic loading and the traditional criterion of the selection is the fatigue limit (σ_{-1}). An approximate estimation of the fatigue limit of steels loaded by alternating symmetric cycling ($R = \sigma_{\min}/\sigma_{\max} = -1$) is about the halve of its tensile strength ($\sigma_{-1}/R_m = 0{,}5$). The fatigue limit measured both on smooth and notched specimens increases with their strength but the differences between σ_{-1} measured on steels with different strengths decrease with increasing level of stress concentration. It is not unusual that fatigue limits measured on poorly machined or not machined welded joints are totally independent on strength and are in the range of 100–200 MPa [4]. Besides welded joints other stress concentrators may be encountered which shorten the initiation stage of the fatigue crack in such an extent that the propagation stage may dominate the life of the structure. For that reason besides the fatigue limit the loading level below which the existing cracks do not propagate i.e. the threshold value of stress intensity factor range (ΔK_0) has to be considered as an important factor of fatigue resistance. It is clear that depending on the structural project and the exploitation of the structure either the initiation stage or the propagation stage will dominate and, therefore, it is important that the fatigue resistance be evaluated separately in the different stages. Among the advantages of the introduction of rolling.

HSLA steels by a controlled schedule of rolling and cooling was the possibility to achieve the required mechanical properties without the necessity of subsequent normalization. In spite of that in order to optimize some sheet and strip properties sometimes an additional heat treatment is incorporated into the processing route consisting of annealing at different temperatures. Annealing below the Ac1 temperature is advantageously used for coils where the measured strengths were higher than the required values or the Charpy impact energy was lower than specified.

The aim of this contribution is to evaluate the influence of low temperature annealing on changes in the fatigue resistance of HSLA steels microalloyed on the basis of Nb, Nb–V, Nb–V–Zr, both in the crack initiation and crack propagation stages.

* **Gejza Rosenberg**
Faculty of Metallurgy, Technical University of Košice, Letná 9, 042 00 Kosice, Slovakia, E-mail: Gejza.Rosenberg@tuke.sk

2. Material and Experimental Procedures

Material

Four commercially produced HSLA steels microalloyed on the basis of Nb (steel B), Nb+V (steel D and 6) and Nb+V+Zr (3) respectively were used for the experiments. Table 1 shows the steels compositions.

The steels designated by B and D had in comparison to steels 3 and 6 higher carbon content but, on the other hand, the carbon equivalents ($C_{ekv.}$ = C+Mn/6 + (Cr+Mo+V)/5 + (Ni+Cu)/15) of steels B and 3 on one side and D and 6 on the other side were comparable ($C_{ekv.}$ = 0,28 and $C_{ekv.}$ = 0.33, respectively). The steel plates were rolled by similar controlled rolling schedules, being the finishing temperatures rolling always in the ranges: $t_{dov.}$ = 835–850 °C and $t_{nav.}$ = 570–580 °C, respectively, while still maintaining tdov $t_{nav.}$ = 260 to 270 °C. The thickness of the rolled plates was the same, 8 mm. The specimens were cut perpendicularly and parallel to the rolling direction, with dimensions of 60 × 150 mm. The mechanical properties were measured in the as delivered condition, without surface machining. Both from the un-annealed material as well as from a set of selected cut pieces annealed for 650°C/25 min fatigue test specimens were machined. On the same specimens hardness was also measured.

Fatigue testing

All fatigue tests were performed at the frequency f = 25 Hz and stress ratio R = 0.03 (notched specimens) and R = −1 (unnotched specimens). Plane bending fatigue tests were conducted on smooth specimens which in the reduced section had $B = 4.1 \pm 0.1$ mm thickness and W = 6 mm width. The evaluation of the fatigue strength in both unnotched and notched test specimens was done for 107 cycles. The surfaces of all specimens were metallographically ground, polished, and in some cases also etched.

The fatigue crack initiation and propagation behavior was investigated on notched specimens in three-point bending at a stress ratio R = 0.03 and frequency of f = 25 Hz. The data were obtained by testing single-edge-notched (SEN) specimens of W = 20 mm (working length L = 4W) width and B = 6 mm thickness containing a 5.0 mm deep electrospark-produced notch. The notch tip radius were ρ = 0.06 mm for FCG or ρ =0.2 mm for fatigue crack initiation experiments.

All specimens were precracked over a length of ≈ 0.7 mm. After crack initiation in the samples at the level of $\Delta K \approx 6$ to 8 $MPam^{1/2}$ the loading was gradually decreased or maintained at a constant level of ΔK with the aim to determine the threshold value of stress intensity factor range (ΔK_{th}), defined by the decrease of the FCG below the level of $da/dN = 2 \times 10^{-7}$ mm/cycle. For both tested conditions minimally three specimens were used for each structural state and direction. Only the FCG data measured at increasing value of ΔK were recorded. The crack length was monitored using an optical microscope and potential drop technique. The loading level was increased in such a way that each additional increase in the ΔK value occurred only after the FCG for the length corresponding to minimally three-fold of the PZ size. Fracture surfaces were examined by a scanning electron microscope.

3. Experimental Results and Discussion

The mechanical properties measured on specimens cut parallel to rolling direction in the as -delivered condition are listed in Table 2.

Mechanical properties and mean grain sizes of tested steels — Table 2

Steel	R_{p02} MPa	R_m MPa	R_{p02}/R_m MPa	A_5 %	Z %	$KCV2$ J.cm^{-2}	d_F μm
B	468	582	0.804	26.4	67.1	171	6.8
D	482	598	0.806	23.2	58.6	128	5.8
6	518	615	0.842	26.5	67.4	165	5.4
3	533	629	0.847	27.1	69.4	192	4.9

Comparing the data in Table 1 it is clear that in spite of the different finishing rolling and coiling temperatures these steels have significantly different mechanical properties. The results in Table 1 show that steel 3 has the highest levels of yield stress and tensile strength also the highest elongation, reduction of area and Charpy impact energy. Steels B and 6 have their strength and plasticity about on the same level. The steel D significantly differs from the others by about 15 per cent lower values of elongation, reduction of area and by 25 per cent lower impact energy.

The microstructural analysis was conducted on sections in the three principal directions in relation to the rolling direction. The microstructures of the investigated steels in the as-delivered condition (the polished planes of the metallographical specimens being parallel with the surface of the strips) are documented on Fig. 1

Chemical compositions of the materials used (mass %) — Table 1.

Steel	C	Mn	Si	P	S	Al	Nb	V	Zr
B	0.090	1.15	0.33	0.014	0.008	0.037	0.035	-	-
D	0.100	1.36	0.28	0.015	0.008	0.054	0.022	0.032	-
6	0.070	1.48	0.13	0.010	0.009	0.040	0.035	0.055	-
3	0.070	1.23	0.28	0.012	0.007	0.058	0.070	0.030	0.06

while the mean grain values are listed in Table1. Generally, the microstructures were very heterogeneous consisting of larger irregular ferritic grains combined with significantly smaller and more or less polyhedric grains. Locally the steels 3,6 and B to a limited extent exhibited acicular ferrite while in the steel B also ferrite with Widmanstätten morphology. In all of the investigated steels except B grains larger than 10 um were present only sporadically the preponderant grain size range was 4 to 8 um. In the steel B in some areas grains of the size about 15 um were observed more frequently i.e. the double of the mean grain size. Except of the steel D all others exhibited on the metallographical sections perpendicular to the strip surface and principally in the plane parallel to the rolling direction elongated grains. This direction dependence of the grain size was clearly detectable in steel B but especially was pronounced only in steels 3 and 6. A detailed metallographical analysis of steels 3 and 6 showed that besides the finer grains of steel 3 they are very similar microstructurally, i.e. by morphology and type of the microstructural constituents. In spite of its mechanical properties steel D exhibited the less heterogeneous microstructure with frequent occurrence of small polyhedric grains located along the grain boundaries of the larger more acicular grains. The perlite in this steel had a more disperse morphology and along the grain boundaries frequently were observed carbides or particles of other phases, sometimes forming a continuous envelop.

The precipitation was investigated by means of carbon extraction replicas in a transmission electron microscope (TEM). From Figs. 2–B to 2–Da which document the as delivered condition it is clear that the sequence with the highest precipitation degree is 2–D, 2–3 and 2–6 respectively, while the lowest degree belongs to steel 2–B, which was micro-alloyed only with 0.03 per cent of Nb. The particles along the grain boundaries were observed mainly in steel 3 and steel 6. The particles in steel 3 had thickness of 100 nm, exceptionally 200 nm (Figs. 2–3a) and in steel D they had a thickness above 500 nm (Fig. 2–Da).

The hardness values measured on annealed specimens listed in Table 2 indicate the highest hardness increase was registered in steels 3 and 6. It confirms the expectation since these steels contained the highest a microalloying addition which is the principal precondition of a successful precipitation hardening. It is supposed that the precipitates were carbides and principally carbonitrides of vanadium for which the highest precipitation rates is considered to be about 600°C [1]. This affirmation is supported by the fact that steel B which did not contain vanadium showed no additional strengthening by annealing (Table 3).

On the other hand, the TEM observation of carbon extraction replicas confirmed that annealing caused an increase in the density of soft precipitates not only in steels 3, 6 and D but also in steels

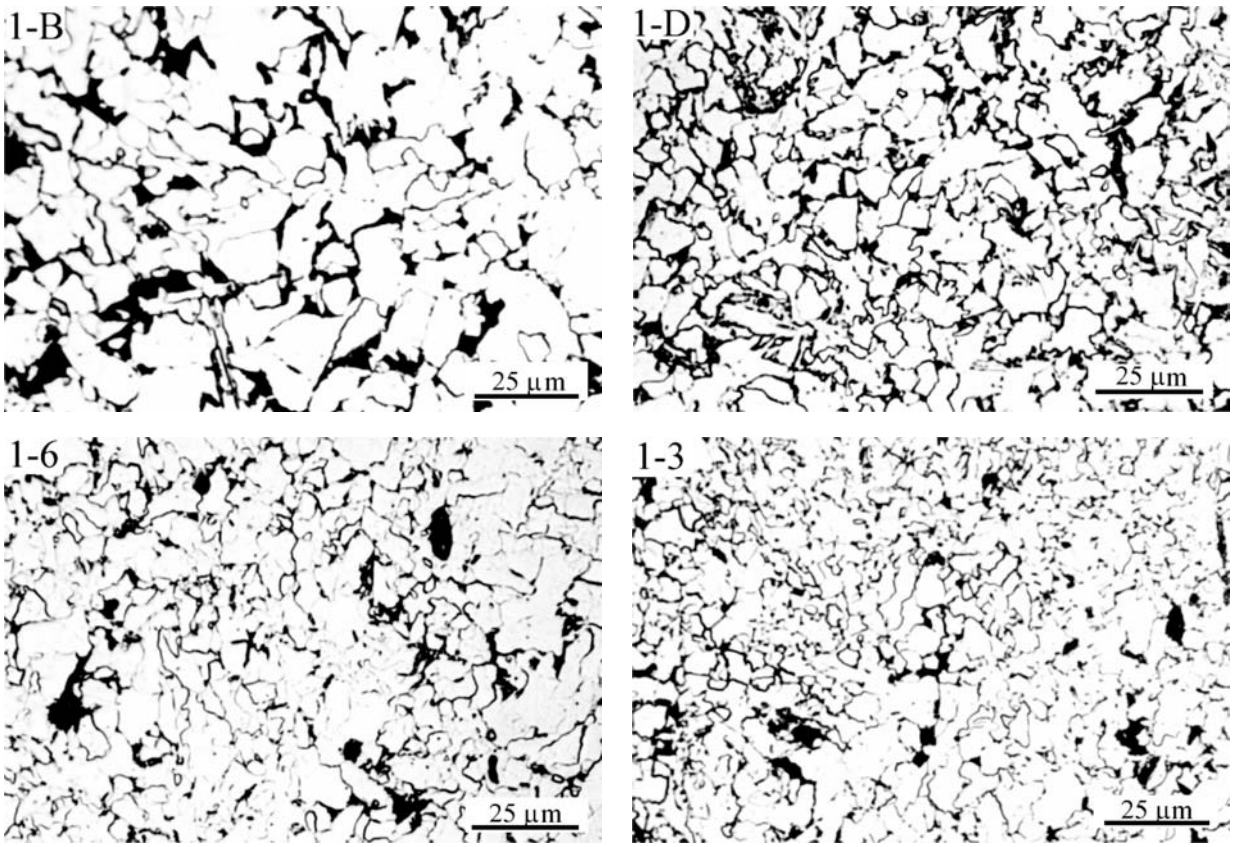

Fig. 1 Microstructure of HSLA steels B, D, 6 and 3

Test results of fatigue limits and hardness before – after annealing — Tab. 3

Steel	*HB* delivered	*HB* annealed	σ_0 MPa	σ_0/R_m	σ_0/HB
B	183	184	327	0.562	1.78
D	186	191	317	0.530	1.66
6	191	203	335	0.545	1.65
3	195	205	341	0.542	1.88

B. It has to be assumed that probably the precipitates AlN also participated in the precipitation process, having the maximal precipitation rate of about 700 °C or rather niobium carbonitrides, the precipitation of which at 600 °C/10 min resulting in a hardness increase of 20 HV was observed also in [5].

The fatigue limit of smooth specimens was investigated only in the annealed condition and on specimens cut parallel to rolling direction, Table 3. This table also contains the calculated ratio σ_{-1}/R_m, where R_m means the tensile strength in un-annealed con-

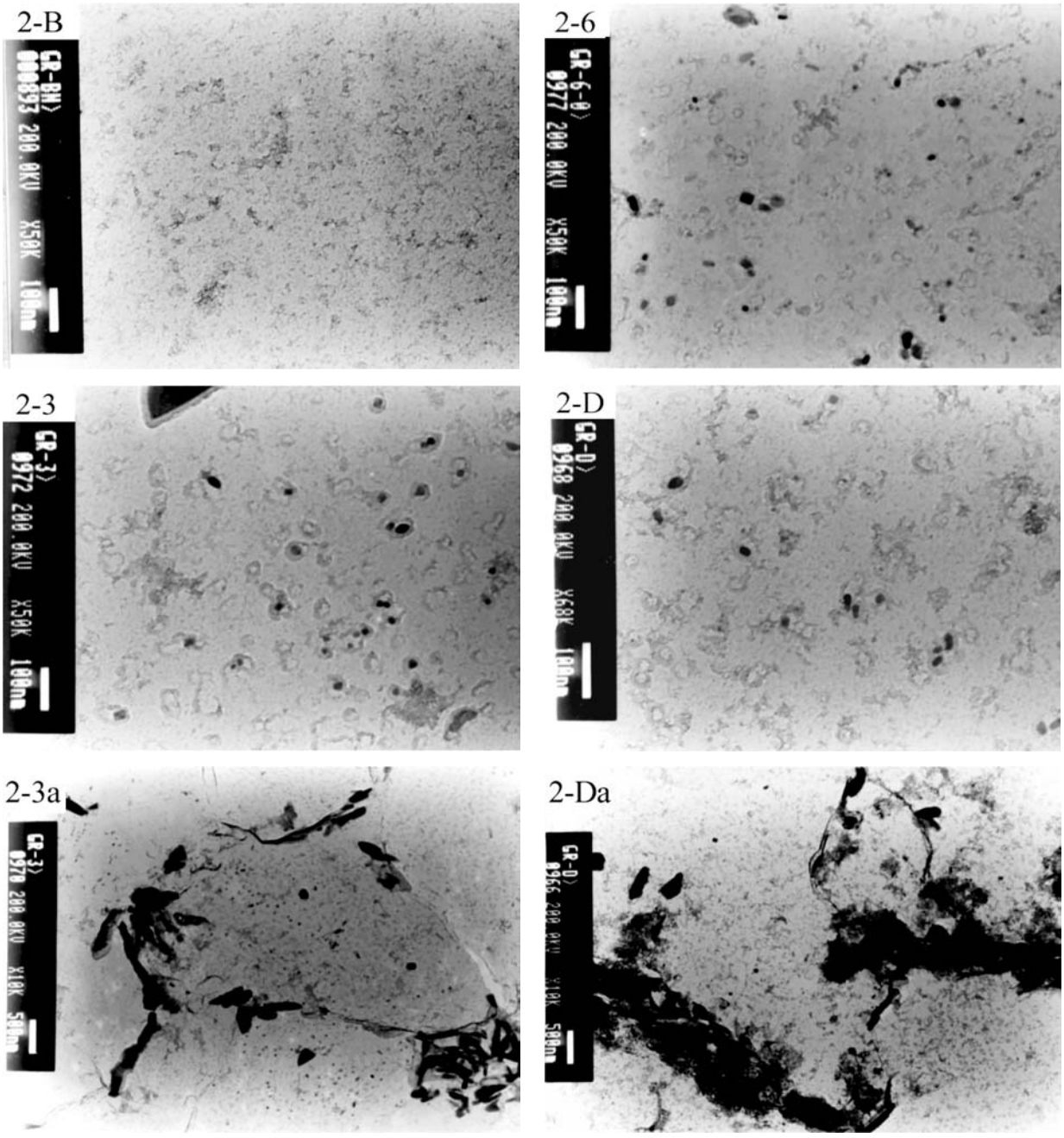

Fig. 2 TEM images of carbon extraction replicas for HSLA steels B, 6, 3 and D

dition from Table 1. The small difference in hardness between annealed and not annealed specimens and the observation that annealing increases the yield stress [5] leads us to suppose that the Rm values did not change by annealing. The relatively high values of the σ_{-1}/R_m ratio in the range 0.53 to 0.56 are in agreement with the value $\sigma_{-1}/R_m = 0.54$ measured in another HSLA steel group [6]. Therefore, we suppose that if the annealing had any influence on σ_{-1}, so it was only slightly positive as a result of hardness increase.

The influence of annealing was clearly observed also by light microscopy. In steels 3, 6 and B the acicular ferrite disappeared or its amount was significantly reduced along with the decomposition of lamellar perlite resulting in the appearance of its less disperse modification. A general statement can be done that annealing resulted in a decrease of the marked microstructural heterogeneity observed in the as -delivered condition. In steel D the microstructural changes were minimal. The most pronounced changes occurred in steels 3 and 6 in which along with the above mentioned features a significant reduction of the elongated grain shape due to rolling direction was observed, being this more pronounced in the central area of the specimens.

The results of microscopical analysis showed a good correlation with the measured values of fatigue crack initiation resistance on notched specimens and crack propagation rate changes at a given level of stress intensity amplitude (ΔK) including the threshold value (ΔK_0). The results are resumed in Table 4.

It can be deduced from Table 4 that fatigue resistance anisotropy occurred only in steels 3 and 6 due to elongated grains in the rolling direction. When cracks grew perpendicularly to the elongated grains the crack propagation rates were significantly lower as in the parallel direction. The crack propagation rate values measured on specimens with cracks oriented parallel to the rolling direction in steels 3 and 6 were the same as in steel B (both on specimens parallel and perpendicular to the rolling direction).

The lowest value of the fatigue crack growth (FCG) resistance was measured in steel D in which independently on the rolling direction the threshold values ΔK_{th} were by 15 per cent lower when compared to steel B. In comparison with steel B the largest difference (as far as 100 per cent) in FCG rate was observed in the range above the threshold value, but also at a loading level of $\Delta K = 20$ MPa.m$^{1/2}$ were difference in the FCG rates marked. The highest threshold values ΔK_{th} and the lowest crack propagation rates at a given level of loading were observed in steels 3 and 6, when the direction of crack growth was perpendicular to the rolling direction. In comparison to steel D cracks grow in this case in the range above the threshold value four times more slowly and at a loading level of $\Delta K = 20$ MPa.m$^{1/2}$ three times more slowly while the threshold values ΔK_{th} are about 50 per cent higher. Attention has to be given to the fact that the threshold value for crack initiation $K_{th,\,\rho=0,2}$ in steels 3 and 6 is lower than the threshold value for crack propagation. This apparently contradictory experimental result can be explicated by the well-known effect of premature crack closure, which occurs more intensively in specimens with a longer fatigue crack [7]. From Table 3 it is clear that the annealing had either no effect on crack growth (steel B) or its influence was negative. Differently from steel D, where the decrease of resistance to fatigue crack growth as well as the decrease of the resistance to crack initiation on notched samples can be considered as insignificant, in steels 3 and 6 a significant degradation of both of the above mentioned characteristics occurred. These results can be explicated by the effect of annealing on suppression of differences in ferritic grain size in both directions relative to rolling direction. Also the fact that steels B, 3 and 6 in the annealed condition show minimal difference both in the threshold values $\Delta K_{th,\rho=0,2}$, ΔK_{th} and fatigue crack growth rates expressed by the parameter $da/dN_{(\Delta K=20}$ is in accordance with the results of the metallographical analysis. The worst properties were observed in steel D which exhibited even after the annealing cycle the threshold values $\Delta K_{th,\rho=0,2}$ and ΔK_{th} by about 20 per cent lower when compared to all of the investigated steels in this work. Microstructures similar to steel D were observed in other HSLA steels annealed at temperatures below Ac1 for a few hours, but not even in this case a significant deterioration of resistance to FCG growth occurred.

It is well known that besides the finishing rolling and coil temperatures exist also many other factors which in certain circumstances may more or less influence the final steel properties. Among the factors that may significantly influence the final properties already in the early stages of the processing is the casting velocity and casting temperature, the heating temperature of slabs as the thermomechanical conditions of the rolling. The carbon content

Influence of annealing on fatigue crack initiation-growth resistance — Table 4.

Microstructure condition	Steel	Direction to *RD*	$\Delta K_{th,\,\rho=0,2}$ MPa.m$^{1/2}$	$da/dN_{\Delta K=20}$ mm/cycles	ΔK_{th} MPa.m$^{1/2}$
Initial condition	B	II, ⊥	6.8	$3.5.10^{-5}$	5.8
	6.3	II	6.7	$3.5.10^{-5}$	5.8
	6. 3	⊥	7.2	$1.5.10^{-5}$	7.6
	D	II, ⊥	5.9	$4.5.10^{-5}$	4.9
Annealed condition	B	II, ⊥	6.8	$3.5.10^{-5}$	5.8
	6. 3	II	6.8	$4.0.10^{-5}$	5.8
	6. 3	⊥	6.8	$4.0.10^{-5}$	5.8
	D	II, ⊥	5.7	$4.5.10^{-5}$	4.8

of steel D was 0.1 per cent, which is slightly above the limit where the liquid steel passes through a peritectic reaction during solidification. The transformation of the primary δ-ferrite to austenite is accompanied by segregation processes and precipitation of dendritic shape particles of the size over 500nm usually along the δ-ferrite boundaries or along the austenite grain boundaries. During the subsequent stages of hot rolling or cold rolling this segregation structure is deformed but the composition of particles except of the carbon content is maintained as is maintained their effect on embrittlement [8, 9]. The embrittlement effect of segregation processes along grain boundaries may be pronounced by precipitation of MnS, AlN inclusions or by nitrides and carbonitrides of the micro-alloying elements (Nb, V, Ti), but also by the possible presence of surface active elements (Sn, As, Sb, Bi) and impurities S, P, Cu, Al [9]. Considering the composition of the steel D (Table 2) along with the fact that observed the particles sizes along the grain boundaries in TEM (Fig 2Da) is comparable with the size of particles formed in the peritectic reaction [10], it can be supposed that exactly the segregation processes due to the solidification of the steel D by peritectic reaction are responsible for the relatively low values of elongation, impact energy and low resistance to fatigue crack initiation and growth observed in notched specimens.

4. Conclusions

The general results of the investigation can be summarized as follows:

1. In all of the investigated steels after an annealing at 650 °C for 25 min relatively high values of the fatigue limit were measured, with σ_0/R_m ratio in the range 0.53 to 0.56.
2. It was confirmed that the threshold values of stress intensity factor amplitude for fatigue crack growth (ΔK_{th}) may be higher than the threshold value for crack initiation on notched specimens with a notch root radius $\rho = 0.2$ mm ($\Delta K_{th,\ \rho=0.2}$), i.e. $\Delta K_{th} > \Delta K_{th,\ \rho=0.2}$.
3. The annealing did not show effect on fatigue crack initiation resistance of micro-alloyed steels in specimens with a notch root radius $\rho = 0.2$, or insignificant (max.5 per cent) decrease of $\Delta K_{th,\ \rho=0.2}$ was found.
4. The annealing caused in most cases a moderate but always detectable decrease in resistance to fatigue crack growth. The effect of annealing was most pronounced in specimens where the cracks grew perpendicularly to the rolling direction, here the threshold values ΔK_{th} decreased by more than 20 per cent. In the range above the threshold value up to the loading level $\Delta K = 20$ MPa.m$^{1/2}$ the measured crack growth rates were twofold higher in the annealed condition than in material that was not annealed.

Dedicated to the memory of Prof. A. Puškár, DrS c., dr. h. c.

References

[1] http://vanadiumtechnologypartnership.org/
[2] http://www.cbmm.com.br/english/sources/techlib/info/hsconstr/hsconstr.htm
[3] JUHÁR Ľ, BANÍK J.: *Final report N. 4 of research project P2-17*, November 1998 (in Slovak).
[4] ROSENBERG, G.: *Proceedings of the International Welding Conference,* Japan-Slovak Welding Symposium, 5-7 March 1996, Vysoké Tatry, str. 327–330.
[5] ZHAO, M-CH. et al.: *Difference in the Role of Non-quench Aging on Mechanical Properties between Acicular Ferrite and Ferrite-Pearlite Pipeline Steels,* ISIJ International, Vol. 45 (2005), No. 1, pp. 116–120.
[6] ABE, T. et al: *Fatigue Behaviour Various Properties HSLA Bar Steels,* Transaction ISIJ International, Vol. 22 (1982), pp. B-152.
[7] ROSENBERG, G.: *The Size of Plastic Zone and Fatigue Crack Growth Behaviour of three Forms of Ti-6Al-2.5Mo-1.5Cr Alloy*, Fatigue & Fracture of Engineering Materials & Structures, 21, 1998, pp. 727–739.
[8] http://www.cbmm.com.br/english/sources/techlib/info/thermhot/f_therho.htm
[9] MAYR, M. et al: *EPMA Investigation of Segregations in Continuously Cast Steel,* AMS, 10, 2004, 55–65].

https://doi.org/10.26552/com.C.2006.4.57-60

KOMUNIKÁCIE COMMUNICATIONS

Milan Blagojevic – Dejan Petkovic *

A NEW APPROACH TO THE INTERPRETATION OF SIGNALS FROM TEMPERATURE SENSORS

A basic approach in adaptive modeling of data acquisition is based on the comparison of real time data with the data previously predicted from the adequate numerical model. Our research was initiated to find a better algorithm for prediction of fire growth in enclosed spaces by means of interpretation of signals from fire sensors. The data obtained from temperature sensors are compared in a real time with predicted data and are used to adjust the numerical model for prediction so that it matches the reality. This adaptive approach has the following primary goals: early warning of fire growth, better alarm decision making, realization of an adaptive threshold (a threshold changing in the time according to the input signal), very small false alarm rate, etc. In this paper we introduce a method that uses smooth spline polynomials for approximation of the collected data and the time sliding window principle. The length of time sliding window varies in the real time and depends on the calculated error.

Keywords: *data acquisition, time sliding window, smoothing spline approximation, adaptive modeling.*

1. Introduction

In the context of data acquisition adaptive modeling uses the comparison of collected data with data predicted from a model to determine behavior of the system during sometime period. Minimization of differences between real and predicted data leads to more appropriate predictions of the system behavior like: system fault detection, detection of an accident situation in the early stage, adaptation of alarm threshold, etc.

In general, the problem of adaptive modeling requires solution of two related problems:

1) To define an adequate method for approximation and extrapolation (prediction) of the acquired data, and
2) To quantify the differences between collected and predicted data and by using this quantification to correct the adaptive model with the main purpose: to minimize those differences.

Functions for approximation can be constructed using the weighted residuals method, WRM. Some of the procedures are the least squares method, point matching method, etc. The simplest choice are the polynomials of arbitrary order which must be less or equal to the number of the remembered data for the current length of time sliding window. Quasi-stationary problems can be described with polynomials of any kind (specially splines of 2nd or 3rd) and prediction of the deterministic process is not a problem. However, the system faults demand a more detailed analysis (such as noise, fault peaks, etc.).

In systems where the collection of data is stationary (polling in equal time distance), the simplest method, which is satisfactorily accurate, is the least squares method with the polynomial approximation of the detected signal. With this approach, the model is represented by a curve which lies between the data, and produces the least sum of square error. According to the problem of adaptive modeling, an arithmetical mean obtained with the mentioned method has to be compared with the real data and the difference obtained in such a way is the condition for decision.

2. Time sliding window and real time reasoning

In real time systems data acquisition demands real time processing. Because of that, the method and corresponding software must provide time sliding. Consequently, it means that in the same program the loop contains the retarded and advanced instruction. Obviously, it is not possible and we have to simulate this algorithm using a sliding window principle.

Comparing the results obtained from extrapolation and data which the software accepts in real time, in every exact moment, the difference can be used to adopt the next extrapolation (the next time window). The extrapolation (prediction) has to be stated on the arbitrary set of previously acquired data. Because of the nature of a real time process, we must use the number of sensor data as small as possible. If we choose to view the set of data in the time window the length of which is constant, consequently we define the time sliding window with a constant length. In our approach the time sliding window has a variable length.

The time sliding window length is variable in time and depends on an error, i.e. the difference between the predicted data and the data that are acquired at every time instant. The measurement of time in every sliding window begins from the relative zero time. The method of variable length of the time sliding window includes feedback that corrects the errors in prediction.

* **Milan Blagojevic, Dejan Petkovic**
Faculty of Occupational Safety, Department of Fire Protection, 18000 Nish, Serbia, E-mail: milan@znrfak.ni.ac.yu

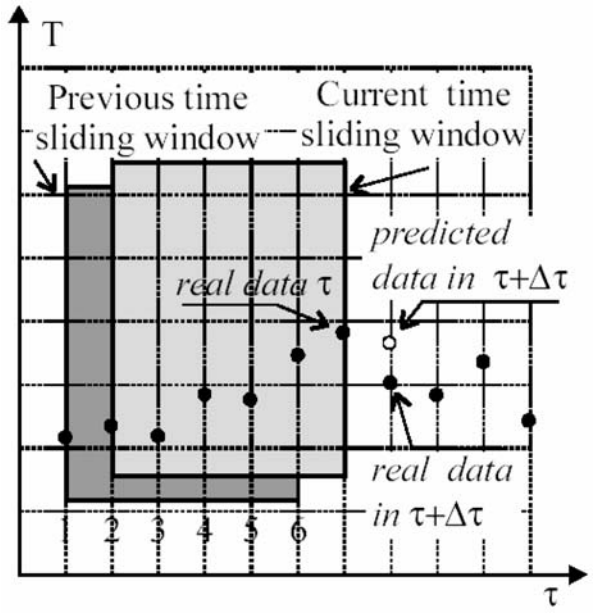

Fig. 1 Time sliding window

3. Outline of the method

Our work is based on the approach which involves numerical signal processing. Data from sensor are used to obtain an acceptable extrapolation function. The next step is to compare the data from sensors to previously expected (predicted) values.

The length of the time sliding window is variable in real time and depends on the calculated error. This is the main problem, i.e. which length of the time sliding window has to be chosen in every time instant. Due to the equal time distance in data acquisition the number of acquired data and the length of the time sliding window are linearly interdependent. Of course, the number of predicted data is arbitrary, but the best results can be obtained with only one next time point. This approach demands that the borders of the time sliding window vary in real time simultaneously with the window. This approach also leads to the best fit between the real time and the predicted data when the difference between those two time series of data is used as a feedback.

The algorithm that uses the time sliding windows principle is described here on data from temperature sensors. In every time instant ($\tau + \Delta\tau$) the algorithm has to compare new data with the previously predicted data and, depending on permitted difference, to expand the window backward until the satisfactory accurate approximation.

The algorithm for the data acquisition subroutine has to be as follows (detailed [2], [3]):

Obviously, the described steps have to be repeated until the mathematical model that describes the real state of a system gives the results which are satisfactorily accurate.

A quantification of the difference between the new data and predicted data can be provided in several ways: through an absolute and relative difference or, better, through tools provided by functional analysis. The framework of functional analysis allows to treat time series as vectors and, consequently, various calculus in that sense through the norm which provides a definition of the length of the vector, inner product which provides the angle between two vector and, finally, minimizing the difference between two vectors by means of a projection coefficient.

The greatest advantage of this real time solution is a small number of iteration, which would have to be made before the best fit is established. Consequently, in buildings or environments with more sensors it should be possible to use information from a variety of systems to make decision.

4. Smoothing spline approximation in time sliding window

Spline functions are the category of very useful non analytic functions which consist of different polynomials on segments (and thereby segmental-analytic) linked in specific points which are called nodes.

; new acquired data in $\tau + \Delta\tau$

1 – approximation and prediction in window of current (initial/last calculated) length
2 – comparing new data with previous predicted data

3 – do until ***(difference between new data and predicted data greater then permitted)***
if ***(maximum length of window not reached)*** **then**
– expand window backward
–approximation and prediction in current window
endif
endd

Fig. 2 Algorithm

The curve is piecewise cubic, that is, the coefficients of the polynomial are different on each interval (segment).

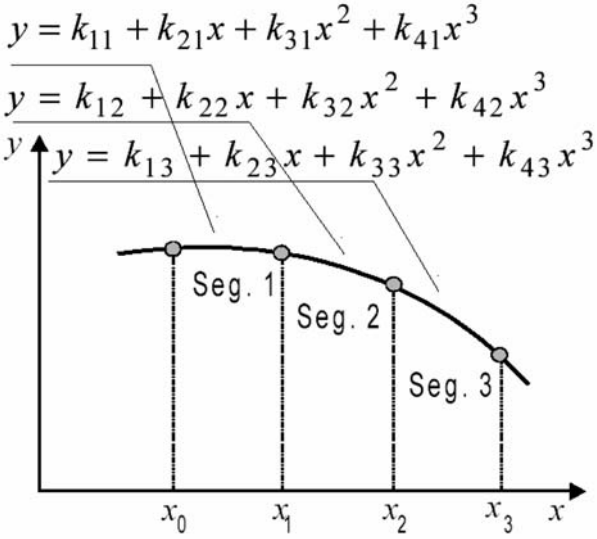

Fig. 3 Spline polynomials

$$y_i(x) = k_{1i} + k_{2i}x + k_{3i}x^2 + k_{4i}x^3, \quad i = 1, 2, ..., m \qquad (1)$$

The curve passes through the given data (x_i, y_i; i, ..., n). The first and second derivatives are continuous at the node points. For natural spline, the second derivatives at end points equal to zero.

For signal identification and, more important, for prediction in the time sliding window, we used a smooth cubic spline approximation of Schoenberg and Reinch with the modification discussed in de Boor [5]. It is a natural cubic spline with knots at all the data abscissas (for uniformly spaced data points), but it does not interpolate the data (x_i, f_i).

The smoothing spline is the unique function, which minimizes

$$\int_s^b S''(x)^2\,dx \qquad (2)$$

Minimization of (1) establishes a compromise between two conflicting goals:

1. to stay close to the given data, and
2. to obtain a smooth function.

These two conflicting goals may be expressed as

$$\sum_{i=1}^{N} \left| \frac{S(x_i) - f_i}{w_i} \right|^2 \le \sigma \qquad (2)$$

where: w – weights,
σ – smoothing parameter, and
N – length of the time sliding window (number of obtained data in window) in every time instant.

The parameter σ has to be chosen somehow and depends on the weights. In [5] it is proposed to choose σ somewhere within $\sqrt{2N}$ of N in case $\sqrt{2N}$ is a good estimate for the standard deviation of the data. That is,

$$N - \sqrt{2N} \le \sigma \le N + \sqrt{2N} \qquad (4)$$

Simply, σ represents a knob which one may set or turn to achieve a satisfactory approximation to the data. More sophisticated choice for σ is based on an estimation of the noise in the data obtained by a process called "cross validation".

The choice of weights depends on the question "have all the data the same importance for approximation" or "which data have more importance for prediction". For example, if we choose the pulse function as weighted function in the time sliding window all the data have the same importance for approximation, with triangle weighted function the "oldest" and the "newest" data have the least importance for approximation. Finally, the best choice for weighted function is the linear function because of the "newest" acquired data have the most importance for prediction.

In our approach, due to the quasistationary nature of temperature in fire phenomena, we have defined weights of f_i in the window uniformly from 0 to 1, where the data on the right border of the window (the last acquired data) have $w = 1$.

5. Numerical experiments

In order to prove the proper choice of smooth spline approximation in the time sliding window, the described method built in simulation software and we made numerical experiments on the several sets of data. The data were chosen in the following way: most of the data have almost the same value except one, two or three data in the sliding window that have significant offset from the signal level (noise, disturbance, etc.).

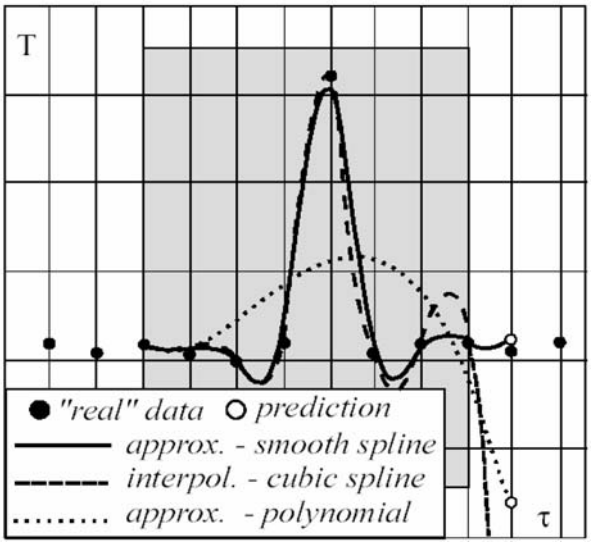

Fig. 4 Interpolation and approximation in window with maximum length

In the first phase of the experiment the comparative analysis between various interpolation and approximation methods was done. The results are shown in Fig. 4 (approximation with polynomial – least squares method, cubic spline interpolation and smoothing spline approximation).

It is obvious from Fig. 4 that for systems which have disturbances and noise it is not possible to use the least squares method to generate a satisfactorily accurate curve to the approximate system behavior. The length of the time sliding window in this example is eight data points, which is maximum for expanding in the algorithm shown in Fig. 2.

Already in this stage of investigation, the experiments show that smoothing spline approximation for various lengths of the time sliding window leads to almost identical predictions. In order to prove that fact a numerical experiment with the time sliding window length of 4, 5, 6, 7 and 8 data points is carried out.

The data for applying smoothing spline approximation for various lengths of the time sliding window and corresponding predictions are shown in table 1 and Fig. 4.

Predictions for various length of window Table. 1

	"Real data"	Approximation data and the predictions for various length of time sliding window				
1	21.000					21.000
2	22.000				22.000	21.995
3	21.000			21.002	21.010	21.023
4	20.000		19.982	19.929	19.878	19.830
5	22.000	22.054	22.275	22.454	22.600	22.730
6	52.000	51.421	51.087	50.879	50.697	50.534
7	21.000	22.134	22.124	22.202	22.289	22.372
8	22.000	21.428	21.522	21.530	21.524	21.514
9	21.000	20.721	20.921	20.857	20.759	20.656
		Smooth spline polynomials for the first time sliding window				
	22.000	$T = 22.054 + 46.914\tau - 105.280\tau^3$				
	52.000	$T = 51.421 - 5.726\tau - 105.280\tau^2 + 174.471\tau^3$				
	21.000	$T = 22.134 - 23.770\tau - 69.192\tau^2 + 69.192\tau^3$				
	22.000	$T = 21.428$				

Obviously, the smoothing spline approximation is almost "insensitive" to non realistic oscillation in data and, the most important from the view of real time processing, the values of prediction practically do not depend on the time sliding window length.

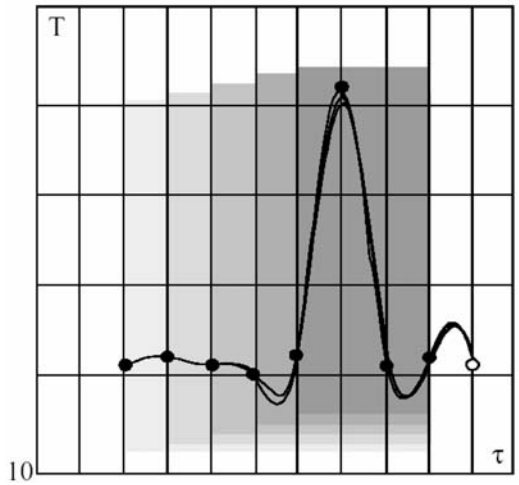

Fig. 5 Approximations and predictions for various window lengths

The results of smoothing spline approximation based on the values from table 1 are shown in Fig. 5.

6. Conclusion

In this paper, the problem how to predict the development of signal from temperature sensors is realized using smoothing spline polynomial in the time sliding window. In this adaptive approach the difference between the predicted value from the model and the acquired value determines the length of the window for the best approximation and extrapolation (prediction). The greatest advantage of spline polynomials usage is that this method of prediction is totally independent of the time sliding window length. On the other hand, the application of functional analysis shows that all comparisons in the sense of vector calculus with various lengths of the time sliding window lead to almost identical values of parameters as relative difference, cosine, etc. Finally, the presented method is very fast and very convenient for real time programming.

References

[1] BLAGOJEVIC, M.: *A new method for adaptation of alarm threshold in fire protection systems*, Ph.D. dissertation, Faculty of Occupational Safety, Nis, SR Yugoslavia, 2001.

[2] BLAGOJEVICH, M., PETKOVICH, D., SIMICH, D.: *A new algorithm for adaptive alarm threshold in fire detection system,* 12th International conference on automatic fire detection ÷ AUBE 2001., Maryland USA, 2001.

[3] BLAGOJEVICH M., PETKOVICH, D.: *Adaptive control and sliding window principle,* System identification and control problems - SICPRO '2000, Moscow, Russia, 2000.

[4] BLAGOJEVIC, M., SIMIC, D., PETKOVIC, D.: *Sliding time window method in fire detection systems,* PREVENTIVE ENGINEERING, year VIII No. 2, Belgrade, SR Yugoslavia, 2001.

[5] DE BOOR, C.: *A practical guide to splines,* Springer-Verlag, New York, USA, 1978.

https://doi.org/10.26552/com.C.2006.4.61-65

komunikácie COMMUNICATIONS

Zoran Čekerevac – Slobodan Ristić *

COMMUNICATIONS: THE WAY OF TRANSMITTING MESSAGES AND COMMUNICATION SKILL

Communication is woven in almost all branches of economy and art, either as a separate skill or as one of the segments in the interdisciplinary approach. It is also a demonstrative and irreplaceable link in the study of various disciplines of management and marketing, as well as in public relations. This paper, after a short basic characteristic of communication, gives detailed analysis about the way of transmitting messages and communication skill. Special attention was paid to the understanding of the sender and the recipient, through the process of coding and decoding of the information. At the end, a communication network established by combining verbal and non-verbal communication systems is analyzed.

Key words: *communication, coding, noise, speech, rhetoric, information*

1. Basic characteristics of communication

Communication is a word of Latin origin. It is derived from a verb meaning "to make common, to report", while the noun meant "community, circulation, report".

The very meaning of the words "communicare" and "communicatio", which lead to the term *communication*, indicates that the essence of communication is in fact a transition from the individual to the collective, a transition which contributes to establishing a community and social behavior.

Communication (by Grinberg, 1998) can also be defined as a process through which a person, a group or an organization (sender) transmits a kind of information (message) to another person, group or organization (recipient). This definition is graphically shown in Figure 1. The diagram helps to better perceive the various phases in the process of communication.

A communication process starts when one party has an idea which it wants to transmit to another party, both parties being an individual, a group or a whole organization.

The sender's task is to transform that idea into a form which can be transmitted to the recipient who will be able to understand it. This process is called *the coding process*, and it represents translating an idea into a form, e.g. written or spoken language, which the recipient can recognize.

This process is of primary significance if communication should be clear.

When a message has been coded, it is ready to be transmitted through one or more channels of communication to the desired recipient, along the ways that information travels, through a telephone line, television or radio signals, by mail or by Internet...The form of coding largely depends on how the information is to be transmitted; however, no matter which channel is used, it is important to transmit the coded message to the desired recipient correctly.

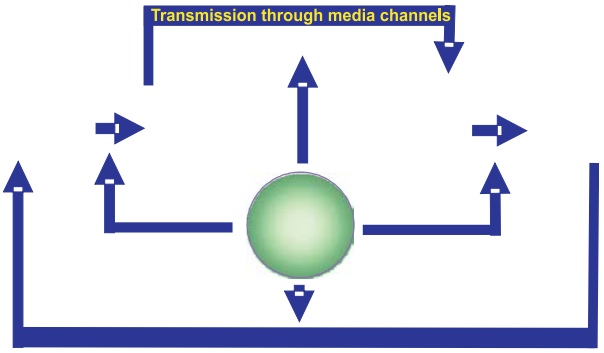

Fig. 1 Communication process

After receiving a message, the recipient starts a decoding process, i.e. returns the message to the form of the sender's original idea. Various sub-processes may be included in this, such as understanding spoken or written words, interpreting facial expressions and the like.

If the recipient has decoded the sender's message correctly, he/she will understand the idea which the sender wanted to transmit. The ability to understand and interpret information is not perfect. As in the case of coding, limitations in the sense of ability to decode some information represent a potential weakness in a communication process. A limitation can be an unclear message as well.

* **Zoran Čekerevac, Slobodan Ristić**
Railway College Belgrade, www.vzs.edu.yu, zoran.cekerevac@hotmail.com

After the message has been finally decoded, the process can be continued by the recipient transmitting a new message to the first sender. This part of the process is called FEEDBACK – and it represents the knowledge of what influence the message has had on the recipient. Having received the feedback, the sender is able to see whether his messages have been understood properly. At the same time, the feedback may convince the recipient that the sender cares for his/her opinion. Once it has been received, the feedback may provoke a new idea with the sender, which may start a new cycle of transmitting information.

In spite of obvious simplicity of the communication process, it rarely functions as ideally as it has been shown here. There are many potential obstacles to effective communication. The factors which damage the clarity of a message are called noise and they can decrease the effectiveness of communication. Noise may be either badly coded (e.g. unclearly written) or badly decoded (e.g. unheard) messages, and also the channels of communication which are full of statics (e.g. the recipient's attention is diverted from the basic message), as well as some other factors (e.g. time pressure, organizational policy...). Noise may cause a distortion of information which is transmitted from one person to another.

2. The way of transmitting messages and communication skill

One of the key purposes of organizing communication is to direct an action, i.e. to make other people behave in a desired way. In order to achieve the aim, the so-called communication bridges are established and obstacles and barriers are overcome. For this purpose, techniques and methods of communication are used and practiced, within different fields and spheres of business environment and social life.

The way of communicating is a skill which can be learnt, practiced and improved. As it has a tendency to create a human, good-quality and esthetic element, communication may also have artistic characteristics. The skill to communicate represents an activity of the spirit which is changed and transformed in time and by experience. It simultaneously points to the art of living, the beauty of a relationship with people, and raises the culture of communication to a higher artistic level.

It may be said that communication is woven in almost all branches of economy and art, either as a separate skill or as one of the segments in the interdisciplinary approach. It is also a demonstrative and irreplaceable link in the study of various disciplines of management and marketing, as well as in public relations.

At the moment of establishing any kind of relation, the following questions should be asked:

- Why do we communicate?
- Who do we communicate with?
- How to be accessible and flexible in that process?
- How to be polite, tactical and patient all the time?
- How to make a profound impression on other people?[1)]

The moment of transmitting information is the most significant in communication. Information is a notice, an announcement, or a fact. It also represents the way of organizing, selecting and creating a certain matter. Information should be reliable, checked, controlled, as well as dynamic. It is not eternal but susceptible to changes. The process of information flow does not consist only of emitting, i.e. transmitting information, but it also requires receiving and decoding a certain message properly, as well as feedback. There is no passive spectator in this process, even if one party in the dialogue is more active in the verbal sense.

In the process of information flow, one party is a sender or transmitter of information and the other is an active recipient. The interaction includes transmitting a message and understanding it properly. Whether the recipient will take and understand a message depends on its contents, the choice of arranged signals, and on the way of communicating the form (the functioning of the system of verbal and non-verbal communication). Public information and speech are sometimes quite wrongly connected only with mass media communication, which narrows the field of action for these categories, and frees a person from responsibility in individual components. Responsibility is equally important in contacts with only one person and when performing in front of a large auditorium. In order to transmit messages and information of different sorts, no matter what type of communication is in question, established signals, i.e. terms, must be chosen.

Public speech is different from everyday speech, because it requires a special application of oratory. Oratory in a modern sense is a complex aspect of verbal communication: it is all-inclusive, informative, argumentative, competent and dynamic. The communicative dynamism is reflected in the way of transmitting messages. In the transmission of information, parts of a statement can be noticed and codes must be chosen, which will lead to revealing the meaning of a message during an information exchange. In order that both participants in a conversation should understand each other, thoughts must be formed in a simple way into an understandable statement by visualizing an idea.

Without entering the theory of meaning, we will only indicate here how to influence recipients of messages in the most appropriate and objective way within a certain communication and behavior. The communicator – speaker – has a complex task: how to transmit a message and meaning in a desired context to the recipient. He/she ought to find a system of signs which will correspond to the broadest public and contribute to a clear, concrete, real and objective delivery of a message. Feedback shows the degree of understanding.

The outline of a communication process is shown in Figure 2.

[1)] M. Marković: Poslovna komunikacija, CLIO, Beograd 2003

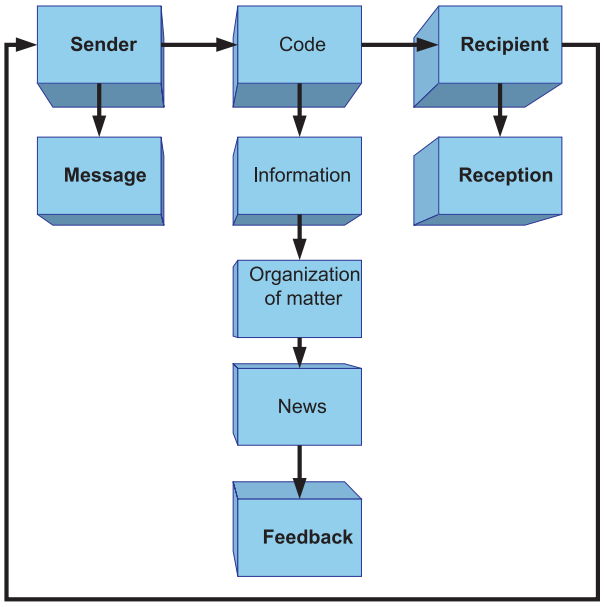

Fig. 2 Communication process with circular flow

Sometimes messages happen to be insufficiently understood, or completely misunderstood and misinterpreted, which causes a communication tension, misunderstanding, and even a conflict. Thus, it is not only important to transmit certain information and ideas, i.e. to pay attention to the contents of a message; the way of transmitting those messages is of crucial significance.

That is why the sentence: "I do not understand" is often heard. It is a good sign of warning which must not be ignored and rejected without thinking. This sentence also offers very important information. It represents a communication bridge for a very skilful communicator, because it is a clear and sincere statement (information) which cannot and must not be ignored. The communicator must try to explain the information, to choose proper terms for the desired idea, and to find another, better and more effective way to transmit the message to the other participant in the communication. Another sentence which is usually heard is: "I do not agree!". Therefore we can say that there are innumerable ways of transmitting and receiving messages. In future, the above mentioned statement could be replaced by another: "I see it in a different way!". The way of forming and transmitting a message contributes to understanding it.

We should consider all levels of meaning which can be noticed in a clear message (text, dialogue, gesture, or voice). It is understandable that there is also a wish and intention to influence listeners or partners in a conversation with a subtext of certain implied messages which are transmitted, and not only with a direct statement. It is particularly noticeable in the sphere of art and political life. Certain variants should therefore be found to make "hidden" messages clear and understandable, and to lead their decoding to understanding them.

Public communication skill does not consist of the quantity of offered information but of the multitude of ideas and matter creation. Communication is not an exchange of sentences but an exchange of ideas formed in a conversation. Speech expression is an important quality in a verbal communication. There are also many signals in the sense of body expressiveness and movements meaning, such as mimic, manual and situational movements, the position of a body in space, etc. The activity in relation to the listener or partner in a conversation can be noticed, first of all, through the opening to the partner or withdrawing from him/her.

Communication skill implies:

- speed;
- economy;
- organization;
- control;
- selectivity;
- trust building.

It is not enough just to have a good idea. It should, in a certain way, be transmitted to the recipient of a message for the purpose of communication. A speech shows the way of the speaker's thinking. People often make mistakes trying to use many words to explain an idea. It is much more important to find adequate images and sounds, i.e. words transformed into understandable and interesting visual impressions and sounds. In that way, the monotony of the sequencing of words in a sentence is broken and the speech can be perceived as a whole. A theoretical discussion and program presentation may seem abstract. Businessmen have no confidence in this method; they demand examples and evidence from practice. An idea will be best presented if it is shown in a simple and practical way – visually and auditory.

Mastering the communication skill may be realized in the following phases:

a) observing and noticing certain characteristics of people and things;
b) classifying these characteristics into groups: important and unimportant; selectively noticing certain features necessary for business communication;
c) adapting behavior, that is selecting certain communicative skills necessary for successful business operations;
d) noticing the reaction of the partner in a conversation;
e) retaining, transforming or completely changing a certain behavior. It should be mentioned that a change in behavior is a skill and not flattering, i.e. giving up or deviating from own attitudes. A change in behavior means adapting to the partner ("walking with him/her"), improvising in looking for various possibilities for a contact, reaching an agreement or a compromise. A change in behavior shows certainty, self-confidence, ability to control a whole process, and a complete domination;
f) noticing the moment of adaptation in the partner in a dialogue, as an attempt to establish bridges in a communication and to show a wish to understand. This moment represents the communicator's first-class skill, for example, in the course of complex negotiations;
g) noticing own mistakes and consequences which those mistakes have or may have on the process as a whole; attempting

to eliminate the mistake without apologizing, but with a change in behavior. To the partner in a conversation, it will be the best sign that tactics has been changed or that there is awareness of a wrong method selected which should be changed or adapted;

h) scoring with no triumph – no one should show that he/she is the winner or has a certain advantage after the negotiations. Confidence and competence should not be proved by enjoying the achieved success and advantage – it goes without saying, because it is a part of the job and professional responsibility for a business operation.[2)]

What causes a misunderstanding? There are many reasons, among which are the following:

- message is not transmitted in an understandable way - problems with terminology;
- conflict of many different ideas – unfocused thinking;
- too much information (overburdening);
- lack of information;
- not understanding or misunderstanding a message;
- not knowing the partner in a conversation;
- noise, disturbance;
- absent-mindedness, being not concentrated;
- deliberate disinformation;
- suppressing, hushing up a misunderstanding.

If a problem turns up in communication, it must be:

- identified and defined, not ignored;
- considered;
- solved.

In various forms of social communication, there are generally two types of clients:

a) clients who are ready to be informed and to satisfy their needs. Cheerful, pleasant and energetic tones are predominant in a conversation with this type of clients;
b) clients who deliberately use a form of aggressive behavior to get an advantage in communication, to impose their own opinion and ideas.

The signs of non-verbal communication are a good indicator of which type of clients is in question, and if they are noticed in time they can give the speaker a certain psychological advantage.

A good relation between the partners in a conversation may be established in the following way:

a) listening to the partner and making deliberate pauses during the speech;
b) applying the technique of cross-examination;
c) ignoring the personal moment and exaggerated emotional reaction (in the case of an aggressive and possessive client);
d) applying a quiet, central and assured tone;
e) applying an active relation, without withdrawing, in order to build up a solid business contact;
f) appearing self-assured in the sense of:
   – body attitude (straight spine),
   – looking at the partner,
   – calm and confident movements,
   – well-balanced movement in space;
g) reaching an agreement or a compromise.

The negotiations with a difficult client may be successfully ended only if the speaker is sure of himself/herself, if he/she is consistent with his/her personal viewpoints and arranges well the time in which he/she will say everything that is necessary in a precise, clear and concise way.

Contacts are established by creating a pleasant atmosphere for conversation, through an activity directed to the listener or partner in the conversation, and the motivation to reach a mutual viewpoint, while respecting the partner's opinion.

Sometimes a speech – words – cannot express primary emotions. The verbal expression of messages may seem too direct and exclusive, particularly when we have to break the news which is not affirmative. Therefore, as a very important system of signs, voice expression and body language (movement, gesture, position, and attitude) can be used to transmit a particular message. Body language allows a certain distance, and it is less likely that the partner in a conversation will be hurt by this way of rejection. Non-verbal communication in a positive way draws attention from a basic, simple and simplified verbal expression to a multi-layered expression.

A communication network is established by combining verbal and non-verbal communication systems. It includes several segments:

a) The speaker's intention – motivation for a conversation or speech. Even Aristotle recognized three types of technical methods of convincing:
   - the first is achieved by the speaker's character,
   - the second is achieved by the mood created in the listener,
   - the third is achieved by the very speech, and the speech should contain three parts:
     - sources from which methods for convincing are derived,
     - the way of making a speech (discussion, style, composing and giving a speech),
     - the arrangement of the parts of a speech;[3)]
b) The dynamic movement of a verbal act – can be followed through an analysis of a conversation. In the contents of every conversation there is a sentence or a part of sentence which is particularly emphasized semantically. It is the most important point in a dialogue – the argument or the focus of a verbal act;

[3)] M. Marinović, Poslovna komunikacija sa poslovnim bontonom, pp. 17-21, CLIO, Beograd 2003

[3)] 4 Aristotel, Retorika 1; Retorika 3; Novi Sad 1997

c) The process of listening – psychological, acoustic and cognitive elements participate in this complex process equally;
d) Non-verbal communication which represents a complex system and can be viewed as a single movement and a series of movements – gestures, and as a pose, the position of a body in space, an arrangement of groups in space, etc.

3. Conclusion

The key purpose of communication is to direct an action, i.e. to make other people behave in a desired way. During that process, communication bridges are established, and obstacles and barriers are overcome. For that purpose, various techniques and methods of communication are used and practiced, keeping in mind a variety of fields, spheres of business environment and social life. The way of communicating is a skill which can be learnt, practiced and improved.

The most important moment in communication of any kind is the preparation which demands creating, opening and completing data bases, and then making a strategic and operational plan. Thus, these plans depend on the essence of an analysis. A situational analysis is a very important moment and consists of the correct answers to the questions: Who communicates? How much/when/where/why, and for what purpose does he/she communicate? The success of a communication act depends on the degree of precision within the answers to the asked questions. That is why it is important to know who the person someone is talking to is (sex, age, profession, status, etc.), how many persons will be present at a business meeting, the meeting place – what it is like, and how large the room in which the meeting will take place is, how much time is available for a presentation, dialogue and listening. Any person that wants to be a good communicator and to master the skill of communication must try to find answers to these questions.

They reveal and show the purpose of a compact process – why we communicate, and particularly what our goal is.

Each communication, in order to be successful, must be carefully and well prepared. Whether it will be successful depends on the communicator, the listener, as well as on the "noise".

References

[1] ARISTOTEL: *Rhetoric 1, Retorika 3*; Novi Sad, 1997
[2] CEKEREVAC, Z., RISTIC, S.: *The Concept, Traits and Characteristics of the Director-Organizer-Manager Personality (In Russian),* In: LXV International Scientific Conference: The Issues and the Prospective of the Railway Transport Development, In: Dniepropetrovsk National University of Railway Transport (DIIT) named after Academician V. Lazaryan, Dniepropetrovsk, May 2005
[3] DVOŘÁK, Z.: *The Possibility of using the geographical information systems in the pipe transport of Military Forces of Slovakia,* In: Zborník 11. Scientific Conference ŽU, pp. 121-126, Žilina, 2003,
[4] GRINBERG, J., Baron, R.: *Behavior in Organisation (in Serbian)*, In: Prentice Hall, 1995, In: Zelnid, Belgrade 1998,
[5] MARINOVIĆ, M.: *Business Communication with Business Bon-Ton (in Serbian)*, In: CLIO, pp. 17–21, Belgrade 2003
[6] MARKOVIĆ, M.: *Business Communication (in Serbian)*, In: CLIO, Beograd 2003., In: CLIO, Beograd 2003.

COMMUNICATIONS – Scientific Letters of the University of Žilina
Writer's Guidelines

1. Submissions for publication must be unpublished and not be a multiple submission.
2. Manuscripts written **in English language** must include abstract also written in English. The submission should not exceed 7 pages (format A4, Times Roman size 12). The **abstract** should not exceed 10 lines.
3. Submissions should be sent: **by e-mail** (as attachment in system Microsoft WORD) to one of the following addresses: *holesa@nic.utc.sk* or *vrablova@nic.utc.sk* or *polednak@fsi.utc.sk* **with a hard copy** (to be assessed by the editorial board) **or on a 3.5″ diskette** with a hard copy to the following address: Zilinska univerzita, OVaV, Univerzitná 1, SK-10 26 Zilina, Slovakia.
4. Abbreviations, which are not common, must be used in full when mentioned for the first time.
5. Figures, graphs and diagrams, if not processed by Microsoft WORD, must be sent in electronic form (as GIF, JPG, TIFF, BMP files) or drawn in contrast on white paper, one copy enclosed. Photographs for publication must be either contrastive or on a slide.
6. References are to be marked either in the text or as footnotes numbered respectively. Numbers must be in square brackets. The list of references should follow the paper (according to **ISO 690**).
7. The author's exact **mailing address of the organisation where the author works, full names, e-mail address or fax or telephone number,** must be enclosed.
8. The editorial board will assess the submission in its following session. In the case that the article is accepted for future volumes, the board submits the manuscript to the editors for review and language correction. After reviewing and incorporating the editor's remarks, the final draft (before printing) will be sent to authors for final review and adjustment.
9. The deadlines for submissions are as follows: September 30, December 31, March 31 and June 30.
10. Topics for the next issues: 1/2007 – Mechatronics in electrotechnical systems, 2/2007 – Educational Sciences in Dimenzions of the Informations Society.

POKYNY PRE AUTOROV PRÍSPEVKOV DO ČASOPISU KOMUNIKÁCIE – vedecké listy Žilinskej univerzity

1. Redakcia prijíma iba príspevky doteraz nepublikované alebo inde nezaslané na uverejnenie.
2. Rukopis musí byť **v jazyku anglickom**. Príspevok by nemal prekročiť 7 strán (formát A4, písmo Times Roman 12 bodové). K článku dodá autor **resumé** v rozsahu maximálne 10 riadkov (v anglickom jazyku).
3. Príspevok prosíme poslať: **e-mailom**, ako prílohu spracovanú v aplikácii Microsoft WORD, na adresu: *holesa@nic.utc.sk* alebo *polednak@fsi.utc.sk* príp. *vrablova@nic.utc.sk* (alebo doručiť na diskete 3,5″) **a jeden výtlačok** článku na adresu Žilinská univerzita, OVaV, Univerzitná1, 010 26 Žilina.
4. Skratky, ktoré nie sú bežné, je nutné pri ich prvom použití rozpísať v plnom znení.
5. Obrázky, grafy a schémy, pokiaľ nie sú spracované v Microsoft WORD, je potrebné doručiť buď v digitálnej forme (ako GIF, JPG, TIFF, BMP súbory), prípadne nakresliť kontrastne na bielom papieri a predložiť v jednom exemplári. Pri požiadavke na uverejnenie fotografie priložiť ako podklad kontrastnú fotografiu alebo diapozitív.
6. Odvolania na literatúru sa označujú v texte alebo v poznámkach pod čiarou príslušným poradovým číslom v hranatej zátvorke. **Zoznam použitej literatúry** je uvedený za príspevkom. Citovanie literatúry musí byť **podľa STN 01 0197 (ISO 690)** „Bibliografické odkazy".
7. K rukopisu treba pripojiť **plné meno a priezvisko autora a adresu inštitúcie v ktorej pracuje, e-mail adresu** alebo číslo telefónu event. faxu.
8. Príspevok posúdi redakčná rada na svojom najbližšom zasadnutí a v prípade jeho zaradenia do niektorého z budúcich čísiel podrobí rukopis recenziám a jazykovej korektúre. Pred tlačou bude poslaný autorovi na definitívnu kontrolu.
9. Termíny na dodanie príspevkov do čísiel v roku sú: 30. september, 31. december, 31. marec a 30. jún.
10. Nosné témy ďalších čísiel: 1/2007 – Mechatronika v elektrotechnických systémoch, 2/2007 – Edukačné vedy v dimenziách informačnej spoločnosti.

kamUNikácie
COMMUNICATIONS

VEDECKÉ LISTY ŽILINSKEJ UNIVERZITY
SCIENTIFIC LETTERS OF THE UNIVERSITY OF ŽILINA
8. ROČNÍK – VOLUME 8

Adresa redakcie:
Address of the editorial office:
Žilinská univerzita
Oddelenie pre vedu a výskum
Office for Science and Research
Univerzitná 1, Slovakia
SK 010 26 Žilina
E-mail: komunikacie@nic.utc.sk, polednak@fsi.utc.sk,

Každý článok bol oponovaný dvoma oponentmi.
Each paper was reviewed by two reviewers.

Časopis je excerpovaný v Compendexe
Journal is excerpted in Compendex

Vydáva Žilinská univerzita
v EDIS – vydavateľstve ŽU
J. M. Hurbana 15, 010 26 Žilina
pod registračným číslom 1989/98
ISSN 1335-4205

It is published by the University of Žilina in
EDIS - Publishing Institution of Žilina University
Registered No: 1989/98
ISSN 1335-4205

Vychádza štvrťročne
Published quarterly

Jednotlivé čísla časopisu sú uverejnené tiež na:
http://www.utc.sk/komunikacie
Single issues of the journal can be found on:
http://www.utc.sk/komunikacie